Geochemistry, Geochronology, and Fluid Inclusion Study of the Newton Epithermal Gold, and Morrison Porphyry Copper Deposits, British Columbia

By

Lijuan Liu

A thesis submitted in partial fulfillment of the requirements for the degree of

Master of Science

Department of Earth and Atmospheric Sciences
University of Alberta

© Lijuan Liu, 2015

Abstract

Petrologic, geochemical, geochronological, and fluid inclusion studies were conducted on the Newton epithermal and Morrison porphyry deposits in central British Columbia, as a part of a large collaborative research project to combine geological, ZTEM, magnetotelluric, and magnetic studies, in order to improve the effectiveness of ZTEM surveys for deep mineral exploration.

Newton is an intermediate-sulfidation epithermal gold deposit, which is spatially and genetically related to a Late Cretaceous volcanoplutonic complex. The mineralized felsic volcanic rocks, feldspar-quartz-hornblende porphyry, and quartz-feldspar porphyry from the volcanoplutonic complex yielded U-Pb zircon ages of 72.1 ± 0.6 Ma (Amarc Resources Ltd., unpublished data, reported in McClenaghan, 2013), 72.1 ± 0.48 Ma (new data), and 70.9 ± 0.5 Ma (Amarc Resources Ltd., unpublished data, reported in McClenaghan, 2013), respectively. A barren diorite intrusion yielded a slightly younger U-Pb age of 69.32 ± 0.43 Ma.

Gold occurs as electrum and gold-silver telluride, which are present as inclusions in disseminated pyrite and marcasite. Three stages of mineralization are recognized: (1) disseminated pyrite with gold inclusions, and rare quartz-pyrite ± molybdenite veins; (2) disseminated marcasite with gold inclusions; (3) polymetallic pyrite-chalcopyrite-sphalerite-arsenopyrite veins. Molybdenite from a porphyry-hosted stage 1 quartz-calcite-pyrite-molybdenite vein yielded a Re-Os data of 72.1 ± 0.3 Ma (McClenaghan, 2013), which is taken to represent the age of mineralization.

A relatively hot and saline hydrothermal fluid was related to stage 1 mineralization, and homogenization temperatures and salinities of fluid inclusions in a stage 1 quartz–pyrite ± molybdenite ± gold vein average 313 ± 51°C (n = 82) and 4.8 ± 0.9 wt.% NaCl equiv. (n = 46), respectively. The predominance of disseminated mineralization suggests that wallrock reaction and cooling were the main controls on gold precipitation, although evidence for boiling was also observed in the veins.

Morrison is a typical porphyry Cu-Au-Mo deposit, spatially and genetically related to Eocene plagioclase-hornblende-biotite porphyry intrusions. The porphyry intrusions are part of a calc-alkaline to high-K calc-alkaline diorite to granodiorite intrusive suite with continental arc

affinity, and yielded a U-Pb age of 52.21 ± 0.37 Ma. The mineralization can be divided into 3 stages: (1) disseminated and vein-type chalcopyrite-bornite; (2) quartz-molybdenite-pyrite veins; and (3) polymetallic dolomite ± quartz-sphalerite-galena-arsenopyrite-chalcopyrite veins. Molybdenite yielded ages of 52.54 ± 0.22 and 53.06 ± 0.22 Ma, which are broadly consistent with the age of the porphyry intrusions, indicating a genetic relationship. Fluid inclusion (Th = 400 to 526°C; salinity = 39.8 to 47.8 wt.% NaCl equiv.), sulfur isotope ($\delta^{34}S$ = -0.2 and 0.8‰ for pyrite and chalcopyrite intergrowths), and oxygen isotope ($\delta^{18}O_{fluid}$ = 3.7 to 6.3‰) data for stage 1 mineralization indicate that the early Cu-Au-bearing fluids were likely of magmatic origin. A cooler and slightly less saline fluid (Th = 320 to 421°C; salinity = 37.0 to 43.1 wt.% NaCl equiv.) was responsible for stage 2 mineralization. Sulfur isotope ($\delta^{34}S$ = -2.1 and -1.2‰ for molybdenite and pyrite, respectively) and oxygen isotope ($\delta^{18}O_{fluid}$ = 0.3 to 3.4‰) data from stage 2 minerals suggest a contribution from meteoric groundwater and sediment-derived S to fluids still dominantly of magmatic origin. Stage 3 was associated with cooler and much more dilute fluids (Th = 163° to 218°C; salinity = 3.1 to 3.9 wt.% NaCl equiv.), with oxygen isotopic compositions of $\delta^{18}O_{fluid}$ ≈ -2 to +4‰ from early vein quartz, and 0.8 to 6.3‰ from late vein dolomite, sulfur isotopic compositions for sphalerite and pyrite of $\delta^{34}S$ = -7.1 and -5.6‰ (respectively), and carbon isotopic compositions from dolomite of $\delta^{13}C$ = 0.6 and 0.7‰. These characteristics suggest that stage 3 fluids were likely dominantly of meteoric water origin (with some wallrock isotopic exchange), and derived C and S from the sedimentary country rocks.

The results of this study will be used to constrain geological and petrophysical models that are being developed to improve the effectiveness of ZTEM surveys.

Preface

This thesis is an original work by Lijuan Liu. No part of this thesis has been previously published except in abstract form:

Liu, L., Richards, J.P., Huebert, J., Abbassi, B., Lee, B., Unsworth, M.J., and Cheng, L-Z., 2014, Geochronology, geochemistry, and fluid inclusion study of the Newton epithermal gold deposit, British Columbia: Prospectors and Developers Association of Canada, Annual meeting abstracts with programs.

Liu, L., Richards, J.P., Huebert, J., Abbassi, B., Lee, B., Unsworth, M.J., and Cheng, L-Z., 2014, Geochronology, geochemistry, and fluid inclusion study of the Newton epithermal gold deposit, British Columbia: Geological Association of Canada, Annual meeting abstract with programs, v. 37, p.166-167

Acknowledgement

This thesis was completed under the supervision of Dr. Jeremy Richards. I would like to express my special appreciation and thanks to my supervisor Dr. Jeremy Richards for support and guidance throughout the duration of my thesis work.

This work was funded by a Strategic Projects Grant from the Natural Sciences and Engineering Research Council of Canada. I am so thankful for the financial support. I also would like to thank my colleagues in this project, Professor Martyn Unsworth, Professor Li zhen Chen, Juliane Hübert, Benjamin Lee, and Bahman Abbassi for assistance, suggestions, and discussion about the work involved in this project.

Amarc Resources Ltd. and Pacific Booker Minerals Inc. are thanked for providing access to drill cores of the Newton and Morrison properties, respectively. I am particularly thankful for the support of Diane Nicolson on the Newton deposit, and Ben Harding and Jean-Baptiste Tary are thanked for field assistance.

I would like to thank Martin von Dollen, Diane Caird, Andy DuFrane, Robert Dokken, and Robert Creaser for their help with sample preparation, XRD analysis, zircon U-Pb dating, and molybdenite Re-Os dating, respectively.

I also would like to thank my colleagues and friends, Rui Wang, Jinxiang Li, Fang An, Jingjing Zhu, Lin Chen, Amir Razavi, Juergen Lang, and Merilie Reyonlds for discussion on my thesis and words of encouragement.

Table of Contents

List of Tables

List of Figures

Chapter 1 Thesis Introduction

1.1 Introduction

Porphyry Cu ± Mo ± Au deposits have important economic significance, and provide 75% of the newly mined Cu, 50% of Mo, and 20% of Au in the world (Sillitoe, 2010). The Canadian Cordillera is a complex accretionary orogen, which hosts a large number of porphyry deposits (McMillan, 1995; Nelson and Colpron, 2007). Major porphyry deposits include the Bell porphyry Cu ± Mo ± Au, Endako porphyry Mo, Gibraltar porphyry Cu, Highland Valley porphyry Cu-Au, and Schaft Creek porphyry Cu-Mo-Au deposits (Bysouth et al., 1995; Casselman et al., 1995; Dirom et al., 1995; Taylor, 1995; Selby et al., 2000; Scott et al., 2008). Most porphyry deposits in the Canadian Cordillera were discovered before the 1970s, and few new discoveries have been made since that time. Any remaining undiscovered deposits are likely covered by younger rock sequences, or occur at depth beneath known deposits, which requires deep-penetrating methods for further exploration. In order to address these exploration challenges, this thesis was conducted within the framework of a large collaborative research project ("Mineral Exploration Under Deep Cover: Improving the Effectiveness of ZTEM Surveys for Porphyry Copper Exploration in the Canadian Cordillera"), with industry partners Amarc Resources Ltd., Geotech Ltd., Gerald G. Carlson, and John A. Chapman, through a Strategic Projects Grant from the Natural Sciences and Engineering Research Council of Canada.

The airborne Z-axis Tipper Electromagnetic survey (ZTEM) is a new electromagnetic method developed by Geotech Ltd. ZTEM measures natural electromagnetic signals in the frequency range of 30−720 Hz, and the relatively low frequency can allows penetration depths of up to 2km (Legault et al., 2009; Holtham and Oldenburg, 2010). Relative contrasts of conductivity are obtained by ZTEM rather than absolute conductivity (Oldenburg et al., 1997), which is helpful for locating targets such as disseminated sulfides with a conductivity contrast to the host rock in porphyry deposits. However, although deep penetration can be achieved in the vertical direction, the ZTEM technique is insensitive to layered (one-dimensional) conductivity structures (Holtham and Oldenburg, 2010), such that the vertical resolution is poor. Consequently, we have applied a combination of geological, magnetotelluric (MT), and magnetic studies to known deposits, in

order to confirm and calibrate ZTEM responses. This thesis provides some of the geological information used in that larger study. Case studies were conducted on the Newton epithermal Au and underlying porphyry system (previous described by McClenaghan, 2013), and the Morrison Cu-Au-Mo porphyry deposit, which are both located in the Stikinia terrane of central British Columbia. Though Newton is an epithermal deposit, it is thought to share similarities in physical properties related to rock units and alteration minerals found in porphyry deposits, and there is evidence for the presence of an underlying porphyry system at depth below the epithermal deposit.

This thesis focuses on the geological characteristics of the two selected deposits, and aims to determine the ore-forming history through petrologic, geochemical, geochronological, and fluid inclusion studies. Detailed geological characteristics, in terms of rock type, alteration, and mineralization are then used by our geophysics colleagues to characterize relevant petrophysical properties, and to reduce the uncertainty of ZTEM survey. The overall project outcomes will improve the effectiveness of ZTEM surveys for deep mineral exploration.

1.2 References

Bysouth, G.D., Campbell, K.V., Barker, G.E., and Gagnier, G.K., 1995, Tonalite-trondhjemite fractionation of peraluminous magma and the formation of syntectonic porphyry copper mineralization, Gibraltar mine, central British Columbia, in Schroeter, T.G., ed., Porphyry Deposits of the Northwestern Cordillera of North America: Canadian Institute of Mining, Metallurgy and Petroleum, Special Volume 46, p. 201-213.

Casselman, M.J., McMillan, W.J., and Newman, K.M., 1995, Highland valley porphyry copper deposits near Kamloops, British Columbia: A review and update with emphasis on the Valley deposit, in Schroeter, T.G., ed., Porphyry Deposits of the Northwestern Cordillera of North America: Canadian Institute of Mining, Metallurgy and Petroleum, Special Volume 46, p. 161-191.

Dirom, G.E., Dittrick, M.P., McArthur, D.R., Ogryzlo, P.L., Pardoe, A.J., and Stothart, 1995, Bell and Granisle porphyry copper-gold mines, Babine region, west-central British Columbia, in Schroeter, T.G., ed., Porphyry Deposits of the Northwestern Cordillera of North America:

Canadian Institute of Mining, Metallurgy and Petroleum, Special Volume 46, p. 256-289.

Holtham, E., and Oldenburg, D.W., 2010, Three-dimensional inversion of ZTEM data: Geophysical Journal International, v. 182, p. 168–182.

Legault, J.M., Kumar, H., Milicevic, B., and Wannamaker, P., 2009, ZTEM tipper AFMAG and 2D inversion results over an unconformity target in northern Saskatchewan: SEG Expanded Abstracts, v. 28, p. 1277-1281.

McClenaghan, L., 2013, Geology and Genesis of the Newton Bulk-Tonnage Gold-Silver Deposit, Central British Columbia: Unpublished M.Sc. thesis, Vancouver, British Columbia, University of British Columbia, 186 p.

McMillan, W.J., Thompson, J.F.H., Hart, C.J.R., and Johnston, S.T., 1995, Regional geological and tectonic setting of porphyry deposits in British Columbia and Yukon Territory, in Schroeter, T.G., eds., Porphyry deposits of the northwestern Cordillera of North America: Canadian Institute of Mining, Metallurgy and Petroleum, Special Volume 46, p. 40–57.

Nelson, J., and Colpron, M., 2007, Tectonics and metallogeny of the British Columbia, Yukon and Alaskan Cordillera, 1.8 Ga to the present, in Goodfellow, W.D., ed., Mineral Deposits of Canada: A Synthesis of Major Deposit-Types, District Metallogeny, the Evolution of Geological Provinces, and Exploration Methods: Geological Association of Canada, Mineral Deposits Division, Special Publication No. 5, p. 755–791.

Oldenburg, D., Li, Y., and Ellis, R., 1997, Inversion of geophysical data over a copper gold porphyry deposit: A case history for Mt Milligan: GEOPHYSICS, v. 62, p. 1419–1431.

Selby, D., Nesbitt, B.E., and Muehlenbachs, K., 2000, Hydrothermal alteration and fluid chemistry of the Endako Porphyry molybdenum deposit, British Columbia: Economic Geology, v. 95, p. 183-202.

Scott, J.E., Richards, J.P., Heaman, L.M., Creaser, R.A., and Salazar, G.S., 2008, The Schaft Creek porphyry Cu-Mo-(Au) deposit, Northwestern British Columbia: Exploration and Mining Geology, v. 17, p. 163-196.

Sillitoe, R.H., 2010, Porphyry copper systems: Economic Geology, v. 105, p. 3–41.

Taylor, H.K., 1995, Western Canadian porphyry deposits – economic perspectives, performances

and prospects, in Schroeter, T.G., ed., Porphyry Deposits of the Northwestern Cordillera of North America: Canadian Institute of Mining, Metallurgy and Petroleum, Special Volume 46, p. 20-39.

Chapter 2 Geochemistry, geochronology, and fluid inclusion study of the Newton epithermal gold deposit, British Columbia

2.1 Introduction

The Newton gold deposit is a significant new discovery in southern British Columbia. It is located roughly 110 km southwest of Williams Lake at 51°47'N and 123°36' W (Fig. 2-1). The disseminated Au mineralization in the Newton area is genetically and spatially associated with Late Cretaceous calc-alkaline felsic volcanic rocks and coeval intrusions (Bordet et al., 2011; McClenaghan, 2013).

Gold mineralization was first discovered by Mr. Newton in 1916 (Pressacco, 2012). The Newton property changed hands several times between 1972–2006, during which time 39 drill holes with a total length of 5762.2 m were completed by Cyprus (10 holes in 1972), Taseko (12 holes in 1982), Rea Gold (5 holes in 1992), and High Ridge (12 holes in 2006) (Pressacco, 2012).

The Newton gold deposit was acquired by Amarc Resources Ltd. in 2009, who completed 89 diamond drill holes with a total length of 27944.5 m between 2009 and 2012. The drilling programs conducted by Amarc successfully intersected Au mineralization, and delineated a new epithermal Au system (McClenaghan, 2013). A resource of 111.5 million tonnes with an average grade of 0.44 g/t Au (0.25 g/t Au cut-off) was reported by Pressacco (2012).

The Newton deposit has characteristics of both porphyry and epithermal deposits, and McClenaghan (2013) classified it as an intermediate sulfidation epithermal system. McClenaghan (2013) conducted a petrologic, geochemical, and geochronological study on the deposit. Here we present additional geochemical and geochronological (U-Pb) data, plus fluid inclusion data from the mineralized veins, in order to further characterize the deposit. This work has been conducted as part of a comprehensive study of the geology and geophysical signatures of porphyry-epithermal systems in British Columbia.

2.2 Tectonic History and Regional geology

The Newton gold deposit is located in the southern Stikinia terrane of the British Columbian Cordillera, and is related to Late Cretaceous volcanoplutonic rocks with continental arc affinity (McClenaghan, 2013).

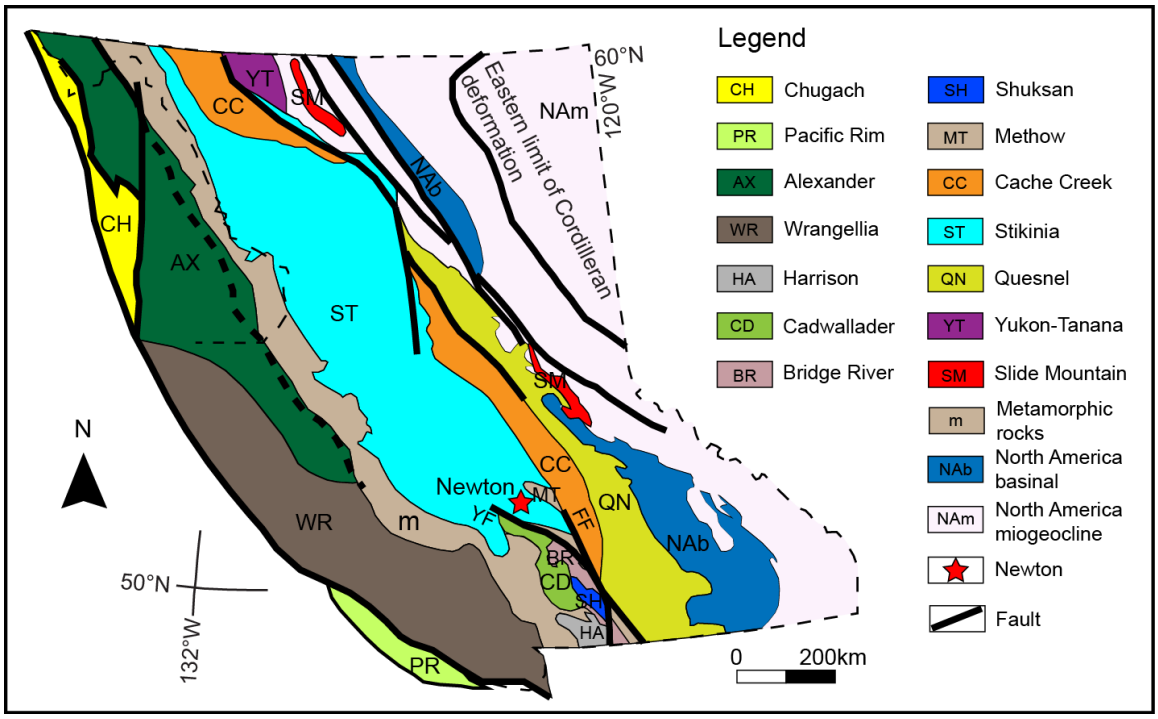

Fig. 2-1. Terrane map of the British Columbian Cordillera, showing the location of the Newton Au deposit in the southern Stikinia terrane. Fault abbreviations: FF-Fraser fault; YF-Yalakom fault. Modified from Nelson and Colpron (2007).

Tectonic history of the British Columbian Cordillera

The Cordillera of British Columbia is a complex amalgamation of the ancient North American passive continental margin, several island arcs, and an accretionary wedge, which has been overlain by later continental arc volcanosedimentary sequences and glacial tills (Nokleberg et al., 2000, 2005). The Cordillera can be divided into several terranes, including the Alexander, Wrangellia, Stikinia, Cache Creek, Quesnel, and Slide Mountain terranes, which abut the North America craton margin, from west to east (Wheeler et al., 1991; Colpron et al., 2006; Nelson and Colpron, 2007; Fig. 2-1). The Phanerozoic tectonic history of British Columbia can be divided into four stages: (1) a passive continental margin developed on the western edge of Laurentia during

the Late Cambrian to the Middle Devonian; (2) the passive continental margin changed to an active margin when the Panthalassa oceanic plate began to subduct beneath the Laurentian craton in the Middle Devonian; back-arc rifting formed island arcs offshore of the continental margin from the Middle Devonian to Early Jurassic; (3) several island arcs were accreted to the margin during the Middle Jurassic to Middle Cretaceous; (4) continental arc magmatism was widespread during the Late Cretaceous to Eocene, and the Newton deposit is genetically associated with this Late Cretaceous magmatism in the Stikinia terrane. Major displacements occurred along strike-slip faults during the Late Cretaceous to Cenozoic.

Stage 1: Neoproterozoic to Middle Devonian: Voluminous sedimentary rocks were deposited on the western margin of the North American continent (Monger and Price, 2002; Fig. 2-1). The sedimentary rocks mainly consist of thick deposits of continental platform carbonate (e.g., the Lower Cambrian Badshot Formation), which change westward into clastic sedimentary rocks (e.g., the lower Paleozoic Lardeau Group in southern British Columbia; Colpron and Price, 1995; Monger and Price, 2002; Nelson and Colpron, 2007).

Stage 2: Middle Devonian to Middle Jurassic: Subduction of the Panthalassa oceanic plate occurred in the Middle Devonian to the Middle Jurassic. A back-arc oceanic basin opened on the continental margin during the Late Devonian–Early Carboniferous, likely in response to slab rollback (Monger and Price, 2002). Fragments of this back-arc basin are thought to be represented by the Slide Mountain terrane, which contains thick mafic volcanic sequences of oceanic affinity (Harms, 1986; Roback, 1994). The Stikinia and Quesnel terranes are thought to represent island arcs formed offshore of the Laurentian margin during this period (Nokleberg et al., 2000; Nelson and Colpron, 2007). Several porphyry and epithermal deposits formed in these two island-arc terranes during the Late Triassic to Middle Jurassic (McMillan et al., 1995).

Stage 3: Middle Jurassic to Middle Cretaceous: The mid- to late Mesozoic tectonic evolution of the British Columbian Cordillera is dominated by terrane collision events. The mid-late Paleozoic back-arc basin is thought to have closed in the Middle Jurassic (Nelson and Colpron, 2007) by collision of the Stikinia, Quesnel, and Slide Mountain terranes with the western North American margin (Gabrielse, 1991). During these accretionary events, the Cache Creek

terrane, a fore-arc assemblage, was enclosed by the Stikinia and Quesnel terranes by counterclockwise rotation of the Stikinia arc (Nelson and Colpron, 2007). The Alexander terrane and Wrangellia terrane are allochthonous terranes, which collided with the margin during the Late Jurassic to Middle Cretaceous (Gabrielse and Yorath, 1991).

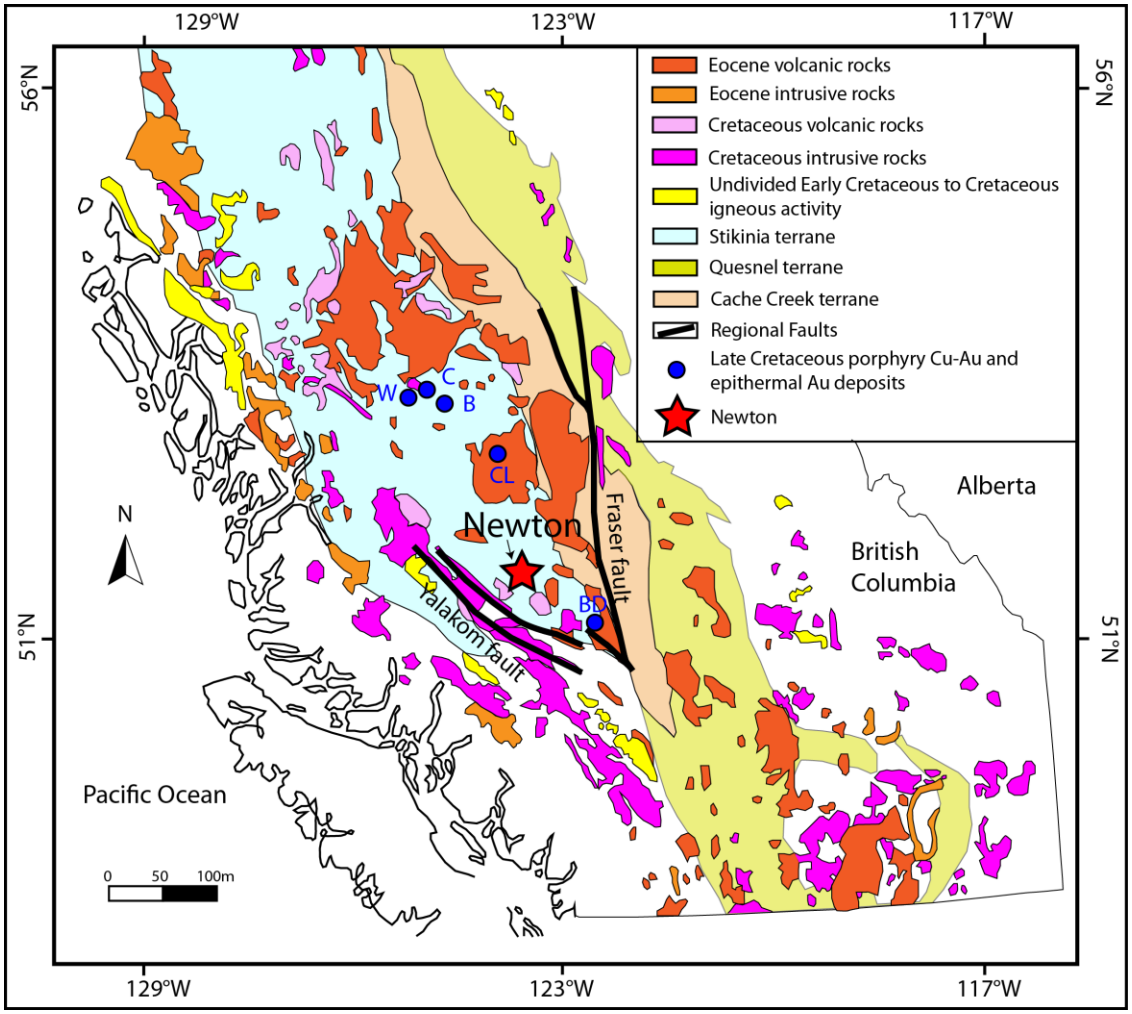

Fig. 2-2. Geological map of the British Columbia Cordillera, showing major terranes, Cretaceous to Eocene volcanic and intrusive rocks, regional faults, and Late Cretaceous-Eocene epithermal gold deposits in the Newton area. Epithermal deposit abbreviations: B-Blackwater; BD-Black Dome; C-Capoose; Cl-Clisbako; W-Wolf. Redrawn from Pressacco (2012).

Stage 4: Middle Cretaceous to Cenozoic: Oblique convergence between the Kula oceanic plate and North American plate led to compressional and transpressional stress regimes in British Columbia during the Middle Cretaceous–late Paleocene (Engebretson et al., 1985).

These compressional and transpressional stresses resulted in regional deformation, crustal thickening, and uplift (e.g., the Sevier and Laramide orogenies; Gillespie and Heller, 1995; English and Johnston, 2004). Major displacements occurred along several extensive strike-slip faults during this period, including the dextral Eocene Tintina, Fraser, and Yalakom faults (Gabrielse et al., 2006). Compression and transpression changed to extension and transtension in southern British Columbia in the Eocene (Parrish et al., 1988), probably in response to a change in obliquity of convergence of the Kula oceanic plate (Nokleberg et al., 2000). Continental arc magmatism continued throughout the Late Cretaceous-Eocene, and is related to a second episode of porphyry and epithermal deposit formation within the accreted terranes, such as the Bulkley intrusive suite (84–64 Ma) and associated porphyry deposits, such as Huckleberry, Whiting Creek, and Emerald Glacier (MacIntyre et al., 1994; Lepitre et al., 1998; McMillan et al., 1995; Riddell, 2011). Epithermal deposits include Newton, Blackwater, Capoose, Black Dome, Wolf, and Clisbako (Fig. 2-2; Nelson and Colpron, 2007; Mihalasky et al., 2011; Pressacco, 2012; McClenaghan, 2013). The Newton property is situated between two regional dextral strike-slip faults, the Yalakom fault to the west and the Fraser fault to the east, which were formed by Eocene crustal-scale transtension (Nelson and Colpron, 2007; Figs. 2-1, 2-2).

The motions between the Pacific and North American plates in this region alternated between convergence and extension in the Neogene (Engebretson et al., 1985; Stock and Molnar, 1988; Atwater, 1989; Edwards and Russell, 1999). Extensional periods caused incipient continental rifting in the western margin of northern North America. Consequently, Neogene to Quaternary alkaline bimodal volcanic rocks are widespread from northwestern British Columbia through the Yukon to eastern Alaska (Edwards and Russell, 1999, 2000). These volcanic rocks cover much of the older sequences, and hinder mineral exploration in many parts of the Cordillera.

Regional geologic setting of the Newton deposit

The Stikinia terrane, which hosts the Newton Au deposit, is mainly composed of four rock units in the Newton area: volcanic and sedimentary rocks of the Early Cretaceous Spences Bridge and Gambier Groups, the Paleogene Endako and Ootsa Lake Groups, the Mio-Pliocene

Chilcotin Group, and Jurassic to early Tertiary intrusive rocks (Fig. 2-3; Massey et al., 2005). The Early Cretaceous Spences Bridge Group consists of andesite and dacite flows and breccias, minor basalt and rhyolite, pyroclastic deposits, sandstone, siltstone, and mudstone (Massey et al., 2005). This unit is conformably overlain by the Early Cretaceous Gambier Group, which is mainly composed of mafic–intermediate–felsic volcanic, pyroclastic, and sedimentary rocks (Massey et al., 2005). Rhyolite from the Gambier Group yielded a U-Pb age of 112.0 ± 0.3 Ma (Lynch, 1995). The Paleogene Endako and Ootsa Lake Groups unconformably overlie the Gambier Group, and consist of mafic to felsic volcanic sequences, and minor sedimentary rocks (Massey et al., 2005).

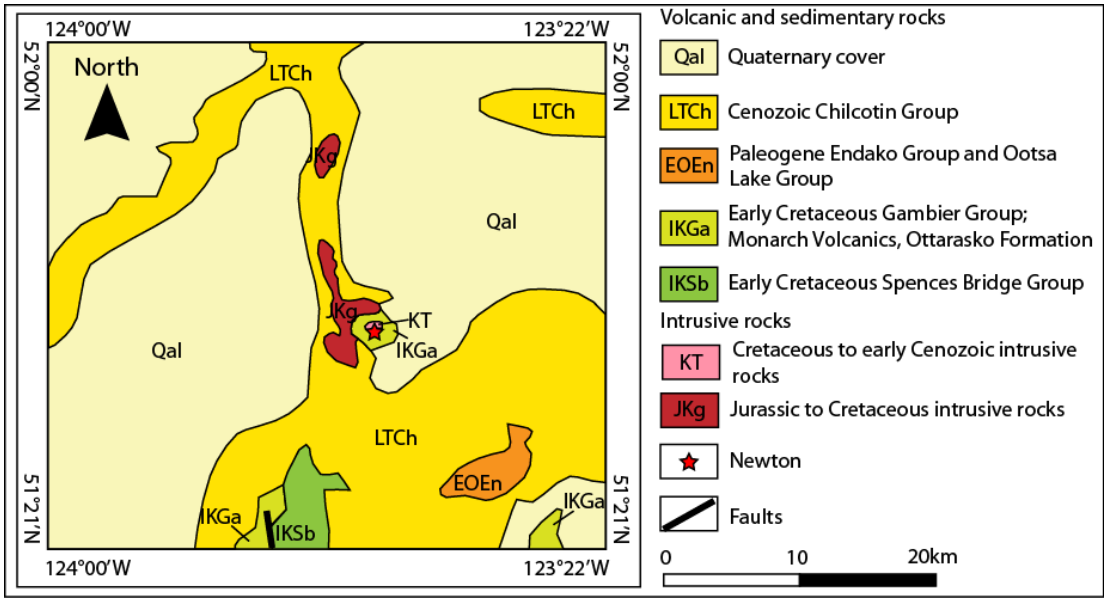

Fig. 2-3. Regional geological map of the Newton area and its surroundings. Modified from Massey et al. (2005).

These sequences are intruded by a wide variety of Jurassic to early Cenozoic dikes and stocks in the Newton area, including felsic porphyry dikes, quartz monzonite, feldspar-quartz-hornblende porphyry, and diorite stocks (McLaren and Rouse, 1989). These rocks are unconformably overlain by the Miocene-Pliocene Chilcotin Group, which mainly consists of basaltic lava flows (Bevier, 1983a, b).

2.3 Newton Deposit Geology

Thick Quaternary glacial till covers most of the Newton property, and outcrop is sparse. Consequently, geological information has primarily been obtained from drill core. Six main lithological units occur on the property: layered mafic volcanic rocks, sedimentary rocks, and felsic volcanic rocks (from the bottom up), which are intruded by quartz-feldspar porphyry, feldspar-quartz-hornblende porphyry, and diorite intrusions (Riddell, 2006; Pressacco, 2012). The quartz-feldspar porphyry and feldspar-quartz-hornblende porphyry bodies mainly occur in the center of the Newton deposit, whereas diorite occurs as a large unmineralized intrusion in the northwest corner of the property, and as minor dikes intruding the central quartz-feldspar porphyry and feldspar-quartz-hornblende porphyry (Fig. 2-4).

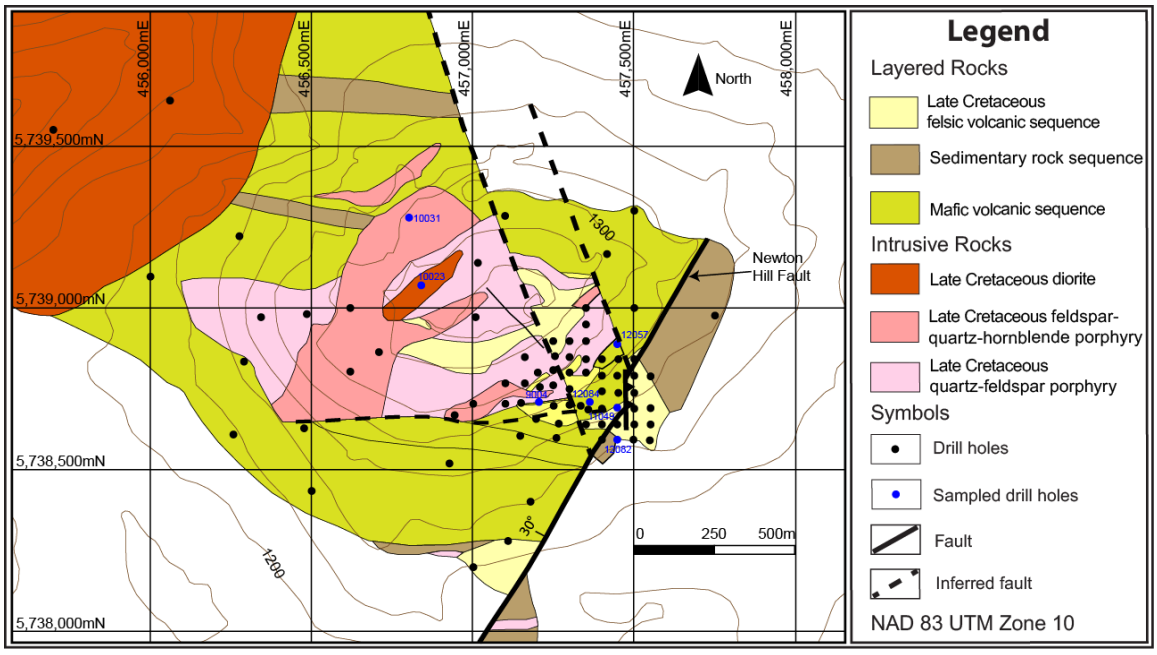

Fig. 2-4. Geological map of the Newton property. Modified from McClenaghan (2013).

The mafic volcanic rocks and sedimentary rocks at Newton have not been dated, but based on regional geological maps (Fig. 2-3), these rocks are thought to be part of the Lower Cretaceous Gambier Group, which includes similar lithologies. The felsic volcanic rocks and quartz-feldspar porphyry have been dated by zircon U-Pb analysis, and yielded ages of 72.1 ± 0.6 Ma and 70.9 ± 0.5 Ma respectively (unpublished data, Amarc Resources Ltd., reported in

McClenaghan, 2013). Gold mineralization at Newton is closely related to these Late Cretaceous felsic volcanic rocks, as well as the quartz-feldspar porphyry and feldspar-quartz-hornblende porphyry intrusions (see below).

McClenaghan (2013) found that the felsic volcanic rocks and quartz-feldspar porphyry had calc-alkaline affinity and were rhyolitic in composition. McClenaghan (2013) also reported a Re-Os molybdenite date of 72.1 ± 0.3 Ma from a porphyry-hosted quartz-calcite-pyrite-molybdenite vein. Oxygen isotopic compositions ($\delta^{18}O$) of 8.4 to 9.5‰ and hydrogen isotopic compositions (δD) of -83.0 to -66.5‰ were also reported for sericite associated with auriferous pyrite and marcasite, and the calculated $\delta^{18}O_{fluid}$ and δD_{fluid} compositions range from 2.5‰ to 6.8‰, and -63 to -46.5‰, respectively (McClenaghan, 2013). Sulfur isotopic compositions ($\delta^{34}S$) of disseminated pyrite, marcasite, and chalcopyrite range from -1.1 to 3.2‰ (McClenaghan, 2013). McClenaghan (2013) interpreted these data to indicate a magmatic source for fluids and sulfur, and therefore likely metals, in the Newton deposit.

Intrusive breccias

Intrusive breccias locally cut the felsic tuff and porphyry intrusions. They consist of subangular to subrounded fragments of felsic tuff, quartz-feldspar porphyry, and feldspar-quartz-hornblende porphyry in a rhyolitic matrix (McClenaghan, 2013). Pressacco (2012) noted that gold mineralization is locally present in the quartz-sericite altered breccias, but the grade of Au in the breccias is not reported.

Mafic volcanic rocks

Mafic volcanic rocks mainly occur in the central part of the Newton deposit, and are thought to correlate with the Lower Cretaceous Gambier Group. This unit is basaltic to andesitic in composition, dark green to dark brown in color, massive in texture, and over 300 m thick on the property (Pressacco, 2012). The rocks are mainly composed of volcaniclastic units, lava flows, and volcanic tuff (Fig. 2-5A), which are epidote-chlorite-altered to varying degrees.

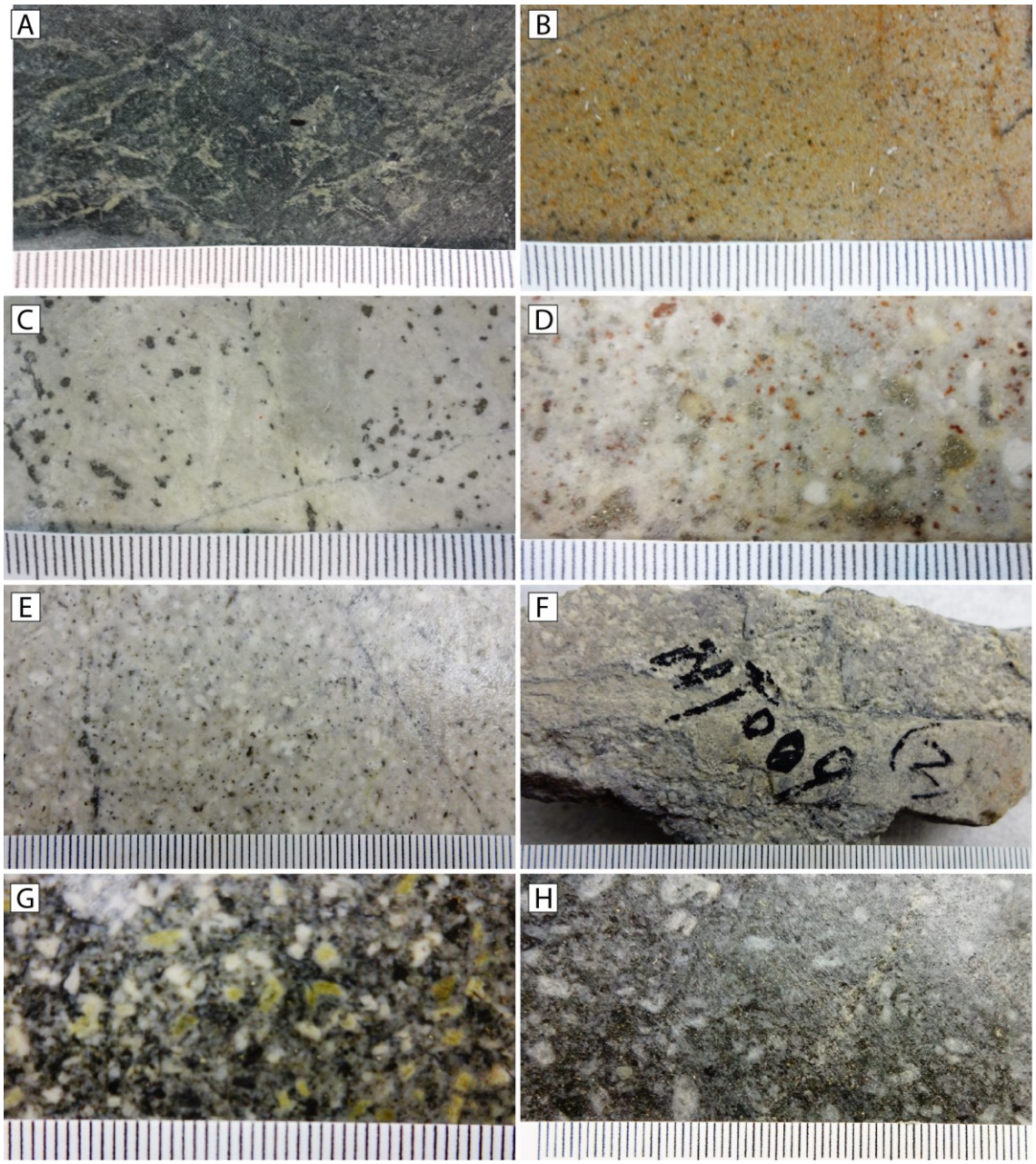

Fig. 2-5. Hand specimens of the main lithological units in the Newton deposit: (A) weak propylitic altered mafic volcanic rock (NT083); (B) weakly propylitic-altered sandstone (NT078); (C) quartz-sericite-altered felsic tuff with disseminated pyrite (NT014); (D) quartz-sericite-altered quartz-feldspar porphyry with disseminated pyrite and a quartz veinlet (NT011); (E) quartz-sericite-altered feldspar-quartz-hornblende porphyry with disseminated marcasite (NT007); (F) kaolinite-altered feldspar-quartz-hornblende porphyry (NT009); (G) chlorite-epidote-altered diorite (NT067); (H) biotite-altered diorite (NT089). The scale divisions are in millimeters.

Sedimentary rocks

Cretaceous sedimentary rocks are primarily located in the eastern part of the Newton property (Fig. 2-4). The unit mainly consists of conglomerates, mudstones, and sandstones (Fig. 2-5B). Contacts between these sedimentary rocks and the mafic volcanic rocks are mostly faulted so their stratigraphic relationship is not clear. However, the presence of some mafic volcanic clasts in the conglomerates suggests that these sediments overlie the mafic volcanic sequences (McClenaghan, 2013).

Felsic volcanic rocks

Felsic volcanic rocks are mainly located in the central and eastern part of the Newton property, and consist dominantly of felsic tuff (Fig. 2-5C) with minor felsic volcaniclastic rocks. The felsic volcanic rocks overlie the sedimentary rocks, and unconformable contacts are observed in drill cores (McClenaghan, 2013). The felsic volcanic rocks are rhyolitic in composition, white to grey in color, and banded to massive in texture. Most felsic volcanic rocks have undergone strong quartz-sericite alteration, and are the primary host rocks for Au mineralization at Newton.

Intrusive rocks

Quartz-feldspar porphyry: The quartz-feldspar porphyry is observed to intrude the sedimentary and felsic volcanic rocks in drill core. It is granitic in composition, and consists of 10–15 vol.% quartz phenocrysts (1–5 mm) and 5–15 vol.% plagioclase phenocrysts (2–5 mm) within a matrix of fine-grained sericite and quartz (<0.05 mm) (Fig. 2-5D). The porphyry has undergone strong quartz-sericite alteration associated with Au mineralization, and most plagioclase phenocrysts have been replaced by fine-grained sericite.

Feldspar-quartz-hornblende porphyry: The feldspar-quartz-hornblende porphyry is observed to intrude the sedimentary and felsic volcanic rocks, but no cross-cutting relationships were seen with the quartz-feldspar porphyry. However, cross sections drawn by McClenaghan (2013) show the feldspar-quartz-hornblende porphyry cross-cutting all the sedimentary and volcanic sequences, as well as the quartz-feldspar porphyry. The feldspar-quartz-hornblende

porphyry is composed of 20–30 vol.% plagioclase phenocrysts (1–3 mm), 10 vol.% quartz phenocrysts (0.5–2 mm), and 5 vol.% hornblende phenocrysts (1–3 mm) set in a fine-grained quartz-feldspar matrix. Like the quartz-feldspar porphyry, the feldspar-quartz-hornblende porphyry has undergone strong sericite alteration associated with gold mineralization, and sericite has replaced most of the plagioclase phenocrysts (Fig. 2-5E).

Diorite: Diorite occurs as a large (>1 km diameter) intrusion to the northwest of the main mineralized zone, and as dikes that cut through the mineralized quartz-feldspar porphyry and feldspar-quartz-hornblende porphyry in the center of the deposit, indicating that it post-dates the main mineralization event. The diorite has experienced propylitic alteration, potassic alteration, and sericite alteration to varying degrees, but this alteration is not associated with mineralization. Relatively fresh diorite (Fig. 2-5G, H) consists of 30–40 vol.% plagioclase phenocrysts (3–5 mm), 15–20 vol.% hornblende phenocrysts (1–5 mm), and 5 vol.% biotite phenocrysts (1–3 mm) in a fine-grained quartz-plagioclase-hornblende matrix. This unit is weakly to strongly magnetic.

Structural setting

Several faults have been identified or inferred on the Newton property, and most appear to post-date mineralization. The Newton Hill Fault is the most significant, and cuts through the main mineralized zone in the eastern part of the property (Fig. 2-4). The hanging wall and footwall of the Newton Hill Fault both contain mineralized felsic volcanic rocks, quartz-feldspar porphyry, and feldspar-quartz-hornblende porphyry. The Newton Hill Fault strikes approximately 027° and dips at ~30° to the northwest, and displays 300–350 m of dip-slip displacement (Pressacco, 2012).

2.4 Alteration and Mineralization

Quartz-sericite, argillic, propylitic, and potassic alteration occur at Newton. Quartz-sericite alteration is widespread in the centre of the property, and is closely associated with gold and base metal mineralization.

Quartz-sericite alteration

Quartz-sericite alteration commonly occurs in the felsic volcanic rocks, quartz-feldspar porphyry, and feldspar-quartz-hornblende porphyry (Fig. 2-6). It is characterized by secondary quartz and sericite, which replaces volcanic glass shards, volcanic fragments, and plagioclase, and infills small fractures. The quartz-sericite alteration is most strongly developed in the felsic volcanic rocks, whereas it is relatively weak in the quartz-feldspar porphyry and feldspar-quartz-hornblende porphyry (McClenaghan, 2013). This may reflect the higher permeability and reactivity (fine-grained, possibly originally glassy groundmass) of the felsic volcanic rocks compared with the quartz-feldspar porphyry and feldspar-quartz-hornblende porphyry (McClenaghan, 2013). This alteration style is only locally present in the diorite (Fig. 2-7A, B).

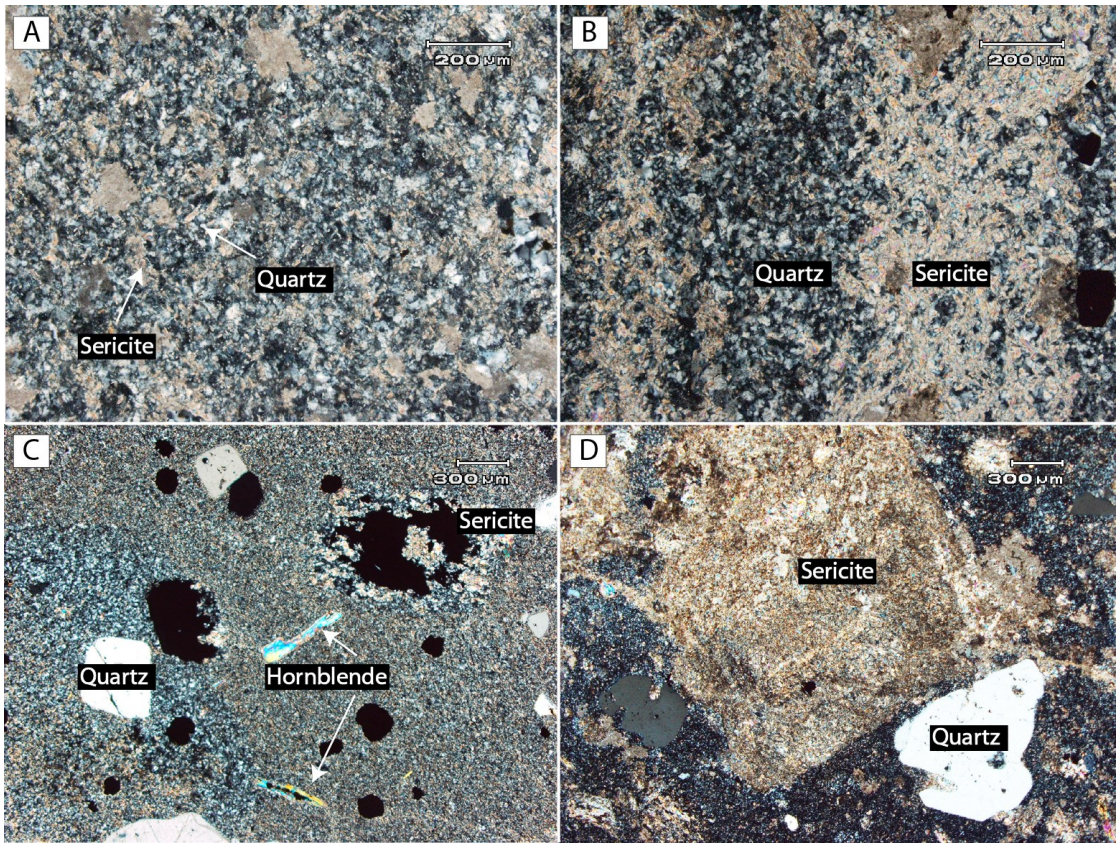

Fig. 2-6. Quartz-sericite alteration in the Newton volcanic and intrusive rocks (taken in cross-polarized light): (A) altered felsic volcanic rocks (NT014); (B) altered felsic flow with banded texture (NT002); (C) altered feldspar-quartz-hornblende porphyry (NT038); (D) altered quartz-feldspar porphyry (NT052).

The quartz-sericite alteration can be divided into two stages:

1. The first stage predominantly consists of quartz, sericite, and pyrite (Fig. 2-5C, D), and is the main alteration style associated with gold mineralization.
2. The second stage is similar but contains more marcasite than pyrite (Fig. 2-5E). This stage is related to relatively high concentrations of base metals, but with lower Au contents.

Argillic alteration

Argillic alteration is not extensively developed at Newton, and was only observed locally in the quartz-feldspar porphyry and feldspar-quartz-hornblende porphyry where it overprints the quartz-sericite alteration (Fig. 2-5F). It is characterized by kaolinite, sericite (relict from the earlier alteration), and carbonates (McClenaghan, 2013), which partially or completely replace plagioclase phenocrysts. This alteration style is also associated with disseminated pyrite and gold. However, it is not clear whether the Au was introduced during the argillic alteration, or is residual from the earlier quartz-sericite alteration.

Propylitic alteration

Propylitic alteration is characterized by secondary epidote, chlorite, and carbonate (Fig. 2-5A, G). Epidote and chlorite are dominant and pervasive, whereas calcite typically occurs in veinlets. This alteration is widespread but variably developed in the mafic volcanic rocks, and is locally present in the diorite (Fig. 2-7C). It does not appear to be associated with gold and base metal mineralization.

Potassic alteration

The least common alteration type at Newton is potassic alteration, which is characterized by the local development of secondary fine-grained biotite in diorite at its contacts with mafic volcanic rocks (Fig. 2-7D; Pressacco, 2012). Locally, the potassic alteration is overprinted by

sericite, and propylitic alteration commonly overprints both potassic and sericitic alteration within the diorite (Fig. 2-5). The potassic alteration is accompanied by pyrite, but is not associated with elevated levels of gold or base metals.

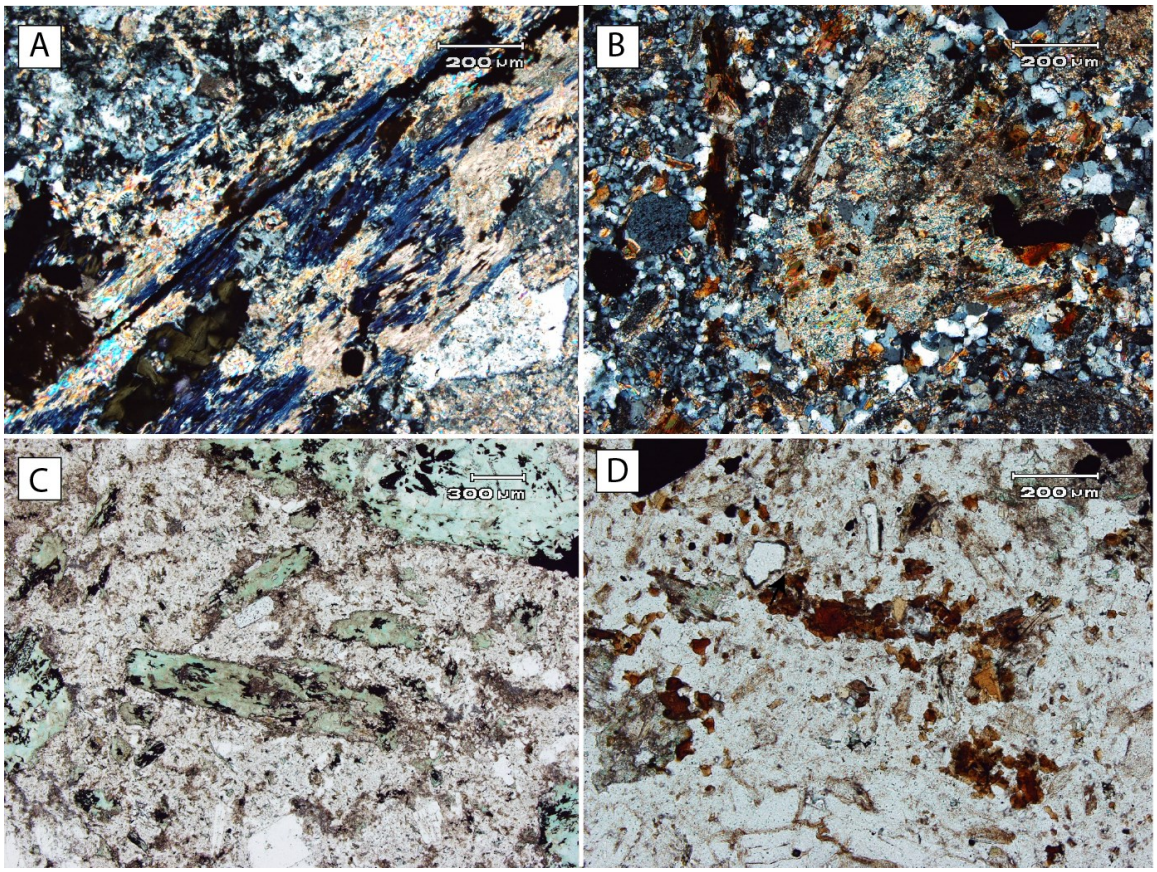

Fig. 2-7. Alteration in diorite (A and B taken in cross-polarized light; C and D in cross-polarized light): (A) sericite alteration overprinted by later chlorite alteration (NT067); (B) sericite alteration overprinting potassic alteration; plagioclase phenocrysts are replaced by secondary sericite (NT091); (C) propylitic alteration: hornblende phenocrysts are replaced by chlorite (NT135); (D) potassic alteration with secondary biotite (NT091).

Mineralization

Ore minerals at Newton mainly consist of electrum, gold-silver tellurides, and base metal sulfides (pyrite, marcasite, chalcopyrite, sphalerite, pyrrhotite, molybdenite, and arsenopyrite; McClenaghan, 2013). The gold-bearing minerals mainly occur as inclusions in these sulfides, especially pyrite and marcasite (Pressacco, 2012). Disseminated mineralization is the

predominant style; veinlet mineralization is also present, but it accounts for less than 1 vol.% of the mineralized rocks (Pressacco, 2012).

Three stages of mineralization have been recognized based on observations of hand samples and petrographic study (Fig. 2-8).

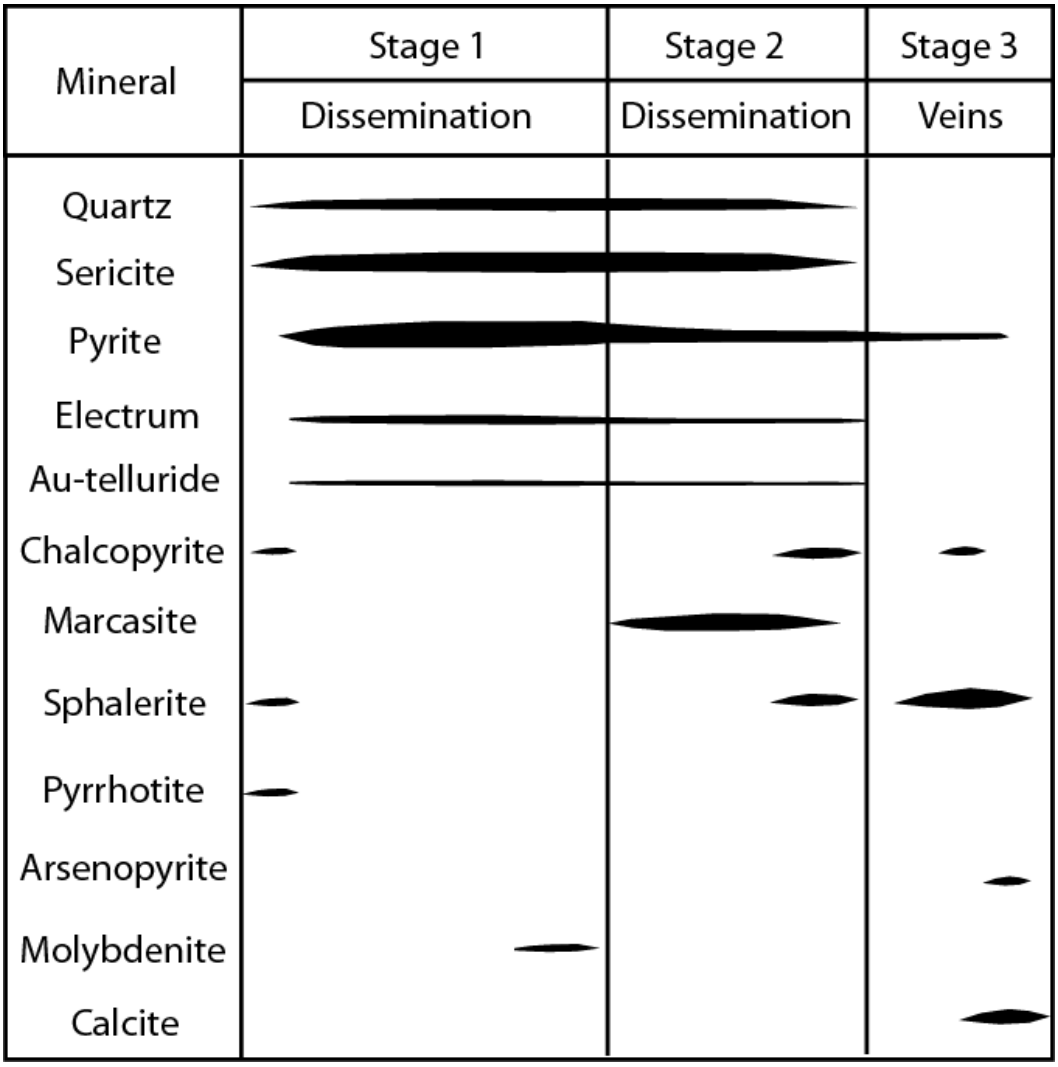

Fig. 2-8. Vein and alteration paragenesis based on hand sample observations and petrographic studies.

1. The earliest stage of Au mineralization is associated with quartz-sericite-pyrite wallrock alteration. The dominant sulfide is disseminated pyrite, which is accompanied by minor chalcopyrite, pyrrhotite, and sphalerite, commonly as small inclusion in pyrite (Fig. 2-9A).

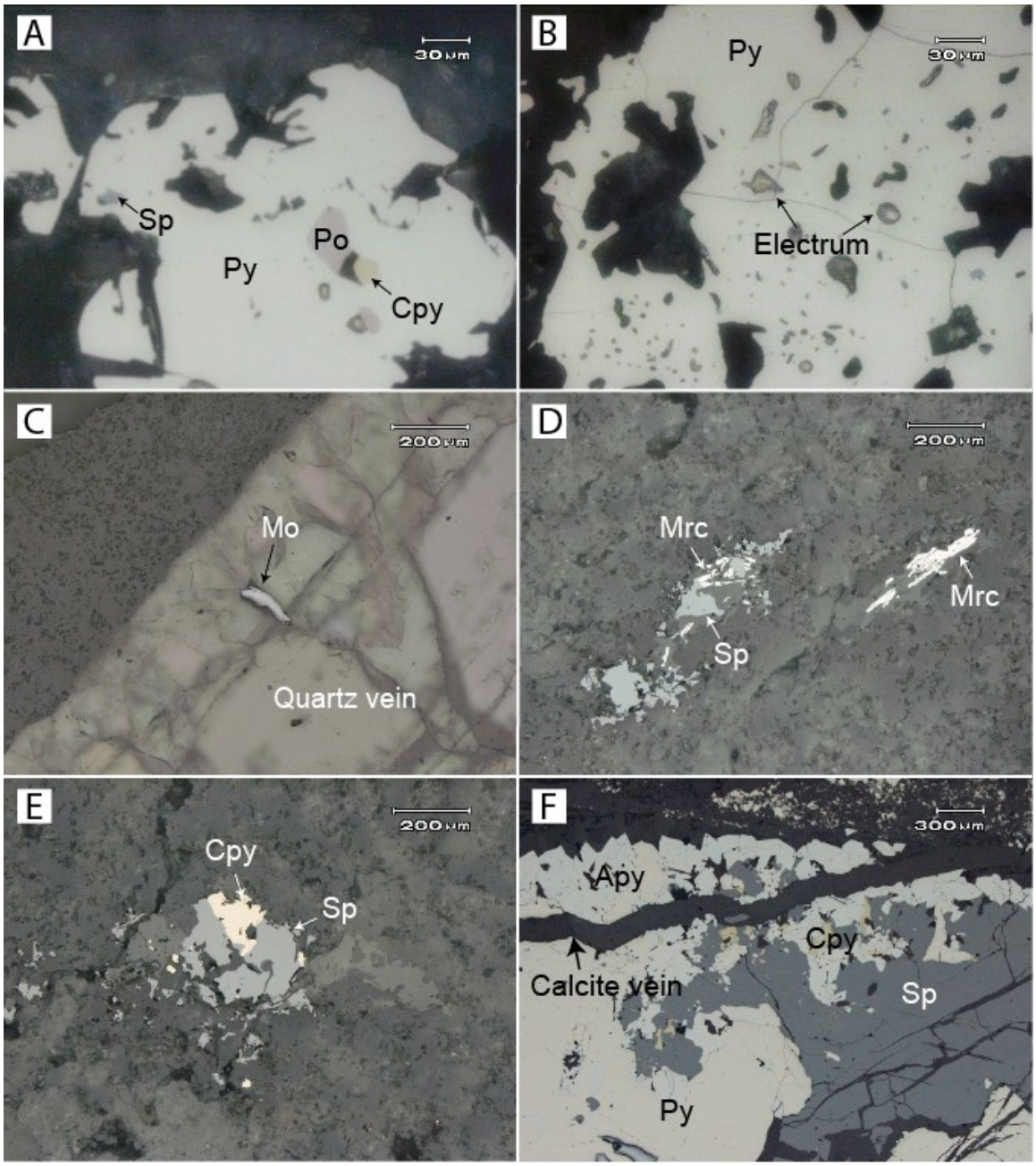

Fig. 2-9. Paragenetic relationships between sulfide minerals (photomicrographs taken in reflected light, except core sample in C): (A) chalcopyrite, sphalerite, and pyrrhotite inclusions in pyrite (quartz-feldspar porphyry; NT011; stage 1 mineralization); (B) electrum inclusions in pyrite (quartz-feldspar porphyry; NT011; stage 1 mineralization); (C) quartz-molybdenite-pyrite vein hosted by quartz-sericite-pyrite-altered felsic volcanic rock (NT060; stage 1 mineralization;); (D) minor sphalerite intergrown marcasite in felsic volcanic rock (NT028; stage 2 mineralization); (E) chalcopyrite intergrown with sphalerite in felsic volcanic rock (NT028; stage 2 mineralization); (F) polymetallic vein: pyrite, arsenopyrite, chalcopyrite, and sphalerite form a layered sequence in the vein, which is cross-cut by a late calcite vein (felsic volcanic host rock; NT062; stage 3 mineralization). Abbreviations: Cpy = chalcopyrite, Mo = molybdenite, Mrc = marcasite, Po = pyrrhotite, Py = pyrite, Sp = sphalerite.

Gold mainly occurs as inclusions of electrum, silver-gold telluride, and gold-bismuth telluride in the pyrite based on description of Pressacco (2012). However, only electrum was observed in this study (Fig. 2-9B). Veins are not common, but where present consist of pyrite veins (Fig. 2-10A), quartz-pyrite veins (Fig. 2-10B), and quartz-molybdenite-pyrite veins (Fig. 2-9C), which are relatively straight and 1–3 mm in width.

2. Stage 2 mineralization is associated with the later quartz-sericite-marcasite alteration. Disseminated marcasite, minor pyrite, chalcopyrite, and sphalerite occur in the felsic volcanic and intrusive rocks (Fig. 2-9D, E; McClenaghan, 2013). Base metal-sulfides are more abundant than in stage 1 (McClenaghan, 2013). Although disseminated mineralization is dominant, minor marcasite veinlets also occur in quartz-sericite-marcasite-altered rocks (Fig. 2-10C). These veinlets are relatively straight, and usually 1–2 mm in width. Pressacco (2012) noted that Au occurs as electrum inclusions in marcasite, but this was not observed in this study.
3. Polymetallic veins occur locally in the sedimentary and felsic volcanic rocks, but are not common. They represent the last stage of mineralization, and cross-cut the disseminated quartz-sericite-pyrite/marcasite mineralization (Fig. 2-10D). Pyrite, chalcopyrite, sphalerite, and arsenopyrite are primary constituents of these veins, commonly with calcite (Figs. 2-9F, 2-10 D). These veins are 1–10 mm in width, and are commonly straight but with various orientations; they lack alteration selvedges. No gold has been reported in these veins.

Molybdenite from a stage 1 quartz-calcite-pyrite-molybdenite vein in the feldspar-quartz-hornblende porphyry has been dated at 72.1 ± 0.3 Ma (McClenaghan, 2013), indicating that the mineralization occurred broadly at the same time as magmatism.

The Newton deposit was interpreted by McClenaghan (2013) to be an intermediate-sulfidation epithermal deposit based on the classifications of Hedenquist et al. (2000) and Sillitoe and Hedenquist (2003). McClenaghan (2013) noted that Newton matches these descriptions in

the following ways: rhyolitic host rocks, primary quartz-sericite alteration, Au and Ag mineralization, and relatively abundant base-metal sulfides (pyrite, marcasite, sphalerite, and galena).

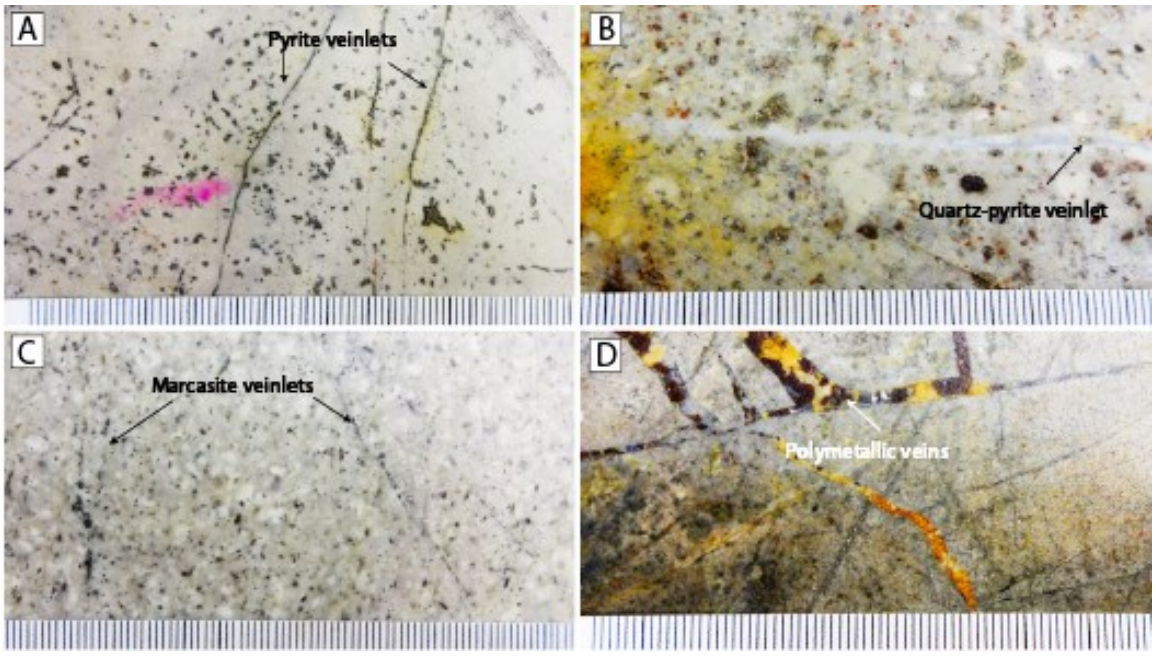

Fig. 2-10. Hand specimens of the main mineralized units in the Newton deposit: (A) quartz-sericite-altered felsic tuff with disseminated pyrite, and pyrite veinlets (NT058); (B) quartz-sericite-altered quartz-feldspar porphyry with a quartz-pyrite veinlet (NT011); (C) quartz-sericite-altered feldspar-quartz-hornblende porphyry with disseminated marcasite and marcasite veinlets (NT007); (D) sandstone cut by polymetallic veins containing sphalerite, chalcopyrite, arsenopyrite, and carbonate. The carbonate on the surface is oxidized to an orange color (NT110).

2.5 Analytical methods

Sample selection

Twenty-eight drill core samples were collected for this study, which are representative of the country rocks, intrusions, alteration facies, and mineralization styles at Newton. Detailed information on these samples is listed in Table 2-1, and sampled drill holes are marked on the geological map in Figure 2-4. All the drill holes in the Table 2-1 are vertical. Fifteen polished thin sections were made for petrographic study, and 5 fluid inclusion sections were made from quartz-sulfide and carbonate-sphalerite veins for fluid inclusion study.

Table 2-1 Sample information from Newton

Sample ID	BH ID	East	North	Elevation (m)	Depth (m)	Samples Interval (m)		Length	Lithology	Alteration
NT002	12084	457350	5738705	1290	651.36	484.00	484.15	0.15	Felsic volcanic rock	Quartz-sericite alteration
NT007	12084	457350	5738705	1290	651.36	613.80	614.02	0.22	Feldspar-quartz-hornblende porphyry	Quartz-sericite alteration
NT009-2	12084	457350	5738705	1290	651.36	634.43	634.53	0.10	Feldspar-quartz-hornblende porphyry	Argillic alteration
NT011	12084	457350	5738705	1290	651.36	176.10	176.40	0.30	Quartz-feldspar porphyry	Quartz-sericite alteration
NT014	12084	457350	5738705	1290	651.36	260.76	260.86	0.10	Felsic volcanic rock	Quartz-sericite alteration
NT028	11049	457449	5738689	1271	511.15	279.60	279.75	0.15	Felsic volcanic rock	Quartz-sericite alteration
NT038	12084	457350	5738705	1290	651.36	104.30	104.40	0.10	Feldspar-quartz-hornblende porphyry	Quartz-sericite alteration
NT047	9004	457203	5738705	1297	350.00	251.30	251.40	0.10	Feldspar-quartz-hornblende porphyry	Quartz-sericite alteration
NT049	9004	457203	5738705	1297	350.00	269.60	269.70	0.10	Quart-feldspar porphyry with a quartz-pyrite-gold vein	Quartz-sericite alteration
NT052	9004	457203	5738705	1297	350.00	304.60	304.70	0.10	Quart-feldspar porphyry	Quartz-sericite alteration
NT056	11037	455697	5739556	1128	181.36	123.94	124.04	0.10	Diorite	Weak potassic alteration
NT058	12057	457447	5738839	1290	348.69	160.20	160.30	0.10	Felsic volcanic rock	Quartz-sericite alteration
NT059	12057	457447	5738839	1290	348.69	180.50	180.60	0.10	Feldspar-quartz-hornblende porphyry	Quartz-sericite alteration
NT060	12057	457447	5738839	1290	348.69	200.00	200.03	0.03	Felsic volcanic rock with a quartz-molybdenite-pyrite vein	Quartz-sericite alteration
NT062	12057	457447	5738839	1290	348.69	292.19	292.29	0.10	Felsic volcanic rocks with a polymetallic vein	Quartz-sericite alteration
NT066	12057	457447	5738839	1290	348.69	338.50	338.65	0.15	Diorite	Weak propylitic alteration

NT067	12057	457447	5738839	1290	348.69	341.94	342.04	0.10	Diorite	Propylitic alteration; sericite alteration locally overprint propylitic alteration
NT078	12082	457450	5738590	1248	405.64	261.50	261.65	0.15	Sandstone	Weak propylitic alteration
NT083	12084	457350	5738705	1290	651.36	56.20	56.34	0.14	Mafic volcanic rock	Weak propylitic alteration
NT089	10023	456841	5739070	1331	309.98	145.85	145.95	0.10	Diorite	Weak potassic alteration
NT090	10023	456841	5739070	1331	309.98	146.35	146.55	0.20	Diorite	Weak potassic alteration
NT091	10023	456841	5739070	1331	309.98	148.80	149.10	0.30	Diorite	Potassic alteration; sericite alteration locally overprint potassic alteration
NT097	10023	456841	5739070	1331	309.98	279.00	279.50	0.50	Feldspar-quartz-hornblende porphyry	Quartz-sericite alteration
NT110	10030	457106	5739277	1329	337.41	196.40	196.50	0.10	Sedimentary rocks with polymetallic veins	Weak propylitic alteration
NT129	10031	456802	5739280	1304	416.66	327.30	328.00	0.70	Feldspar-quartz-hornblende porphyry	Quartz-sericite alteration
NT134	9004	457203	5738705	1297	350.00	296.30	296.50	0.20	Diorite	Weak propylitic alteration
NT135	9004	457203	5738705	1297	350.00	299.30	299.45	0.15	Diorite	Propylitic alteration
NT137	11037	455697	5739556	1128	181.36	105.90	106.58	0.68	Diorite	Weak propylitic alteration

*UTM grid zone: 10; UTM datum: NAD 83

Lithogeochemical analysis

Five feldspar-quartz-hornblende porphyry and 5 diorite samples were collected for whole-rock geochemical analysis. Lithogeochemical analyses were conducted at Activation Laboratories Ltd. (Ancaster, Ontario, Canada) using a combination of methods including instrumental neutron activation analysis and fusion inductively coupled plasma mass spectrometry (Actlabs code 4E Research + ICP/MS). Based on reproducibility of standards and duplicates, accuracy is typically within 5 relative % for major elements, and 10 relative % for minor and trace elements.

Zircon U-Pb dating

Zircons were separated from two samples of drill core with lengths of 1–2 m by crushing, Wilfley table heavy mineral separation, magnetic separation, heavy-liquid separation, and handpicking. Selected zircons were mounted in epoxy, and polished to expose their cores. The zircons were analyzed using a Nu-Plasma multiple collector inductively coupled plasma-mass spectrometer (MC-ICP-MS; Nu Instruments, UK) coupled to a frequency quintupled (λ = 213 nm) Nd:YAG laser ablation system (New Wave Research, USA) in the Radiogenic Isotope Facility at the University of Alberta. Details of the analytical setup and protocols employed are described in Simonetti et al. (2005). Laser pit dimensions were 30 μm diameter and approximately 20–30 μm deep. A 30 s blank analysis prior to ablation was made for determination of ^{204}Hg contributions, and was followed by 30 s ablations on samples. Zircon reference materials GJ1-32 and LH94-15 were used to correct instrumental bias, drift, and laser induced U-Pb fractionation. Standards were analyzed after every 10 unknowns, and the 2σ reproducibility of the standards was ~3% for U/Pb and 1% for ^{207}Pb/^{206}Pb. Reported errors are a quadratic combination of the within run precision and the external reproducibility of the standards. All U-Pb plots were generated using the Isoplot software (Ludwig, 2003), and concordia intercept ages were derived by anchoring to a common Pb value of 0.83 ± 0.06 (Stacey and Kramers, 1975).

Fluid inclusion measurements

Fluid inclusion analyses were conducted using a Linkham THMSG600 microthermometric stage mounted on an Olympus BX50 microscope. Fluid inclusions were cooled to -100°C, and then final ice melting temperatures, clathrate melting temperatures, and total homogenization temperatures were recorded during reheating. The salinities of aqueous, CO_2 clathrate-bearing, and halite-bearing inclusions were calculated using final ice melting, final CO_2 clathrate melting, and halite dissolution temperatures, based on the equations of Bodnar (1993), Bozzo et al. (1975), and Sterner et al. (1988), respectively. Bozzo et al. (1975) noted that their equation strictly applied only to fluid inclusions that contained liquid CO_2 at the point of clathrate melting, but Diamond (1992) noted that presence or absence of a CO_2 liquid phase actually had little effect on salinity calculations. Liquid CO_2 was not observed in our fluid inclusions, but on the basis of Diamond's (1992) findings, we have used Bozzo et al.'s (1975) equation for salinity estimation. Synthetic fluid inclusion standards from Syn Flinc were used for calibration. Reported measurements are accurate to ±0.2°C below 10°C, and ±2°C above 10°C.

2.6 Geochemistry

Ten new whole-rock geochemical analyses of feldspar-quartz-hornblende porphyry and diorite are listed in Table 2-2. These analyses are combined with 21 analyses of felsic volcanic rocks and quartz-feldspar porphyry reported by McClenaghan (2013) to assess the compositional range and geochemical affinity of the Newton igneous suite. All of the samples show some degree of alteration, but selected samples showed the least alteration of available material.

Major element compositions and lithological classification

Major element data for igneous rock samples from the Newton deposit were recalculated on a volatile-free basis, and plotted on a total alkali–silica classification diagram (Fig. 2-11). The least-altered feldspar-quartz-hornblende porphyry samples plot in the fields of granodiorite and granite, and the quartz-feldspar porphyry samples plot in the granite field. McClenaghan identified two samples of felsic volcanic rock and quartz-feldspar porphyry as "least altered", but all other samples show moderate to strong degrees of alteration (mostly phyllic). Because all of the

Table 2-2 Major and trace element analysis of igneous rock samples from Newton

Sample ID	NT038	NT047	NT056	NT059	NT066	NT090	NT097	NT129	NT134	NT137
Rock-type	Feldspar-quartz-hornblende porphyry	Feldspar-quartz-hornblende porphyry	Diorite	Feldspar-quartz-hornblende porphyry	Diorite	Diorite	Feldspar-quartz-hornblende porphyry	Feldspar-quartz-hornblende porphyry	Diorite	Diorite
Alteration	Quartz-sericite alteration	Quartz-sericite alteration	Weak potassic alteration	Quartz-sericite alteration	Weak propylitic alteration	Weak potassic alteration	Quartz-sericite alteration	Quartz-sericite alteration	Weak propylitic alteration	Weak propylitic alteration
wt.%										
SiO_2	69.76	66.64	64.34	65.04	61.04	59.37	66.39	62.57	56.56	65.17
Al_2O_3	14.80	14.44	15.14	13.14	15.74	15.55	13.52	14.45	15.84	15.46
Fe_2O_3	3.80	2.18	6.20	8.91	6.61	6.74	4.58	4.34	7.63	6.35
CaO	0.32	3.62	3.89	0.25	3.73	3.57	2.04	2.82	4.01	4.50
MgO	0.55	0.70	2.10	0.30	2.10	2.75	0.94	1.41	3.26	1.63
Na_2O	0.13	1.44	3.33	0.17	3.04	3.22	1.28	3.37	2.34	3.26
K_2O	3.80	3.47	1.78	3.91	2.53	2.05	5.18	2.91	3.15	1.62
TiO_2	0.25	0.23	0.64	0.21	0.65	0.72	0.25	0.47	0.83	0.65
P_2O_5	0.09	0.09	0.11	0.08	0.27	0.28	0.07	0.17	0.32	0.11
MnO	0.01	0.03	0.07	0.02	0.06	0.04	0.09	0.03	0.04	0.07
LOI	4.48	5.36	1.66	6.28	4.22	4.39	5.21	5.74	5.41	1.17
Total	97.99	98.20	99.26	98.31	99.99	98.68	99.54	98.27	99.39	99.99
ppm										
Cs	2.0	2.5	3.1	0.6	1.8	2.7	2.2	2.3	5.8	1.6
Tl	1.02	0.85	0.76	1.23	1.31	0.82	1.26	0.78	1.30	0.62
Rb	80	52	47	88	69	53	99	64	72	42
Ba	1069	869	1232	773	1028	924	1739	1075	1620	846

Th	6.52	6.25	3.09	5.80	4.32	4.20	5.88	6.00	3.46	3.10
U	1.91	3.58	1.74	1.76	2.18	2.25	2.82	3.36	2.44	1.72
Nb	6.4	6.6	3.9	6.4	5.6	5.7	5.5	5	5.7	3.8
Ta	0.61	0.62	0.26	0.59	0.37	0.42	0.55	0.53	0.40	0.28
La	18.1	15.3	10.8	18.5	20.5	19.1	21	16.7	19.4	11.2
Ce	33.2	29.1	22.4	32.1	37.2	37	38	30.2	39	23.8
Pr	3.79	3.52	3.05	3.72	4.97	4.74	4.43	3.62	5.04	3.22
Sr	28	108	310	26	633	611	169	467	1021	327
P	393	393	480	349	1178	1222	306	742	1397	480
Nd	12.5	13.4	13.0	12.9	19.4	18.3	15.5	13.8	20.3	13.6
Zr	101	116	97	102	110	115	92	107	103	103
Hf	2.6	2.9	2.5	2.7	2.6	2.8	2.5	2.6	2.4	2.7
Sm	2.11	2.30	3.41	1.99	3.72	3.55	2.51	2.49	3.76	3.42
Eu	0.55	0.61	0.87	0.70	0.95	1.10	0.66	0.72	1.24	0.87
Ti	1498	1402	3824	1283	3884	4327	1468	2799	4951	3920
Gd	1.33	1.67	3.52	1.37	2.83	2.51	1.55	1.75	2.79	3.58
Tb	0.19	0.24	0.58	0.17	0.44	0.33	0.22	0.25	0.36	0.62
Dy	1.06	1.31	3.73	0.94	2.43	1.75	1.21	1.35	1.93	3.86
Y	5	8	22	5	13	9	6	8	9	24
Ho	0.20	0.24	0.78	0.17	0.45	0.33	0.22	0.25	0.36	0.79
Er	0.59	0.70	2.25	0.51	1.23	0.91	0.66	0.74	0.98	2.37
Tm	0.10	0.11	0.34	0.08	0.18	0.13	0.11	0.11	0.14	0.37
Yb	0.72	0.78	2.29	0.59	1.24	0.81	0.73	0.74	0.88	2.44
Lu	0.12	0.13	0.35	0.11	0.20	0.13	0.11	0.12	0.13	0.37

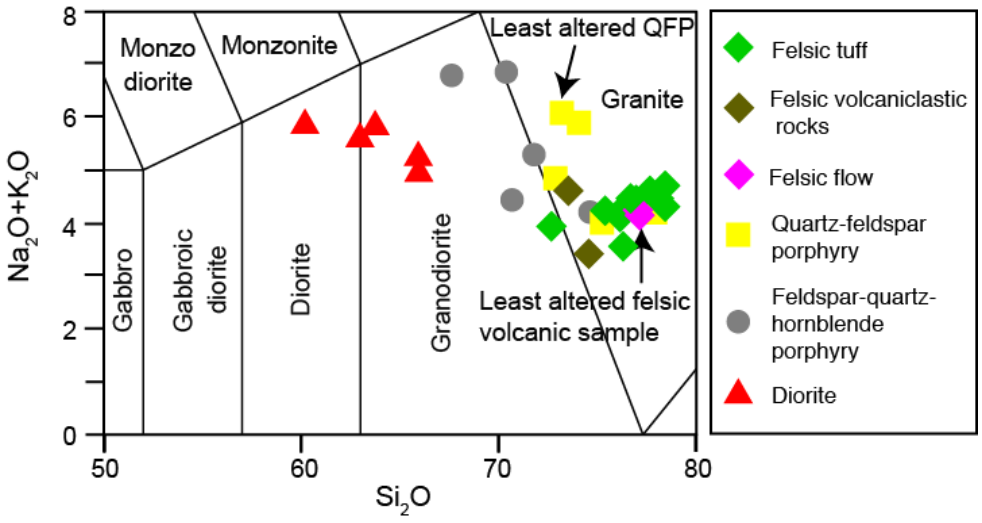

Fig. 2-11. Total alkali (Na_2O+K_2O) versus silica diagram (Middlemost, 1994) showing the compositions of igneous rocks from the Newton area. The felsic volcanic rock and quartz-feldspar porphyry data are from McClenaghan (2013).

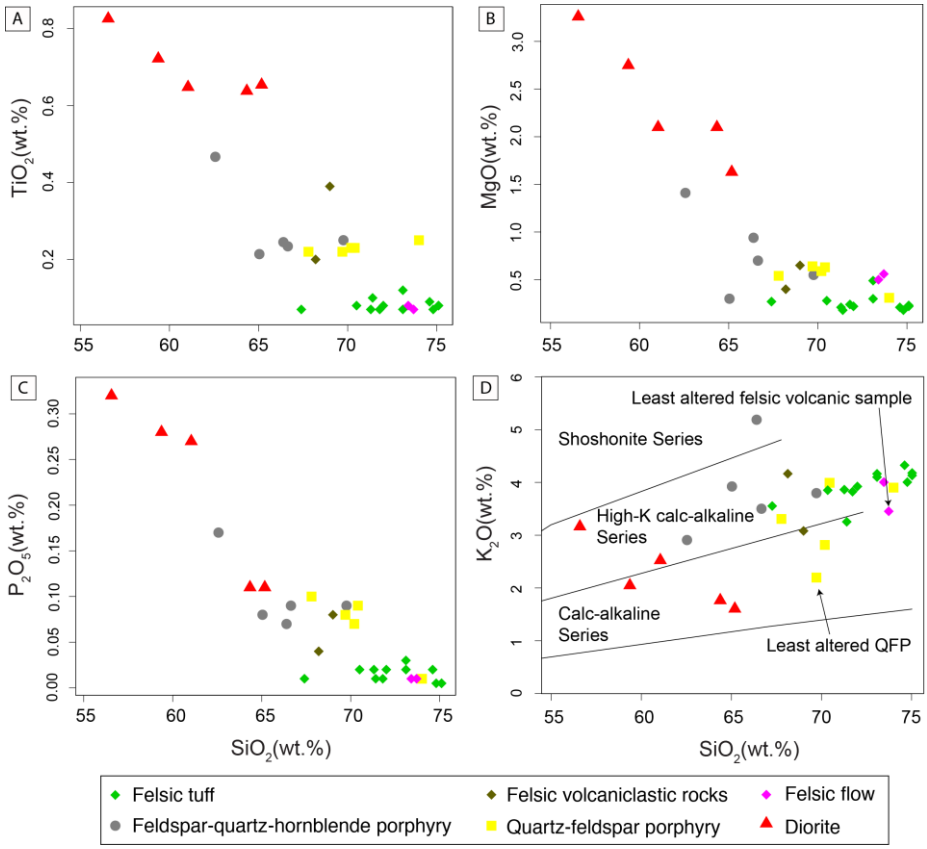

Fig. 2-12. Harker diagrams showing variations of (A) TiO_2, (B) MgO, (C) P_2O_5, and (D) K_2O versus SiO_2 for igneous rocks from the Newton property. Data for felsic volcanic rocks and quartz-feldspar porphyry are from McClenaghan (2013).

samples plotted here are altered to varying degrees, caution must be exercised when using the total alkali–silica diagram for lithological classification purposes. However, the data plot fairly tightly, and the compositions of the two least-altered volcanic and quartz-feldspar porphyry samples are similar to more altered equivalents. We therefore consider that alteration has not affected these rocks to a degree that would change their broad lithological classification. On this basis, the data suggest a typical calc-alkaline trend from dioritic to granitic compositions for the intrusive rocks, and dacite to rhyolite for the volcanic rocks (Fig. 2-11).

Concentrations of TiO_2, MgO, and P_2O_5 are plotted relative to SiO_2 in Figure 12A–C, and show reasonably well correlated inverse trends, suggesting a cogenetic relationship though fractionation of ferromagnesian silicates, magnetite, and apatite. Potassium shows greater scatter relative to SiO_2, likely due to the effects of hydrothermal alteration, but the data nevertheless group within the calc-alkaline to high-K calc-alkaline fields in Figure 2-12D, consistent with a volcanic arc origin.

Trace element compositions

Due to varying degrees of alteration, plots using immobile elements Y, Yb, Ta, Nb, are used for tectonic discrimination (Fig. 2-13). All samples plot in the field of volcanic arc rocks. Trace element data for igneous rock samples from the Newton deposit are plotted on primitive mantle-normalized trace element and chondrite-normalized rare earth element (REE) diagrams in Figures 2-14 and 2-15.

The samples display broadly similar patterns on primitive mantle-normalized trace element diagrams (Fig. 2-14), with relative enrichments in incompatible large-ion lithophile elements (LILE) and distinctive depletions in Nb, Ta, and Ti, characteristic of arc-related magmas (Gill, 1981; Briqueu et al., 1984; Brown et al., 1984). The suite also shows depletions in Sr and P, which, along with Ti, are more pronounced in the felsic volcanic rocks, reflecting fractionation of feldspar, apatite, and magnetite respectively. The more mafic diorites show positive anomalies for Sr, which may indicate minor plagioclase feldspar accumulation. The diorites also have higher

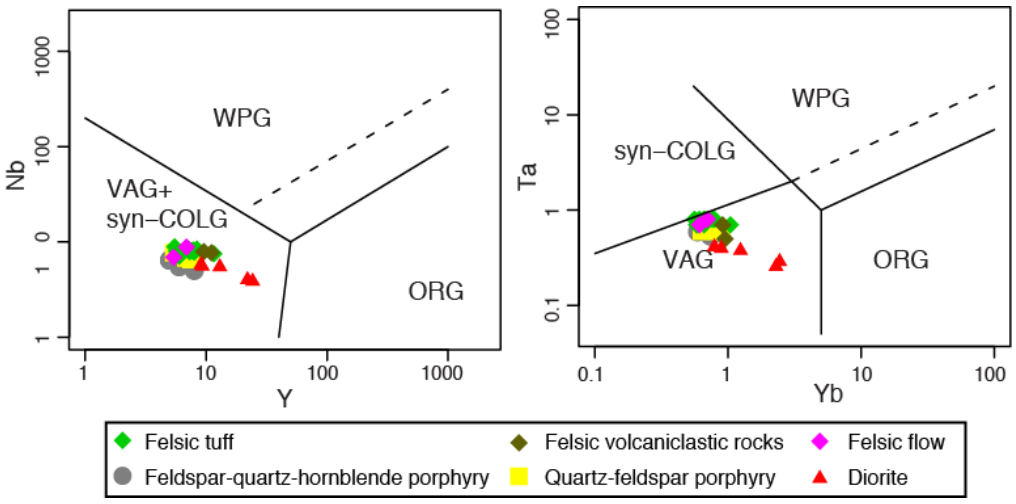

Fig. 2-13. Tectonic discrimination diagrams for igneous rocks from the Newton property (after Pearce et al., 1984). Abbreviations: collisional granites (COLG), ocean ridge granites (ORG), volcanic arc granites (VAG), and within plate granites (WPG).

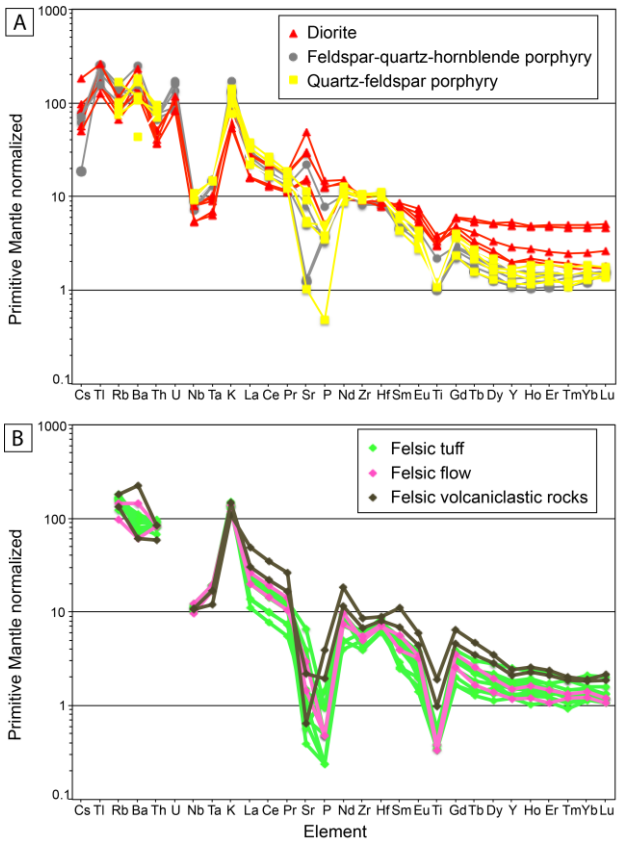

Fig. 2-14. Primitive mantle-normalized trace element diagrams for samples of (A) intrusive and (B) extrusive rocks from Newton (primitive mantle normalization values from Sun and McDonough, 1989). Data for felsic volcanic rocks and quartz-feldspar porphyry are from McClenaghan (2013).

concentrations of compatible elements such as middle and heavy REE (MREE, HREE) compared to the more evolved rocks.

On chondrite-normalized rare earth element diagrams (Fig. 2-15), the quartz-feldspar porphyry, feldspar-quartz-hornblende porphyry, and felsic volcanic rock samples show listric-shaped REE patterns (steep slopes from light REE (LREE) to MREE, and shallow to flat slopes from MREE to HREE; La/Yb = 11.7 to 36.0), suggesting that amphibole fractionation was important (Sisson, 1994). In contrast, the diorite samples show slightly shallower slopes from LREE to MREE, and flat slopes from MREE to HREE, consistent with their less evolved compositions relative to the felsic rocks (La/Yb = 4.6 to 23.6).

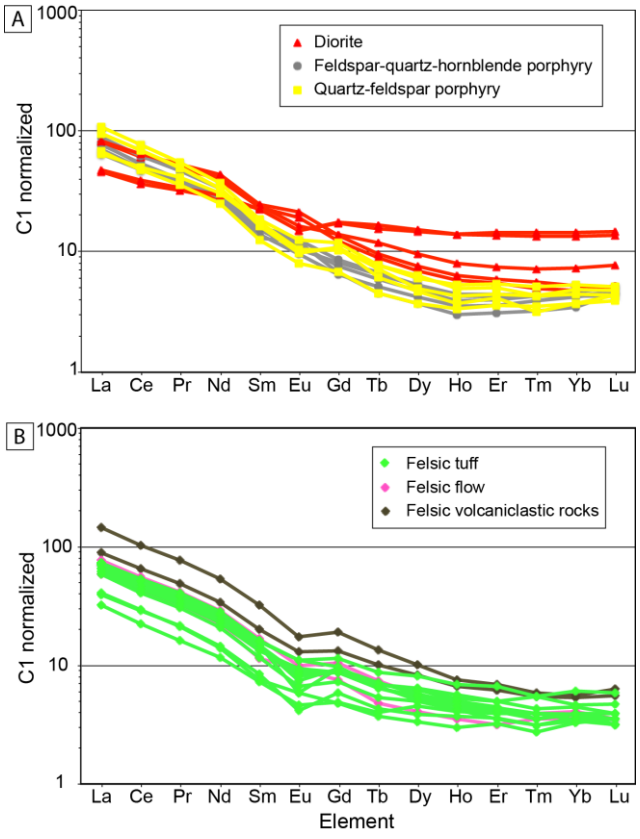

Fig. 2-15. C1 Chondrite-normalized REE diagrams for samples of (A) intrusive and (B) extrusive rocks from Newton (normalization values from Sun and McDonough, 1989). Data for felsic volcanic rocks and quartz-feldspar porphyry are from McClenaghan (2013).

The more felsic rocks (quartz-feldspar porphyries and volcanic rocks) display small negative Eu anomalies (Figs. 2-15 and 2-16), indicative of feldspar fractionation. The lack of significant negative Eu anomalies in the more mafic lithologies (Figs. 2-15A and 2-16) indicates that plagioclase fractionation was not important during early crystallization of the parental magmas, but small positive anomalies for some diorite samples are consistent with some later-stage plagioclase accumulation, as also indicated by elevated Sr concentrations (Fig. 2-14A).

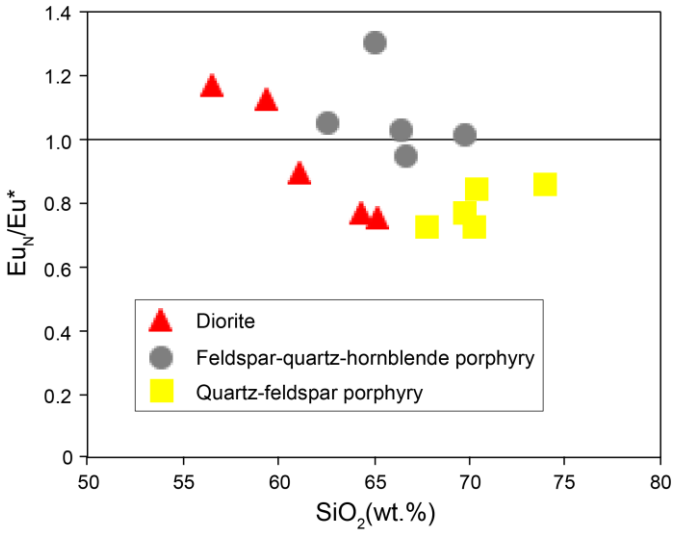

Fig. 2-16. Eu anomaly vs SiO_2 diagram for samples of igneous rocks from Newton (Eu_n / Eu* = Eu_n / √ Sm_n*Gd_n).

2.7 Geochronology (zircon U-Pb dating)

The felsic volcanic rocks and quartz-feldspar porphyry have been dated by Amarc Resources Ltd. (reported in McClenaghan, 2013). The felsic volcanic rock sample yielded an age of 72.1 ± 0.6 Ma, which is a weighted mean age of two zircon grains with a low degree of certainty (McClenaghan, 2013). The quartz-feldspar porphyry sample yielded an age of 70.9 ± 0.5 Ma (MSWD = 1.8; McClenaghan, 2013). In order to better understand the relationships between the felsic volcanic rocks and the three phases of intrusions (diorite, feldspar-quartz-hornblende porphyry, quartz-feldspar porphyry), the feldspar-quartz-hornblende porphyry and diorite were dated in this study. The feldspar-quartz-hornblende porphyry sample was collected from drill hole

10031 (Fig. 2-4) at a depth of 328 m, and the diorite sample was collected from drill hole 10023 (Fig. 2-4) at a depth of 146 m.

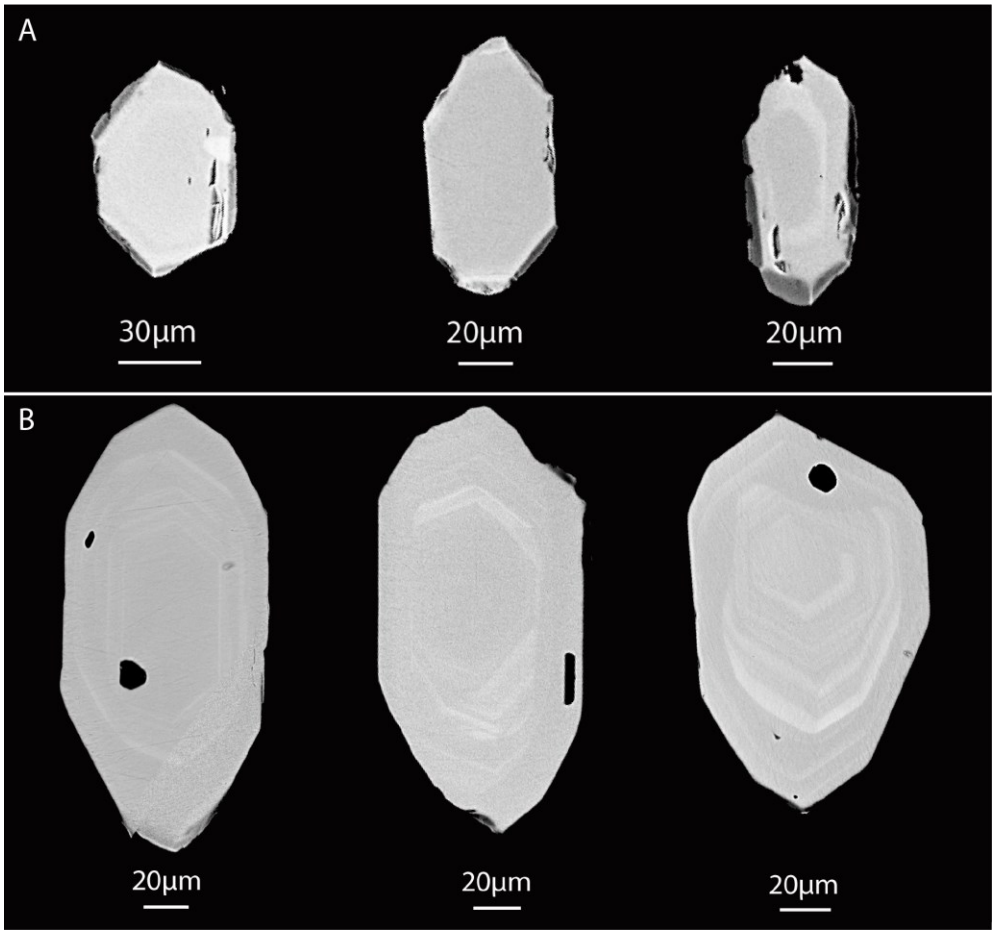

Fig. 2-17. Backscattered electron images of typical zircons from the feldspar-quartz-hornblende porphyry (A, NT129) and diorite (B, NT090). Zircons from the diorite are slightly larger than from the feldspar-quartz-hornblende porphyry, and show clear magmatic oscillatory zoning from center to margin. Dark areas are small inclusions of other minerals, which were avoided during analysis.

The analyzed zircons are clear, colorless, euhedral, and prismatic, which are the characteristics features of magmatic zircons. Oscillatory zoning is well developed in zircons from the diorite (as seen in the backscattered electron SEM images), whereas zircons from the feldspar-quartz-hornblende porphyry are largely unzoned (Fig. 2-17). Variations in the brightness of the different zones are attributed to different proportions of trace elements such as Hf, Y, and REE (Hoskin, 2000).

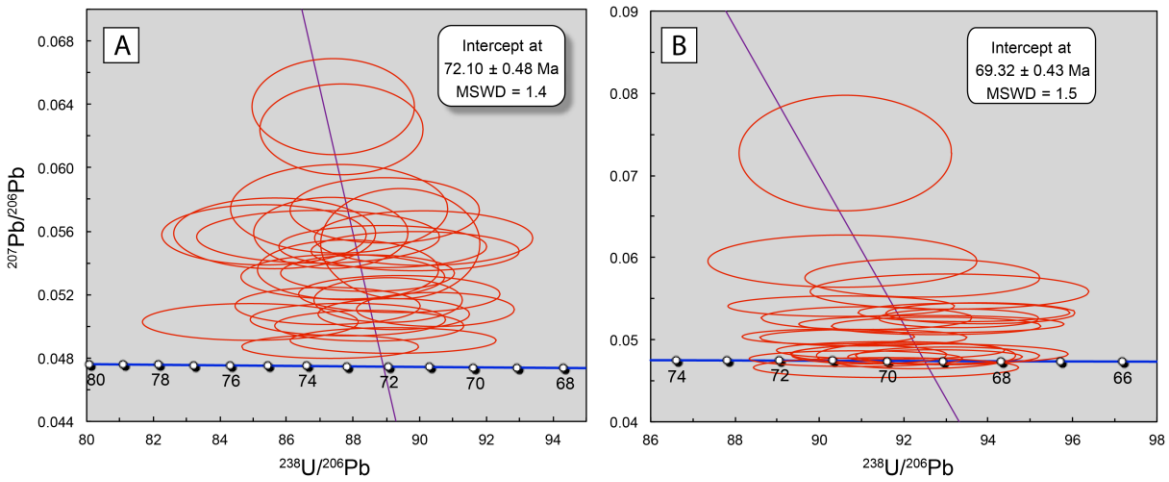

Fig. 2-18. U-Pb Concordia diagrams for zircon laser ablation ICPMS data from the feldspar-quartz-hornblende porphyry (A, NT129) and diorite (B, NT090). The error ellipses are 2 sigma.

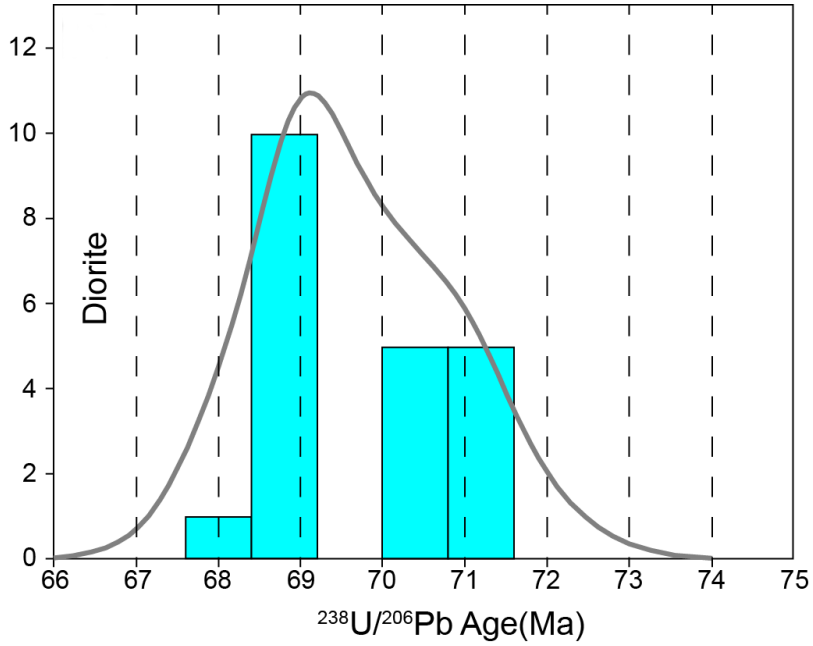

Fig. 2-19. Zircon U-Pb $^{238}U/^{206}Pb$ age histograms and relative probability curves for the diorite sample (NT090).

U-Pb dating results for zircons from the feldspar-quartz-hornblende porphyry (NT129) and diorite (NT090) are listed in Table 2-3 and plotted on Concordia diagrams in Figure 2-18. The feldspar-quartz-hornblende porphyry sample contains a relatively homogeneous population of concordant zircons, which yielded a U-Pb concordia intercept age of 72.10 ± 0.48 Ma (n = 25,

Table 2-3 Zircon U-Pb data of feldspar-quartz-hornblende porphyry and diorite from Newton

Sample name	$^{207}Pb/^{206}Pb$	2 s	$^{207}Pb/^{235}U$	2 s	$^{206}Pb/^{238}U$	2 s	r	$^{207}Pb^*/^{206}Pb^*$ age (Ma)	2 s error (Ma)	$^{207}Pb^*/^{235}U$ age (Ma)	2 s error (Ma)	$^{206}Pb^*/^{238}U$ age (Ma)	2 s error (Ma)	% discordance
Feldspar-quartz-hornblende porphyry														
NT_129_1	0.05077	0.00080	0.07846	0.00205	0.01121	0.00023	0.799	230	36	77	2	72	1	69.2
NT_129_2	0.05356	0.00154	0.08407	0.00322	0.01138	0.00029	0.660	353	64	82	3	73	2	79.8
NT_129_3	0.05106	0.00087	0.07782	0.00213	0.01105	0.00024	0.781	244	39	76	2	71	2	71.3
NT_129_4	0.05166	0.00115	0.07998	0.00242	0.01123	0.00023	0.676	270	50	78	2	72	1	73.8
NT_129_5	0.05474	0.00101	0.08399	0.00285	0.01113	0.00032	0.839	402	41	82	3	71	2	82.7
NT_129_6	0.06242	0.00234	0.09820	0.00431	0.01141	0.00026	0.520	689	78	95	4	73	2	89.9
NT_129_7	0.04871	0.00060	0.07693	0.00213	0.01145	0.00028	0.895	134	29	75	2	73	2	45.5
NT_129_8	0.06386	0.00247	0.10074	0.00453	0.01144	0.00026	0.507	737	80	97	4	73	2	90.6
NT_129_9	0.05521	0.00284	0.08514	0.00476	0.01118	0.00024	0.391	421	111	83	4	72	2	83.4
NT_129_10	0.05589	0.00183	0.08824	0.00347	0.01145	0.00025	0.552	448	71	86	3	73	2	84.1
NT_129_11	0.05312	0.00115	0.08353	0.00299	0.01140	0.00033	0.796	334	48	81	3	73	2	78.6
NT_129_12	0.05129	0.00096	0.08106	0.00260	0.01146	0.00030	0.813	254	42	79	2	73	2	71.4
NT_129_13	0.05335	0.00094	0.08319	0.00248	0.01131	0.00027	0.808	344	39	81	2	72	2	79.4
NT_129_14	0.05565	0.00136	0.08824	0.00371	0.01150	0.00039	0.815	438	53	86	3	74	3	83.7
NT_129_15	0.05043	0.00084	0.07915	0.00253	0.01138	0.00031	0.854	215	38	77	2	73	2	66.4
NT_129_16	0.05586	0.00182	0.08993	0.00392	0.01168	0.00034	0.663	447	71	87	4	75	2	83.7
NT_129_17	0.05028	0.00095	0.08164	0.00297	0.01178	0.00037	0.856	208	43	80	3	75	2	64.0
NT_129_18	0.05577	0.00155	0.09012	0.00365	0.01172	0.00034	0.726	443	61	88	3	75	2	83.5
NT_129_19	0.05741	0.00228	0.09039	0.00453	0.01142	0.00035	0.607	507	85	88	4	73	2	86.1
NT_129_20	0.05203	0.00095	0.08026	0.00266	0.01119	0.00031	0.834	287	41	78	2	72	2	75.4
NT_129_21	0.05503	0.00108	0.08536	0.00297	0.01125	0.00032	0.824	413	43	83	3	72	2	83.0

NT_129_22	0.05556	0.00141	0.08501	0.00332	0.01110	0.00033	0.761	435	55	83	3	71	2	84.1
NT_129_23	0.05731	0.00168	0.08884	0.00349	0.01124	0.00029	0.664	504	63	86	3	72	2	86.2
NT_129_24	0.04910	0.00066	0.07590	0.00238	0.01121	0.00032	0.903	153	31	74	2	72	2	53.3
NT_129_25	0.05003	0.00079	0.07796	0.00239	0.01130	0.00030	0.857	197	36	76	2	72	2	63.5
Diorite														
NT090_1	0.04870	0.00087	0.07323	0.00220	0.01091	0.00026	0.804	133	41	72	2	70	2	47.8
NT090_2	0.04660	0.00099	0.07016	0.00247	0.01092	0.00031	0.797	29	50	69	2	70	2	-143.3
NT090_3	0.04769	0.00078	0.07236	0.00203	0.01101	0.00025	0.812	84	38	71	2	71	2	15.9
NT090_4	0.04807	0.00131	0.07181	0.00247	0.01084	0.00023	0.608	103	63	70	2	69	1	32.5
NT090_5	0.04816	0.00090	0.07283	0.00182	0.01097	0.00018	0.662	107	44	71	2	70	1	34.6
NT090_6	0.04803	0.00088	0.07118	0.00188	0.01075	0.00021	0.724	101	43	70	2	69	1	31.8
NT090_7	0.04825	0.00101	0.07185	0.00257	0.01080	0.00031	0.812	112	49	70	2	69	2	38.3
NT090_8	0.04791	0.00070	0.07123	0.00166	0.01078	0.00020	0.780	95	34	70	2	69	1	27.4
NT090_9	0.05956	0.00259	0.09070	0.00474	0.01104	0.00032	0.551	588	92	88	4	71	2	88.4
NT090_10	0.05262	0.00113	0.07962	0.00247	0.01097	0.00025	0.722	313	48	78	2	70	2	77.9
NT090_11	0.05189	0.00085	0.07722	0.00249	0.01079	0.00030	0.861	281	37	76	2	69	2	75.7
NT090_12	0.05408	0.00102	0.08237	0.00253	0.01105	0.00027	0.790	374	42	80	2	71	2	81.5
NT090_13	0.05585	0.00175	0.08273	0.00353	0.01074	0.00031	0.680	447	68	81	3	69	2	85.0
NT090_14	0.05024	0.00082	0.07608	0.00209	0.01098	0.00024	0.802	206	38	74	2	70	2	66.2
NT090_15	0.07272	0.00575	0.11065	0.00910	0.01104	0.00025	0.276	1006	153	107	8	71	2	93.5
NT090_16	0.05321	0.00104	0.07820	0.00216	0.01066	0.00021	0.707	338	44	76	2	68	1	80.2
NT090_17	0.05167	0.00087	0.07680	0.00212	0.01078	0.00024	0.794	271	38	75	2	69	2	74.9
NT090_18	0.05332	0.00092	0.07869	0.00220	0.01070	0.00024	0.788	342	39	77	2	69	2	80.4
NT090_19	0.05753	0.00191	0.08580	0.00355	0.01082	0.00027	0.595	512	72	84	3	69	2	86.9
NT090_20	0.05260	0.00093	0.07773	0.00189	0.01072	0.00018	0.687	311	40	76	2	69	1	78.3
NT090_21	0.05036	0.00074	0.07697	0.00182	0.01108	0.00021	0.784	212	34	75	2	71	1	66.8

MSWD = 1.4, Fig. 2-18A). The diorite sample contains a slightly more complicated population of zircons, which yielded a U-Pb concordia intercept age of 69.32 ± 0.43 Ma (n = 21, MSWD = 1.5, Fig. 2-18B). A $^{238}U/^{206}Pb$ age histogram for these zircons (Fig. 2-19) suggests the presence of two populations of zircon in the diorite sample, one with an age close to the bulk sample at ~69 Ma, and a smaller group with slightly older ages ~71 Ma. This older group has an age similar to that of the feldspar-quartz-hornblende porphyry and felsic volcanic rocks, and may represent xenocrystic or antecrystic zircon inherited from slightly earlier intrusions within the same magmatic complex. Alternatively, the younger (~69 Ma) ages may reflect minor Pb-lose, and the true age of the diorite may be essentially coeval with the other igneous rocks at ~71 Ma.

2.8 Fluid inclusions

Quartz veins are not common at Newton. Workable primary and pseudosecondary fluid inclusions were only found in two quartz vein samples, which are both related to stage 1 mineralization. One sample is a quartz-pyrite vein (with electrum inclusions in pyrite) hosted by quartz-feldspar porphyry (sample NT049) from borehole 9004 at a depth of 270 m. The other sample is a quartz-molybdenite-pyrite vein hosted by felsic volcanic rocks (sample NT060) from borehole 12057 at a depth of 200 m. No quartz veins related to stage 2 mineralization were found, and sphalerite from a stage 3 polymetallic sulfide vein mineralization was too opaque to observe fluid inclusion.

A total of 96 quartz-hosted fluid inclusions was analyzed. Only primary and pseudosecondary inclusions were analyzed (Fig. 2-20; criteria of Roedder, 1984, and Goldstein, 2003), and necked or leaked inclusions were avoided. Primary inclusions were mostly observed in growth zones, whereas pseudosecondary inclusions occur in micro-fractures developed during crystal growth. Measured inclusions ranged in size between 3–7 μm with a few up to 10 μm. Most fluid inclusions are present in groups as fluid inclusion assemblages, in which the vapor/liquid phase ratios are constant (Fig. 2-20A; Goldstein and Reynolds, 1994; Goldstein, 2003). A few fluid inclusions occurred as larger isolated inclusions, which are interpreted to be primary in origin.

Three distinct fluid inclusion types have been recognized. Type 1 inclusions are two-phase liquid-rich inclusions, and occur in both samples. CO_2 was not seen as a separate liquid or vapor phase, and no melting events were observed at -56.6°C during heating that would indicate the presence of CO_2. However, some inclusions displayed subtle melting events at temperatures above 0°C, indicating that small amounts of CO_2 are present as CO_2 clathrate. Therefore the type 1 inclusions can be subgrouped into type 1a inclusions (without CO_2 clathrate) and type 1b inclusions (with CO_2 clathrate).

Type 2 inclusions are two-phase vapor-rich inclusions, and also occur in both samples. It is difficult to observe phase changes in these predominantly dark inclusions, so no microthermometric data could be obtained from them (Bodnar et al., 1985). Primary type 2 inclusions occur together with liquid-rich type 1 inclusions in one fluid inclusion assemblage from the quartz-pyrite-gold vein (NT049), and this is taken to be evidence that boiling occurred in this vein sample (Fig. 2-20C). Boiling was also likely occurring in the other quartz-molybdenite-pyrite vein, as evidenced by the presence of type 2 vapor-rich fluid inclusions in this sample (NT060). However, they were not observed in the same assemblages as type 1 inclusions, so the identification of boiling is not definitive for this sample.

Type 3 fluid inclusions contain three- or four-phases, including halite and in some cases opaque daughter minerals, in addition to liquid and vapor phases (Fig. 2-20B). Halite crystals were recognized by their cubic morphology and relatively slow dissolution during heating. Type 3 inclusions are rare, and only occur locally at the edges of the quartz-molybdenite-pyrite vein (NT060). Type 3 inclusions are therefore thought to represent early stage fluids.

Homogenization temperature and salinity measurements

Homogenization temperature and salinity data are presented in Figures 2-21 and 2-22, and Table 2-4.

Quartz-pyrite-gold vein sample (NT049): Type 1a fluid inclusions from the quartz-pyrite-gold vein sample homogenized by bubble disappearance at temperatures ranging from 210° to 415°C (average = 327° ± 48°C; n = 47). Fluid salinities for type 1a inclusion (as measured from

ice melting temperatures) range from 4.0 to 6.0 wt.% NaCl equiv. (average = 5.2 ± 0.7 wt.% NaCl equiv., n = 24).

Type 1b inclusions from this sample homogenized at similar temperatures to type 1a inclusions (316° to 355°C; average = 343° ± 15°C, n = 6). Salinities calculated from clathrate melting temperature are more scattered because of the lower precision of this method (0.8 to 7.1 wt.% NaCl equiv.; average = 4.0 ± 2.4 wt.% NaCl equiv., n = 6), but overlap the tighter range of type 1a inclusions.

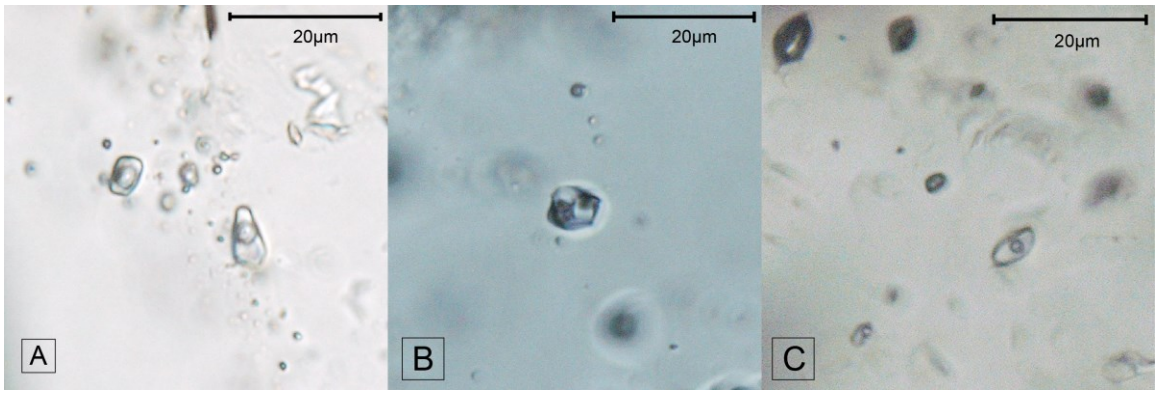

Fig. 2-20. Transmitted light photomicrographs showing primary fluid inclusions from stage 1 mineralization: (A) type 1 fluid inclusion assemblage from a quartz-pyrite vein (NT049); (B) type 3 primary multi-phase inclusion (liquid-vapor-halite/opaque mineral) from a quartz-molybdenite-pyrite vein (NT060); (C) type 1 liquid-rich inclusion with type 2 vapor-rich inclusions in a primary fluid inclusion assemblage from a quartz-pyrite vein (NT049).

The homogenization temperatures and salinities of type 2 vapor-rich fluid inclusions could not be measured due to the small amount of liquid present, but type 1a inclusions in the same assemblage range from 293°–369°C (average = 329° ± 32°C, n = 7) and 4.3–6.0 wt.% NaCl equiv. (average = 5.3° ± 0.6°C, n = 7).

Quartz-molybdenite-pyrite vein sample (NT060): Type 1a fluid inclusions from the quartz-molybdenite-pyrite vein sample homogenized by bubble disappearance at temperatures ranging from 205° to 388°C (average = 294° ± 49°C; n = 35). Fluid salinities for type 1a inclusion range from 2.9 to 6.4 wt.% NaCl equiv. (average = 4.5 ± 1.0 wt.% NaCl equiv., n = 22).

Table 2-4 Fluid inclusion data from Newton

Fluid inclusion number	Fluid inclusion assemblage ID	Tm_{ice} (°C)	$Tm_{CO2\ clathrate}$ (°C)	Tm_{halite} (°C)	Th(°C)	Salinity (wt % NaCl equiv.)	Type
Quart-pyrite vein (NT049)							
1	A	-3.5			307	5.7	1a
2		-3			306	5.0	1a
3		-3.6			293	5.9	1a
4		-3.3			361	5.4	1a
5		-2.6			369	4.3	1a
6		-3.7			355	6.0	1a
7		-2.9			310	4.8	1a
8	B	-3.4			356	5.6	1a
9		-3.6			320	5.9	1a
10					411		1a
11					410		1a
12					367		1a
13	C	-3.2			375	5.3	1a
14		-3.3			290	5.4	1a
15		-2.7			305	4.5	1a
16		-2.7			362	4.5	1a
17					320		1a
18					368		1a
19					280		1a
20					342		1a
21	*	-3.7			253	6.0	1a
22	*	-2.4			305	4.0	1a
23	*	-3.2			214	5.3	1a
24	*	-2.8			268	4.6	1a

25	*	-3.6			285	5.9	1a
26	*	-3.4			354	5.6	1a
27	*	-2.4			244	4.0	1a
28	*	-3.4			302	5.6	1a
29	*	-3			243	5.0	1a
30	*	-3.4			305	5.6	1a
31	*	-2.4			210	4.0	1a
32	D				300		1a
33					356		1a
34					354		1a
35					366		1a
36					328		1a
37					369		1a
38	E				372		1a
39					415		1a
40	F				345		1a
41					328		1a
42	G		6.2		355	7.1	1b
43			7.2		352	5.4	1b
44					360		1a
45					356		1a
46					344		1a
47					348		1a
48	H		9.6		316	0.8	1b
49			8.7		343	2.6	1b
50			8.8		336	2.4	1b
51					332		1a
52					316		1a

53	*		7.2		355	5.4	1b
Quartz-molybdenite-pyrite vein (NT060)							
1	A	-3.3			318	5.4	1a
2		-3.6			330	5.9	1a
3		-3.1			322	5.1	1a
4		-3.7			338	6.0	1a
5	B	-3.5			370	5.7	1a
6		-3			308	5.0	1a
7	*	-1.9			252	3.2	1a
8	*	-1.8			205	3.1	1a
9	*	-2.2			252	3.7	1a
10	*	-2.6			320	4.3	1a
11	*	-2.8			254	4.6	1a
12	*	-2			258	3.4	1a
13	*	-2.4			267	4.0	1a
14	*	-2.3			232	3.9	1a
15	*	-3.1			330	5.1	1a
16	*	-2.8			260	4.6	1a
17	*	-4			360	6.4	1a
18	*	-2.9			300	4.8	1a
19	*	-2			220	3.4	1a
20	*	-2.7			217	4.5	1a
21	*	-1.9			301	3.2	1a
22	*	-1.7			230	2.9	1a
23	*		7.6		268	4.7	1b
24	*		8.3		358	3.4	1b
25	*		8.6		389	2.8	1b
26	*		7.7		241	4.5	1b

27	*				385		1a
28	*				388		1a
29	*				323		1a
30	*				354		1a
31	*				352		1a
32	*				269		1a
33	*				291		1a
34	*				287		1a
35	*				276		1a
36	*				276		1a
37	*				278		1a
38	*				315		1a
39	*				242		1a
40	C			260	335	35.1	3
41				255	355	34.8	3
42				244	340	34.2	3
43	*			260	340	35.1	3

* Isolated fluid inclusions

Type 1b inclusions from this sample homogenized at similar temperatures to type 1a inclusions (241° to 389°C; average = 314° ± 71°C, n = 4). Salinities calculated from clathrate melting temperature also overlap (at the lower end) the range for type 1a inclusions (2.8 to 4.7 wt.% NaCl equiv.; average = 3.8 ± 0.9 wt.% NaCl equiv., n = 4).

Early type 3 hypersaline fluid inclusions homogenized finally by halite daughter crystal dissolution at temperatures ranging from 335° to 355°C (average = 343° ± 9°C; n = 4), indicating salinities of (34.2 to 35.1 wt.% NaCl equiv.; average = 34.8 ± 0.5 wt.% NaCl equiv., n = 4). The vapor bubble disappeared at lower temperatures (244°–260°C; average = 255° ± 8°C; n = 4).

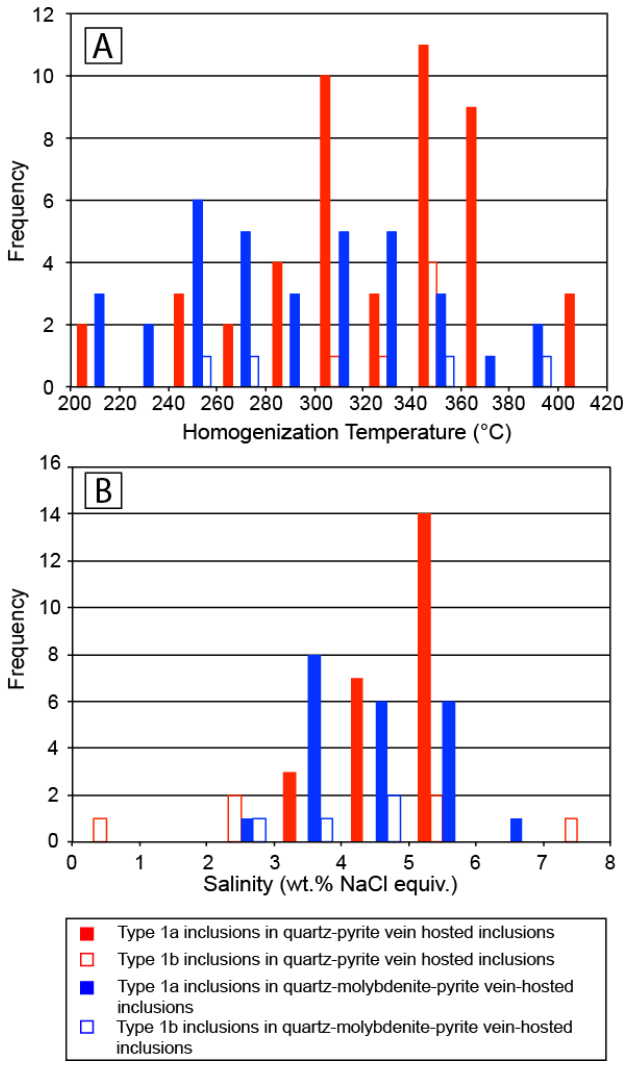

Fig. 2-21. Histograms showing homogenization temperature and salinity distribution for type 1 fluid inclusions from quartz-pyrite (NT049) and quartz-molybdenite-pyrite (NT060) veins.

Pressure

Because there is evidence of boiling in at least one vein sample, homogenization temperatures are assumed to be close to the real trapping temperatures for most of the type 1 fluid inclusions, and no pressure corrections have been made to homogenization temperatures (Roedder and Bodnar, 1980; Bodnar and Vityk, 1994). The average homogenization temperature and fluid salinity of all type 1a inclusions is 313° ± 51°C (n = 82), and 4.8 ± 0.9 wt.% NaCl equiv. (n = 46). Therefore assuming that the hydrothermal fluid is a pure H_2O-NaCl system with a temperature of ~310°C and salinity of ~5 wt.% NaCl equiv., the trapping pressure for fluid inclusions related to stage 1 mineralization can be estimated to be ~95 bars, equivalent to a depth of 1160 m (assuming hydrostatic pressure conditions), based on the data of Haas (1971). However, the presence of small amounts of CO_2 in some type 1b inclusions may mean that fluid pressures (and therefore depths) were slightly greater; the estimates provided here are therefore considered to be minimum values.

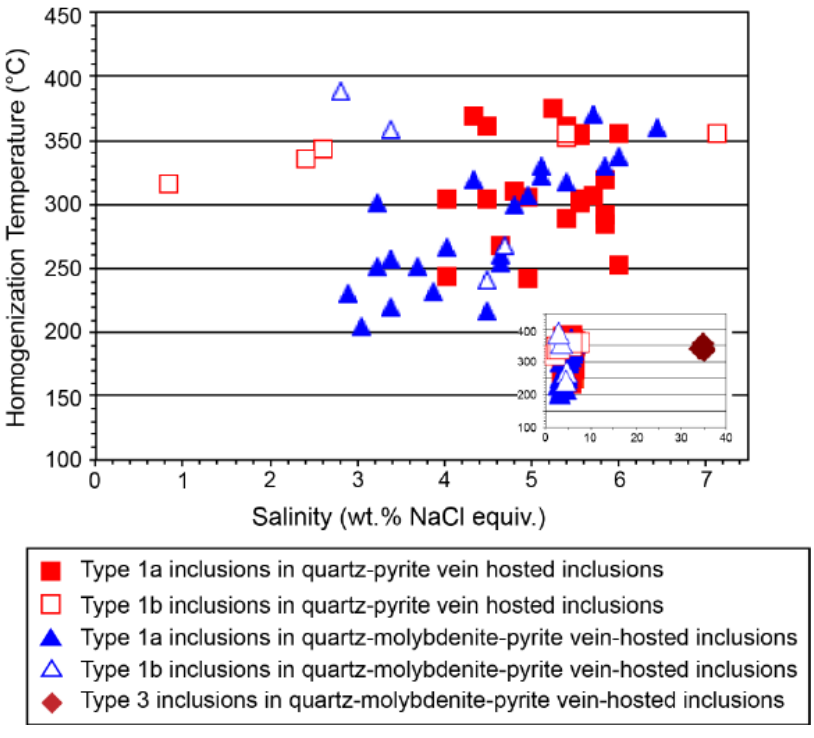

Fig. 2-22. Salinity versus homogenization temperature plot for inclusions from quartz-pyrite (NT049) and quartz-molybdenite-pyrite (NT060) veins.

2.9 Discussion

Timing and petrogenesis

The felsic volcanic rocks, feldspar-quartz-hornblende porphyry, quartz-feldspar porphyry, and post-mineralization diorite at Newton yielded U-Pb zircon ages of 72.1 ± 0.6 Ma, 72.10 ± 0.48 Ma, 70.9 ± 0.5 Ma, and 69.32 ± 0.43 Ma respectively (McClenaghan, 2013; this study). These ages indicate that the magmatic activity at Newton is broadly coeval, and spanned a time period of ~ 3 m.y. (~72–69 Ma), or possibly only ~1 m.y. if the true age of the diorite is closer to 71 Ma, as suggested by the bimodal population of zircon ages for this samples (the younger ages ~69 Ma reflecting minor Pb-loss). A single Re-Os date on hydrothermal molybdenite (72.1 ± 0.3 Ma) reported by McClenaghan (2013), is consistent with the ages of the felsic volcanic rocks and feldspar-quartz-hornblende porphyry, but is slightly older than the age of the main quartz-feldspar porphyry host rock. This slightly inconsistent result cannot be explained at this time, but may relate to problems comparing data from two different geochronological systems, and also to the difficulty of resolving minor Pb-loss in young samples dated by LA-ICP-MS. Broadly, however, the molybdenite age is consistent with a cogenetic relationship between the magmatic and hydrothermal activity at ~72 Ma.

The felsic volcanic rocks, quartz-feldspar porphyry, feldspar-quartz-hornblende porphyry, and diorite are also broadly cogenetic in terms of their geochemical compositions, and they are assumed to have been derived from the same parent magma. Because the most mafic rock, the diorite, is the youngest intrusion, the data cannot be modelled as a simple fractionation trend. However, the diorite is likely reflective of the composition of the more mafic end-member in this suite, and the more evolved lithologies may have evolved from a similar, earlier dioritic magma at depth.

The diorite contains hornblende phenocrysts, which indicates that the magma contained at least 4 wt.% H_2O (Naney, 1983). High magmatic water contents also can suppress early crystallization of plagioclase, which is evidenced by the absence of europium anomalies in the normalized REE patterns for the diorites (because plagioclase preferentially partitions Eu^{2+} relative to Eu^{3+} and other REE; Hanson, 1980). However, the absence of Eu anomalies can also

be explained by relatively oxidizing conditions, under which Eu is mainly present as Eu^{3+} (and is therefor not partitioned into plagioclase). Thus, the diorites are interpreted to be either relatively hydrous or oxidized, or both, which are favorable characteristics for the formation of porphyry and related epithermal deposit (Candela, 1992; Richards, 2003).

Immobile trace element and major element compositions suggest that the Newton igneous suite is of calc-alkaline, continental arc affinity, with compositions ranging from diorite to granite. Listric-shaped REE patterns combined with the lack of europium anomalies in more mafic rocks suggest that the suite was hydrous, and evolved by early fractionation of amphibole (± titanite; Gromet and Silver, 1983; Green and Pearson, 1985; Rollinson, 1993).

Characteristics of ore-forming fluids:

Fluid inclusions from two vein samples from stage 1 mineralization record similar temperatures and salinities. Data for type 1a two-phase (liquid + vapor) inclusions from a quartz-sericite-pyrite vein indicate an average homogenization temperature of 327° ± 48°C (n = 47) and salinity of 5.2 ± 0.7 wt.% NaCl equiv. (n = 24). Data from a quartz-molybdenite-pyrite vein overlap this composition but show a trend from a relatively high temperature and saline composition (370°C; 5.7 wt.% NaCl equiv.) to a lower temperature and less saline fluid (~205°C; 3.1 wt.% NaCl equiv.). This trend is not observed in individual fluid inclusion assemblages, indicating that in situ fluid mixing was not occurring. Instead, the trend can be correlated with vein paragenesis, with the high temperature and salinity fluids occurring near the vein margins, and lower temperature and salinity fluids occurring towards the vein center. This trend is further supported by the presence of rare hypersaline fluid inclusions near the margin of this quartz-molybdenite-pyrite vein. The presence of vapor-rich fluid inclusions in some assemblages indicates that trapping conditions were at or near the two-phase boundary, and homogenization temperatures of type 1 fluid inclusions have not therefore been corrected for pressure. A minimum estimate of trapping pressure for fluids of this composition and temperature is ~95 bars (equivalent to a depth of around 1160 m assuming hydrostatic pressure conditions, but the observed presence of minor

amounts of CO_2 in some fluid inclusions may indicate higher fluid pressures (and depths). The deposit was therefore likely formed at ~1–2km depth.

McClenaghan (2013) conducted oxygen and deuterium isotopic analyses on sericite related to stage 1 and 2 mineralization. Sericite separated from stage 1 mineralization has $\delta^{18}O$ compositions of 8.4 to 9.5‰ (average = 8.7 ± 0.4‰, n = 6) and δD of -75.8 to -66.5‰ (average = -71.0 ± 3.8‰, n = 6). Assuming that sericite is in equilibrium with hydrothermal fluids, McClenaghan (2013) calculated the isotopic composition of these hydrothermal fluids using the fractionation equations of Sheppard and Gilg (1996) at an estimated temperature of 335°C (similar to the average trapping temperature of type 1a fluid inclusions determined in this study, 313°C). The $\delta^{18}O_{fluid}$ compositions range from 5.7 to 6.8‰ (average = 6.0 ± 0.4‰, n = 6), and δD_{fluid} ranges from -55.8 to -46.5‰ (average = -51.0‰ ± 3.8, n = 6; McClenaghan, 2013). McClenaghan (2013) concluded that these fluid compositions are broadly consistent with a primary magmatic water origin ($\delta^{18}O_{magmatic\ water}$ = +5.5 to +10.0‰; $\delta D_{magmatic\ water}$ = -50 to -90‰; Sheppard, 1977).

Isotopic compositions of fluid in equilibrium with sericite from stage 2 mineralization, calculated at 235°C, are $\delta^{18}O_{fluid}$ = 2.5 to 3.5‰ (average = 2.9 ± 0.4‰, n = 5) and δD_{fluid} = -63.0 to -50.3‰ (average = -57.5 ± 5.5‰, n = 5), suggesting possible mixing between magmatic fluids and meteoric groundwaters in this later stage (McClenaghan, 2013).

McClenaghan (2013) also measured the S isotopic composition of sulfides from different mineralization stages, and found that pyrite from stage 1 mineralization has $\delta^{34}S$ values of 1.2 to 3.2‰ (average = 2.1 ± 0.6‰, n = 10), whereas stage 2 marcasite and chalcopyrite ranged from -1.1 to 3.5 (average = 1.8 ± 1.5‰, n = 6). These compositions are also consistent with a magmatic origin for sulfur in the hydrothermal system (expected composition of magmatic sulfide is $\delta^{34}S$ = 0 ± 2‰; Marini et al., 2011).

Newton has been classified as an intermediate-sulfidation epithermal gold deposit (McClenaghan, 2013), although the quartz-sericite alteration and relatively high fluid temperatures place it in the deeper parts of the spectrum of epithermal deposits, close to the

porphyry environment. This interpretation is supported in this study by the observation of halite-bearing inclusions in the stage 1 quartz-molybdenite-pyrite vein, and the presence of potassic alteration in the diorite. Therefore, we propose that the Newton deposit formed near the transition zone between porphyry and epithermal environments. This interpretation implies the potential for porphyry-type mineralization at depth below the currently explored levels, as also suggested by geophysical data (work in preparation).

Ore depositional processes

Gold is mainly present as inclusions in disseminated pyrite and marcasite in quartz-sericite alteration, and auriferous veins are relatively rare. Consequently, wall rock reaction appear to be the main control on the precipitation of gold from the magmatic hydrothermal fluids, although minor gold may have been precipitated during boiling in the rare quartz-sulfide veins observed. If it is assumed that gold was dissolved as bisulfide complexes (e.g., $Au(HS)_2^-$; Seward, 1989, 1991), then wallrock sulfidation reactions accompanied by cooling may have been responsible for its coprecipitation with pyrite and marcasite, through reactions such as:

$FeO_{(wallrock)} + 2\ H_2S + ½\ O_2 = FeS_2 + 2\ H_2O$ (eq. 1)

$2\ Au(HS)_2^- + FeO_{(wallrock)} + 2\ H^+ = 2\ Au + FeS_2 + 2\ H_2S + H_2O$ (eq. 2) (Mikucki, 1998)

Newton compared with other intermediate-sulfidation epithermal deposits

Epithermal deposits can be classified into high-, intermediate-, and low-sulfidation systems in term of their sulfidation state (Hedenquist et al., 2000; Einaudi et al., 2003; Sillitoe and Hedenquist, 2003). The main characteristics of the Newton deposit are compared with Sillitoe and Hedenquist's (2003) description of intermediate-sulfidation (IS) epithermal deposit in Table 2-5, and key similarities include:

1. The Newton deposit is genetically related to calc-alkaline andesitic-rhyolitic arc magmas.
2. The main wallrock alteration mineral at Newton is sericite.
3. Sulfide abundance in mineralized rocks at Newton is ~5 to 10%.

4. Key sulfide minerals are pyrite, marcasite, sphalerite, galena, and minor chalcopyrite.
5. The main metal enrichments are Ag, Au, Zn, and Pb, with minor Mo and As.
6. Telluride minerals locally occur as inclusions in pyrite and marcasite.
7. Magmatic fluids were primarily responsible for mineralization at Newton, with some contribution at later stages from meteoric groundwaters.

Newton differs to some extent from typical IS deposits by being dominated by disseminated mineralization, whereas vein type mineralization is more common in other deposits (Sillitoe and Hedenquist, 2003). The disseminated mineralization style at Newton might be related to the transpressional tectonic setting thought to have prevailed at the time of its formation (Nelson and Colpron, 2007), which may have limited the formation of extensional fractures and veins, leading to more dispersed mineralization styles. Similar disseminated IS-type mineralization is found in the San Cristobal deposit in the Altiplano of Bolivia, which is interpreted to have formed in a compressional tectonic setting (Lamb et al., 1997; Buchanan, 2000; Sillitoe and Hedenquist, 2003). In contrast, IS deposits formed in extensional tectonic environments tend to be vein or breccia-hosted, such as the Arcata deposit in Peru, and the Fresnillo deposit in Mexico (Noble et al., 1990; Albinson et al., 2001; Sillitoe and Hedenquist, 2003).

Two other IS Au-Ag deposits of similar age and disseminated mineralization style occur in the southern Stikinia terrane of central British Columbia: the Blackwater and Capoose deposits (Fig. 2-2; Bordet et al., 2013; McClenaghan; 2013). The timing of magmatism and mineralization at these three deposits is similar (72 to 67 Ma), suggesting a pulse of transpression-related magmatism and mineralization in this region in the Late Cretaceous (Andrew, 1988; Lane and Schroeter, 1997; Friedman et al., 2001; Christie et al., 2014).

The Newton deposit appears to be transitional to underlying porphyry type alteration (and potentially mineralization), as indicated by the presence of rare hypersaline fluid inclusions in early vein stages, the local presence of potassic alteration, and geophysical data (work in prep.) This is consistent with the commonly observed spatial and genetic relationship between shallow IS and deeper porphyry systems, such as the coupled Acupan and Antamok IS and the Ampucao

porphyry deposits in the Baguio district, and the Victoria IS and Far Southeast porphyry deposits in the Mankayan district of the Philippines (Cooke et al., 1996, 2011; Chang et al., 2011).

Table 2-5 Comparison of Newton to other intermediate-sulfidation epithermal deposits described by Sillitoe and Hedenquist (2003)

	Characteristics of intermediate sulfidation deposits (from Sillitoe and Hedenquist, 2003)	Characteristics of the Newton deposit
Genetically related volcanic rocks	Principally andesite to rhyodacite and locally rhyolite	Rhyodacite to rhyolite
Mineralization style	Veins and breccias, minor disseminations	Disseminated
Key alteration minerals	Sericite; adularia generally uncommon	Sericite
Silica gangue	Vein-filling crustiform and comb quartz	Quartz veins are not well developed
Carbonate gangue	Common in veins, typically including manganiferous varieties	Carbonate is only associate with stage 3 polymetallic-sulfide veins
Other gangue	Barite and manganiferous silicates present locally	Rare
Sulfide abundance	5–>20 vol.%	~5–10 vol.%
Key sulfide species	Sphalerite, galena, tetrahedrite-tennantite, chalcopyrite	Pyrite, marcasite, sphalerite, galena, and minor chalcopyrite
Main metals	Ag-Au, Zn, Pb, Cu	Ag-Au, Zn, Pb
Minor metals	Mo, As, Sb	Mo, As

2.10 Conclusion

The Newton epithermal deposit is hosted by a Late Cretaceous volcanoplutonic complex with continental arc affinity, and consists of felsic volcanic rocks (72.1 ± 0.6 Ma; Amarc Resources Ltd., unpublished data, reported in McClenaghan, 2013) intruded by coeval quartz-feldspar porphyry (70.9 ± 0.5 Ma; Amarc Resources Ltd., unpublished data, reported in McClenaghan, 2013) and feldspar-quartz-hornblende porphyry (72.10 ± 0.48 Ma; this work) stocks and dikes, and a late diorite body (69.32 ± 0.43 Ma; this work). The timing of gold mineralization was constrained by Re-Os dating of molybdenite in a quartz-calcite-pyrite-molybdenite vein at 72.1 ± 0.3 Ma (McClenaghan, 2013). Gold is mainly present as electrum and gold-silver telluride in disseminated pyrite and minor marcasite associated with quartz-sericite

alteration in the felsic volcanic rocks and porphyries. Three stages of mineralization are recognized: stage 1 disseminate pyrite with gold and minor quartz-pyrite ± molybdenite veins; stage 2 disseminated marcasite with gold; and stage 3 polymetallic-sulfide-carbonate veins (pyrite-chalcopyrite-sphalerite-arsenopyrite-calcite). Stages 1 and 2 are related to quartz-sericite alteration, whereas the stage 3 veins cut across quartz-sericite altered rocks, and lack noticeable alteration selvedges. New fluid inclusion data combined with stable isotope data from McClenaghan (2013) indicate that a relatively hot and saline fluid (~313°C, ~4.8 wt.% NaCl equiv.) of probable magmatic origin was likely responsible for the first stage of mineralization. The coprecipitation of gold with pyrite/marcasite in the sericitized wallrocks likely reflects a combination of cooling and wallrock sulfidation reactions, while lesser gold may have been precipitated in rare quartz-sulfide veinlets by boiling.

Newton is thought to be typical of deep intermediate-sulfidation-style gold deposits related to the shallow parts of porphyry systems, and there is some evidence in the presence of rare hypersaline fluid inclusions and localized potassic alteration for the presence of such a system at depth, although this has not been explored to date.

2.11 References

Albinson, T., Norman, D.I., Cole, D., and Chomiak, B., 2001, Controls on formation of low-sulfidation epithermal deposits in Mexico: Constraints from fluid inclusion and stable isotope data: Society of Economic Geology Special Publication 8, p. 1–32.

Andrew, K.P.E., 1988, Geology and genesis of the Wolf precious metal epithermal prospect and the Capoose base and precious metal porphyry-style prospect, Capoose Lake area, central British Columbia: MSc. thesis, University of British Columbia, Vancouver, 334 p.

Atwater, T., 1989, Plate tectonic history of the northeast Pacific and western North America, in Winterer, E.L., Hussong, D.M., and Decker, R.W., eds., The eastern Pacific Ocean and Hawaii: Boulder, Colorado, Geological Society of America, Geology of North America, v. N, p. 21–72.

Bevier, M.L., 1983, Implications of Chemical and Isotopic Composition for Petrogenesis of

Chilcotin Group Basalts, British Columbia: Journal of Petrology, v. 24, p. 207–226.

Bevier, M.L., 1983, Regional stratigraphy and age of Chilcotin Group basalts, south-central British Columbia: Canadian Journal of Earth Sciences, v. 20, p. 515–524.

Briqueu, L., Bougault, H., Joron, J.L., 1984, Quantification of Nb, Ta, Ti and V anomalies in magmas associated with subduction zones: petrogenetic implications: Earth and Planetary Science Letters, v. 68, p. 297–308.

Brown, G.G., Thorpe, R.S., and Webb, P.C., 1984, The geochemical characteristics of granitoids in contrasting arcs and comments on magma sources: Journal of the Geological Society, v. 141, p. 413–426.

Bodnar, R.J., Burnham, C.W., and Sterner, S.M., 1985, Synthetic fluid inclusions in natural quartz. III. Determination of phase equilibrium properties in the system H_2O-NaCl to 1000°C and 1500 bars: Geochimica et Cosmochimica Acta, v. 49, p. 1861-1873

Bodnar, R.J., 1993, Revised equation and table for determining the freezing point depression of H_2O-NaCl solutions: Geochimica et Cosmochimica Acta, v. 57, p. 683–684.

Bodnar, R.J., and Vityk, M.O., 1994, Interpretation of microthermometric data for H_2O-NaCl fluid inclusions, in DeVivo, B., and Frezzotti, M.L., eds., Fluid inclusions in minerals: Methods and applications: Blacksburg, VA, Virginia Polytechnic Institute and State University, p. 117–130.

Bordet, E., Hart, C, and McClenaghan, L., 2011, Epithermal-style Au-Ag mineralization in Cretaceous to Eocene felsic volcanic complexes, central British Columbia, western Canada, in: Barra, F., Reich, M., Campos, E., Tornos, F., eds., Let's Talk Ore Deposits Proceedings of the Eleventh Biennial SGA Meeting Ediciones Universidad Catolica del Norte, Antofagasta, Chile, p. 714–716.

Bozzo, A.T., Chen, H.S., Kass, J.R., and Barduhn, A.J., 1975, The properties of the hydrates of chlorine and carbon dioxide: Desalination, v. 16, p. 303–320.

Buchanan, L.J., 2000, The geology of the San Cristobal deposit: Society of Mining Engineers, Abstracts with Programs, Annual Meeting, p. 60.

Candela, P.A., 1992, Controls on ore metal ratios in granite-related ore systems: An experimental

and computational approach: Transactions of the Royal Society of Edinburgh, Earth Sciences, v. 83, p. 317–326.

Chang, Z., Hedenquist, J.W., White, N.C., Cooke, D.R., Roach, M., 2011, Exploration Tools for Linked Porphyry and Epithermal Deposits: Example from the Mankayan Intrusion-Centered Cu-Au District, Luzon, Philippines: Economic Geology, v. 106, p. 1365–1398.

Christie, G., Lipiec, I.T., Simpson, R.G., Horton, J., Borntraeger, B., 2014, Technical report on feasibility study of the Blackwater Gold deposit, British Columbia: New Gold Inc. NI43–101 Report, 336 p.

Colpron, M., and Price, R.A., 1995, Tectonic significance of the Kootenay terrane, southeastern Canadian Cordillera: An alternative model: Geology, v. 23, p. 25–28.

Colpron, M., Nelson, J.L. and Murphy, D.C., 2006, A tectonostratigraphic framework for the pericratonic terranes of the northern Canadian Cordillera, in Colpron, M. and Nelson, J.L., eds., Paleozoic Evolution and Metallogeny of Pericratonic Terranes at the Ancient Pacific Margin of North America, Canadian and Alaskan Cordillera: Geological Association of Canada Special Paper 45, p. 1–23.

Cooke, D.R., McPhail, D.C., and Bloom, M.S., 1996, Epithermal gold mineralization, Acupan, Baguio district, Philippines: Geology, mineralization, alteration, and the thermochemical environment of ore deposition: Economic Geology, v. 91, p. 243–272.

Cooke, D.R., Deyell, C.L., Waters, P.J., Gonzales, R.I., and Zaw, K., 2011, Evidence for Magmatic-Hydrothermal Fluids and Ore-Forming Processes in Epithermal and Porphyry Deposits of the Baguio District, Philippines: Economic Geology, v. 106, p. 1399–1424.

Diamond, L.W., 1992, Stability of CO_2 clathrate hydrate + CO, liquid + CO_2 vapour + aqueous KCl-NaCl solutions: Experimental determination and application to salinity estimates of fluid inclusions: Geochimica et Cosmochimica Acta, v. 56, p. 273–280.

Edwards, B.R., and Russell, J.K., 1999, Northern Cordilleran volcanic province: A northern Basin and Range: Geology, v. 27, p. 243–246.

Edwards, B.R., and Russell, J.K., 2000, Distribution, nature, and origin of Neogene-Quaternary magmatism in the northern Cordilleran volcanic province, Canada: GAS bulletin, v. 112, p.

1280–1295.

Einaudi, M.T., Hedenquist, J.W., and Inan, E., 2003, Sulfidation state of hydrothermal fluids: The porphyry-epithermal transition and beyond: Society of Economic Geologists Special Publication 10, p. 285−313.

Engebretson, D.C., Cox, Allan, and Gordon, R.G., 1985, Relative motions between oceanic and continental plates in the Pacific Basin: Geological Society of America, Special Paper 206, 59 p.

English, J.M., and Johnston, S.T., 2004, The Laramide Orogeny: What were the Driving Forces?: International Geology Review, v. 46, p. 833–838.

Friedman, R., Diakow, L., Lane, R., and Mortensen, J., 2001, New U Pb age constraints on latest Cretaceous magmatism and associated mineralization in the Fawnie Range, Nechako Plateau, central British Columbia: Canadian Journal of Earth Sciences, v. 38, p. 619–637.

Gabrielse, H., 1991, Late Paleozoic and Mesozoic terrane interactions in north-central British Columbia: Canadian Journal of Earth Sciences, v. 28, p. 947–957.

Gabrielse, H., and Yorath, C.J., 1991, The Cordilleran orogen in Canada. Geoscience Canada, v. 16, p. 67–83.

Gabrielse, H., Murphy, D.C. and Mortensen, J.K., 2006, Cretaceous and Cenozoic dextral orogen-parallel displacements, magmatism and paleogeography, north-central Canadian Cordillera, in Haggart, J.W., Monger, J.W.H., and Enkin, R.J., eds., Paleogeography of the North American Cordillera: Evidence For and Against Large-Scale Displacements: Geological Association of Canada Special Paper 46, p. 255–276.

Gill, J.B., 1981, Orogenic andesites and plate tectonics: New York, Springer-Verlag, 390 p.

Gillespie, J.M., and Heller, P.L., 1995, Beginning of foreland subsidence in the Columbian-Sevier belts, southern Canada and northwest Montana: Geology, v. 23, p. 723–726.

Goldstein, R.H., 2003, Petrographic analisys of fluid inclusions, in Samson, I., Anderson, A., and Marshall, D., eds., Fluid inclusions: Analysis and interpretation: Mineralogical Association of Canada, Short Course Handbook, v. 32, p. 9–53.

Goldstein, R.H., and Reynolds, T.J., 1994, Systematics of fluid inclusions in diagenetic minerals:

Society of Economic Paleontologists and Mineralogists, Short Course Handbook, v. 31, 199 p.

Green, T.H., and Pearson, N.J., 1985. Experimental determination of REE partition coefficients between amphibole and basaltic to andesitic liquids at high pressure. Geochimica et Cosmochimica Acta, v. 49, p. 1465–1468.

Gromet, L.P., Silver, L.T., 1983. Rare earth element distributions among minerals in a granodiorite and their petrogenetic implications. Geochimica et Cosmochimica Acta, v. 47, p. 925–939.

Haas, J.L., 1971, The effect of salinity on the maximum thermal gradient of a hydrothermal system at hydrostatic pressure: Economic Geology, v. 66, p. 940–946.

Hanson, G., 1980, Rare earth elements in petrogenetic studies of igneous systems: Annual Review of Earth and Planetary Sciences, v. 8, p. 371–406.

Harms, T. A., 1986, Structural and tectonic analysis of the Sylvester Allochthon, SW McDame map area, northern British Columbia: Implications for paleogeography and accretion, Ph.D. thesis, University of Arizona, Tucson, America, 80 p.

Hedenquist, J.W., Arribas, A., Gonzalez-Urien, E., 2000, Exploration for epithermal gold deposits: Reviews in Economic Geology, v. 13, p. 245–277.

Hoskin, P.W.O., 2000, Patterns of chaos: Fractal statistics and the oscillatory chemistry of zircon: Geochimica et Cosmochimica Acta, v. 64, p. 1905–1923.

Lamb, S., Hoke, L., Kennan, L., and Dewey, J., 1997, Cenozoic evolution of the Central Andes in Bolivia and northern Chile: Geological Society [London] Special Publication 121, p. 237–264

Lane, R.A., and Schroeter, T.G., 1997, A review of metallic mineralization in the Interior Plateau, central British Columbia, in: Diakow, L.J., and Newell, J.M., eds., Interior Plateau Geoscience Project, Summary of Geological, Geochemical and Geophysical Studies, BCGS Survey Branch Open File 1996-2, p. 237–256.

Lepitre, M.E., Mortensen, J.K. Friedman, R.M., and Jordan, S.J., 1998, Geology and U-Pb geochronology of intrusive rocks associated with mineralization in the northern Tahtsa

Lake district, west-central British Columbia, in Geological Fieldwork 1997, British Columbia Ministry of Energy and Mines, Paper 1998-1, p. 1–32.

Ludwig, K.R., 2003, Isoplot/Ex, a geochronological toolkit for Microsoft Excel, Version 3.00: Berkeley Geochronology Center, Special Publication No. 4, p. 1–43.

Lynch, G., 1995, Geochemical polarity of the Early Cretaceous Gambier Group, southern Coast Belt, British Columbia: Canadian Journal of Earth Sciences, v. 32, p. 675–685.

MacIntyre, D.G., Ash, C., and Britton, J., 1994, Geological compilation, Skeena-Nass area, west-central British Columbia, NTS 93E, L, M; 94D; 103G, H, I, J, P; 104A, B: British Columbia Ministry of Energy, Mines and Petroleum Resources, Open File 1994–14.

Marini, L., Moretti, R., and Accornero, M., 2011, Sulfur Isotopes in Magmatic-Hydrothermal Systems, Melts, and Magmas: Reviews in Mineralogy & Geochemistry, v. 73, p. 423–492

Massey, N.W.D., MacIntyre, D.G., Desjardins, P.J., Cooney, R.T., 2005, Digital geology map of British Columbia; whole province: British Columbia Ministry of Energy, Mines and Petroleum Resources, Open-File 2005–01.

McClenaghan, L., 2013, Geology and Genesis of the Newton Bulk-Tonnage Gold-Silver Deposit, Central British Columbia: Unpublished M.Sc. thesis, Vancouver, British Columbia, University of British Columbia, 186 p.

McLaren, G., and Rouse, J., 1989, Geology and Geochemistry of the Taseko Lakes Area (NTS 092O/3, 4, 5, 6): British Columbia Ministry of Energy, Mines and Petroleum Resources, Open File 1989–25.

McMillan, W.J., Thompson, J.F.H., Hart, C.J.R., and Johnston, S.T., 1995, Regional geological and tectonic setting of porphyry deposits in British Columbia and Yukon Territory, in Schroeter, T.G., ed., Porphyry deposits of the northwestern Cordillera of North America: Canadian Institute of Mining, Metallurgy and Petroleum, Special Volume 46, p. 40–57.

Middlemost, E.A.K., 1994, Naming materials in the magma/igneous rock system: Earth-Science Reviews, v. 37, p. 215–224.

Mihalasky, M.J., Bookstrom, A.A., Frost, T.P., and Ludington, S., 2011, Porphyry Copper Assessment of British Columbia and Yukon Territory, Canada: U.S. Geological Survey

Scientific Investigations Report 2010-5090-C, v.1.1, 128 p.

Mikucki, J.E., 1998, Hydrothermal transport and depositional processes in Archean lode–gold systems: A review: Ore Geology Review, v. 13, p. 307–321.

Monger, J., and Price, R., 2002, The Canadian Cordillera: Geology and Tectonic Evolution: CSEG Recorder, v. 2, p.17–36.

Naney, M.T., 1983, Phase equilibria of rock-forming ferromagnesian silicates in graniticsystems: American Journal of Science, v. 283, p. 993–1033.

Nelson, J., and Colpron, M., 2007, Tectonics and metallogeny of the British Columbia, Yukon and Alaskan Cordillera, 1.8 Ga to the present, in Goodfellow, W.D., eds., Mineral Deposits of Canada: A Synthesis of Major Deposit-Types, District Metallogeny, the Evolution of Geological Provinces, and Exploration Methods: Geological Association of Canada, Mineral Deposits Division, Special Publication No. 5, p. 755–791.

Noble, D.C., Eyzaguirre, V.R., and McKee, E.H., 1990, Precious-metal mineralization of Cenozoic age in the Andes of Peru: Circum-Pacific Council for Energy and Mineral Resources, Earth-Science Series, v. 11, p. 207–212.

Nokleberg, W.J., Parfenov, L.M., Monger, J. W. H., Norton, I.O., Khanchun, A.I., Stone, D.B., Scotese, C.R., Scholl, D.W., and Fujita, K., 2000, Phanerozoic Tectonic Evolution of the Circum-North Pacific: U.S. Geological survey Professional Paper 1626, 122 p.

Nokleberg, W.J., Bundtzen, T., Eremin, R.A., Ratkin, V.V., Dawson, K.M., Shpikerman, V.V., Goryachev, N.A., Byalobzhesky, S.G., Frolov, Y.F., Khanchuck, A.I., Koch, R.D., Monger, J.W.H., Pozdeev, A.A., Rozenblum, I.S., Rodionov, S.M., Parfenov, L.M., Scotese, C.R. and Sidorov, A.A., 2005, Metallogenesis and tectonics of the Russian Far East, Alaska and the Canadian Cordillera: U.S. Geological Survey Professional Paper 1697, 397 p.

Parrish, R.R., Carr, S.D., and Parkinson, D.L., 1988, Eocene extensional tectonics and geochronology of the southern Omineca Belt, British Columbia and Washington: Tectonics, v. 7, p. 181–212.

Pearce, J.A., Harris, N.B.W., and Tindle, A.G., 1984, Trace element discrimination diagrams for the tectonic interpretation of granitic rocks: Journal of Petrology, v. 25, p. 956-983.

Peccerillo, A., and Taylor, S.R., 1976, Geochemistry of Eocene calc-alkaline volcanic rocks from the Kastamonu area, northern Turkey: Contributions to Mineralogy and Petrology, v. 58, p. 63–81.

Pressacco, R., 2012, Technical report on the initial mineral resource estimate for the newton project, central British Columbia, Canada: Amarc Resources Ltd. NI43–101 report, 154 p.

Richards, J.P., 2003, Tectono-magmatic precursors for porphyry Cu-(Mo-Au) deposit formation: Economic Geology, v. 98, p. 1515–1533.

Riddell, J. M., 2006, Geology of the Southern Nechako Basin NTS 92N, 92O, 93B, 93C, 93F, 93G: British Columbia Ministry of Energy, Mines and Petroleum Resources, Open-File 2006–01.

Riddell, J., 2011, Lithostratigraphic and tectonic framework of Jurassic and Cretaceous Intermontane sedimentary basins of south-central British Columbia: Canadian Journal of Earth Sciences, v. 48, p. 870–896.

Roback, R. C., Sevigny, J. H., Walker, N. W., 1994, Tectonic setting of the Slide Mountain terrane, southern British Columbis: Tectonics, v. 13, p. 1242–1258.

Roedder, E., and Bodnar, R.J., 1980, Geologic pressure determinations from fluid inclusion studies: Annual Review of Earth and Planetary Sciences, v. 8, p. 263–301.

Roedder, E., 1984, Fluid inclusions: Reviews in Mineralogy, v. 12, 644 p.

Rollinson, H., 1993, Using Geochemical Data: Evaluation, Presentation, Interpretation, 352 p.

Seward, T.M., 1989, The hydrothermal chemistry of gold and its implications for ore formation: Boiling and conductive cooling as examples, in: Keays, R.R., Ramsay, W.R.H., Groves, D.I., eds., The Geology of Gold Deposits: The Perspective in 1988, Economic Geology Monograph Series, v. 6, p. 398–404.

Seward, T.M., 1991, The hydrothermal geochemistry of gold, in: Foster, R.P., ed., Gold Metallogeny and Exploration, p. 37–62.

Sheppard, S.M.F., 1977, Identification of the origin of oreforming solutions by the use of stable isotopes: Geological Society, London, Special Publications, v. 7, p. 25–41.

Sheppard, S., and Gilg, H., 1996, Stable isotope geochemistry of clay minerals: Clay Minerals, v.

31, p. 1–24.

Sillitoe, R.H., and Hedenquist, J.W., 2003, Linkages between volcanotectonic settings, ore-fluid compositions, and epithermal precious-metal deposits: Society of Economic Geologists Special Publication 10, p. 315−343.

Sisson, T.W., 1994, Hornblende-melt trace-element partitioning measured by ion microprobe: Chemical Geology, v. 117, p. 331–344.

Simonetti, A., Heaman, L.M., Hartlaub, R.P., Creaser, R.A., MacHattie, T.G., Bohn, C., 2005, U–Pb zircon dating by laser ablation-MC-ICP-MS using a new multiple ion counting Faraday collector array: Journal of Analytical Atomic Spectrometry, v .20, p. 677–686.

Stacey, J.S., and Kramers, J.D., 1975, Approximation of terrestrial lead isotope evolution by a two-stage model: Earth and Planetary Science Letters, v. 26, p. 207–221.

Sterner, S.M., Hall, D.L., and Bodnar, R.J., 1988, Synthetic fluid inclusions. V. Solubility relations in the system NaCl-KCl-H_2O under vapor-saturated conditions: Geochimica et Cosmochimica Acta, v. 52, p. 989–1005.

Stock, J., and Molnar, P., 1988, Uncertainties and implications of the Late Cretaceous and Tertiary position of North America relative to the Farallon, Kula, and Pacific plates: Tectonics, v. 7, p. 1339–1384.

Sun, S.S., and McDonough, W.F., 1989, Chemical and isotopic systematics of oceanic basalts: Implications for mantle composition and processes. Geological Society of London Special Publication, v. 42: p. 313–345.

Umhoefer, P.J. and Schiarizza, P., 1996, Latest Cretaceous to early Tertiary dextral strike-slip faulting on the southeastern Yalakom fault system, southeastern Coast belt, British Columbia: Geological Society of America Bulletin, v. 108, p. 768–785.

Wheeler, J.O., Brookfield, A.J., Gabrielse, H., Monger, J.W.H., Tipper, H.W. and Woodsworth, G.J., 1991, Terrane map of the Canadian Cordillera: Geological Survey of Canada, Map 1713A, scale 1: 2 000000.

Chapter 3 The Morrison porphyry Cu-Au-Mo deposit, Babine Lake area, British Columbia

3.1 Introduction

The Morrison porphyry deposit is located in the northern Babine Lake area of central British Columbia (Fig. 3-1). Several porphyry copper deposits related to early Cenozoic dioritic to granitic porphyry intrusions occur in this area, including the Bell, Granisle, Nakinilerak, Dorothy, North Newman, South Newman, Hearne Hill, and Morrison deposits (Fig. 3-2; Carson and Jambor, 1974; Carter, 1982; Zaluski et al., 1994; Nokleberg et al., 2005). However, only three of these deposits contain resources that are considered economic or close to economic: the Bell (77.2 million tonnes @ 0.48% Cu), Granisle (52.7 million tonnes @ 0.43% Cu), and Morrison (207 million tonnes @ 0.39% Cu) (Carson and Jambor, 1974; Carson and Jambor, 1976; Fahrni et al., 1976; Dirom et al., 1995; Simpson and Geo, 2007). The Bell and Granisle deposits were important past Cu-Au producers but both closed in 1992, whereas the Morrison deposit has not yet been mined to date (Carter et al., 1995; Simpson and Geo, 2007).

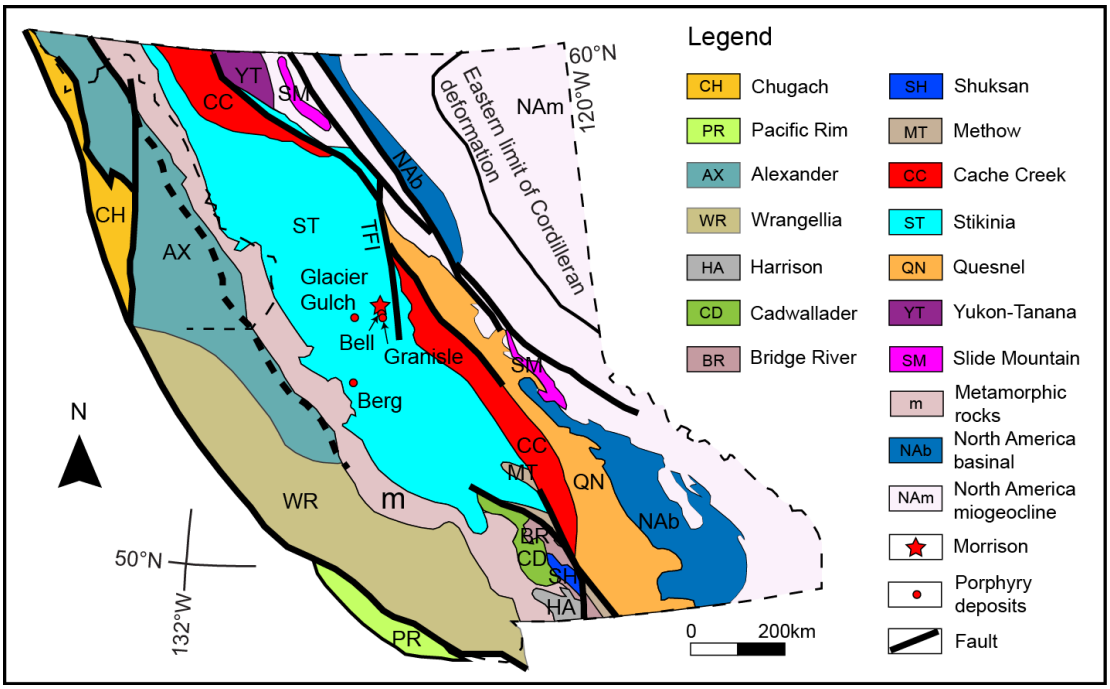

Fig. 3-1. Terrane map of the British Columbian Cordillera, showing the location of the Morrison and other early Cenozoic porphyry Cu deposits in the central Stikinia terrane. Fault abbreviation: TFI = Takla-Finlay-Ingenika fault system. Modified from Nelson and Colpron (2007).

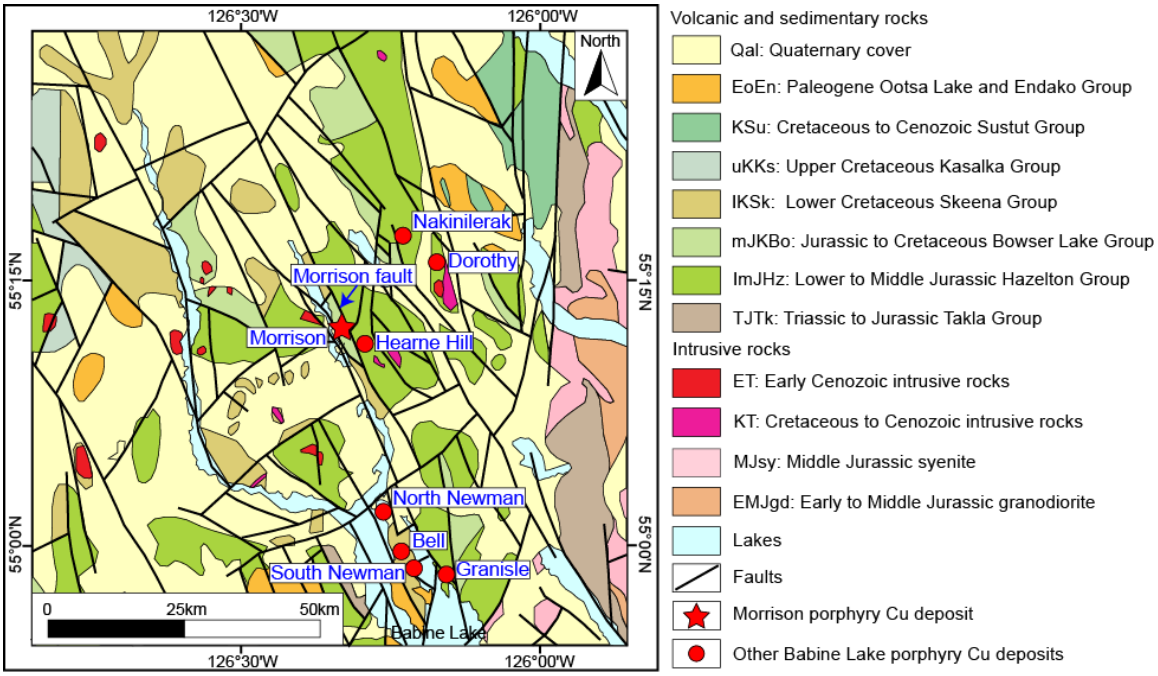

Fig. 3-2. Regional geological map of the Babine Lake area and its surroundings. Modified from Massey et al. (2005).

The Morrison porphyry Cu-Au-Mo deposit is located 65 km northeast of Smithers in central British Columbia (55°11'N, 126°18'W), and is spatially associated with Eocene dioritic to granodioritic plagioclase-hornblende-biotite porphyry stocks and dikes, which intruded siltstones and greywackes of the Middle to Upper Jurassic Ashman Formation of the Bowser Lake Group (Carson and Jambor, 1976; Simpson and Geo, 2007).

The Morrison deposit was first discovered by Noranda Mines Limited in 1963 during a stream sediment sampling program (Simpson and Geo, 2007). A comprehensive study was conducted at the deposit from 1963–1973, including geological mapping and diamond core drilling (95 holes with a total length of 13,890 m; Carson and Jambor, 1976; Simpson and Geo, 2007). Two mineralized zones were outlined northwest and southeast of a small central lake, which are interpreted to be offset by a fault (the East Fault in Fig. 3-3).

Pacific Booker Minerals acquired the Morrison property in 1997, and drilled a further 96 holes (26,202 m) by 2007 (Simpson and Geo, 2007). This work has defined a measured and

indicated resource of 207 Mt with average grades of 0.39% Cu, 0.2 g/t Au, and 0.005% Mo (0.3% Cu equiv. cut-off; Simpson and Geo, 2007).

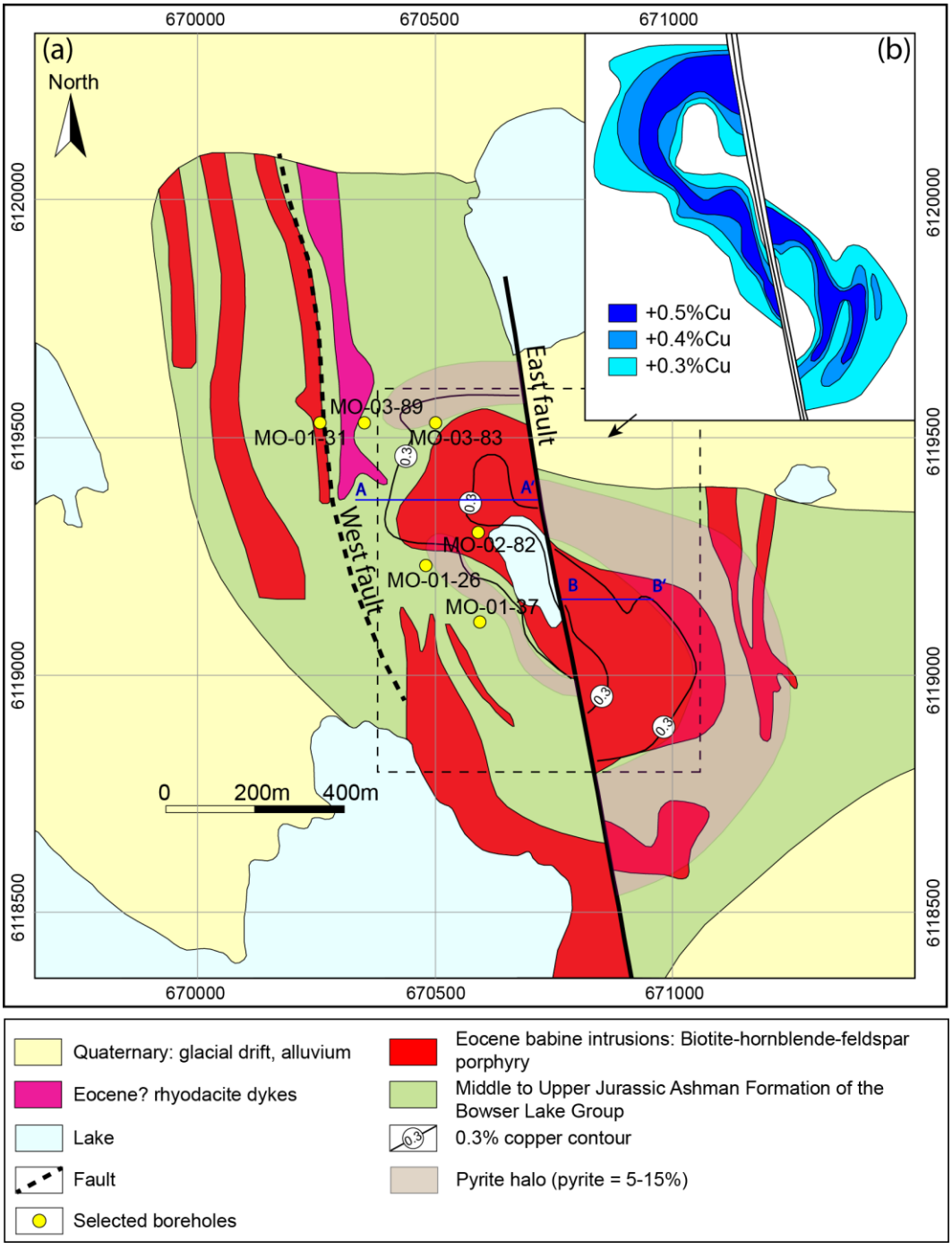

Fig. 3-3. (a) Geological map of the Morrison porphyry Cu deposit; (b) Copper contour map. Cross-section lines for figure 3-4 are shown on the map. Modified from Carson and Jambor (1976) and Simpson and Geo (2007).

Previous studies of the Morrison Cu-Au-Mo deposit were undertaken in the 1970s by Carson and Jambor (1976), and consisted of detailed geological descriptions and assay data. More recently, Ogryzlo and Dirom (1995) reported whole-rock geochemical analyses for several intrusions from other Babine Lake area.

A K-Ar age of 52.1 ± 2.1 Ma was reported for the plagioclase-hornblende-biotite porphyry intrusion at Morrison by Carter (1982), and a more accurate $^{40}Ar/^{39}Ar$ age of 53.2 ± 0.5 Ma was reported by MacIntyre et al. (2001).

The aim of this study is to describe the geological features, determine the ore-forming history, and identify the main controls on ore formation at Morrison. We present new petrological and whole-rock geochemical data for the porphyry intrusions associated with the deposit, geochronological data for one of the intrusions (zircon, U-Pb) and hydrothermal molybdenite (Re-Os), and stable isotope and fluid inclusion data from different stages of mineralized veins. The data confirm that Morrison is typical of early Eocene porphyry Cu-Au-Mo deposits in central British Columbia.

3.2 Tectonic Setting and Regional Geology

Tectonic setting

The Morrison deposit is located in the central Stikinia terrane of the Canadian Cordillera (Fig. 3-1). The Canadian Cordillera comprises a number of allochthonous island arcs, oceanic terranes, and pericratonic terranes, which accreted to the western margin of the North American craton during the Middle Jurassic to late Mesozoic (Monger, 1977; Monger and Irving, 1980; Monger et al., 1982; Gabrielse et al., 1991; Monger and Price, 2002; Nelson and Colpron, 2007). As one of the allochthonous island arcs, the Stikinia terrane hosts a significant number of porphyry copper deposits, which formed both prior to and after the accretion events.

The Stikinia island arc was initiated in the Late Devonian, in response to subduction of the Panthalassa oceanic plate beneath ancestral North America (Nelson and Colpron, 2007; Logan and Mihalynuk, 2014). The Stikinia arc was separated from ancestral North America by a back-arc basin (Nelson and Colpron, 2007). The growth of the arc ceased during the Late

Permian to Middle Triassic following collision with the Kutcho island arc, which gave rise to uplift and erosion (the Tahltanian orogeny; Souther, 1971, 1972; English et al., 2003; Logan and Mihalynuk, 2014). Arc construction recommenced in the Late Triassic with deposition of new volcanic and sedimentary rocks. Consequently, the Stikinia terrane consists of a Devonian to Permian assemblage of volcanic rocks and carbonate sedimentary rocks (named the Stikinia assemblage), overlain by a Triassic to Jurassic sequence of volcanic and associated sedimentary rocks (e.g., the Triassic to Jurassic Takla Group and the Early to Middle Jurassic Hazelton Group in the Babine lake area; Massey et al., 2005; Logan and Mihalynuk, 2014). A suite of Late Triassic to Middle Jurassic intrusive rocks is associated with an early pulse of porphyry Cu mineralization in the Stikinia terrane (McMillan et al., 1995).

Several island arc terranes, such as Stikinia, Cache Creek, and Quesnellia, collided with the continental margin in the Middle Jurassic, resulting in closure of the middle Paleozoic-Mesozoic back-arc basin (Monger and Price, 2002; Nelson and Colpron, 2007). The Stikinia terrane then became part of a continental arc, with renewed deposition of volcanic and sedimentary rocks, including the Jurassic to Cretaceous Bowser Lake Group, Lower Cretaceous Skeena Group, Cretaceous to Tertiary Sustut Group, and the Paleogene Ootsa Lake and Endako Groups in the Babine Lake area (Fig. 3-2; Massey et al., 2005). The tectonic regime of the Cordillera at this time (Early Jurassic to late Paleocene) was characterized by compression and transpression during the Early Jurassic to late Paleocene, but changed to extension and transtension during the late Paleocene to Eocene.

Late Cretaceous to early Cenozoic intermediate-to-felsic plutons intruded the Mesozoic volcanic and sedimentary rocks along deep-seated strike-slip faults (Nokleberg et al., 2005; Nelson and Colpron, 2007), and are associated with a second pulse of post-accretionary porphyry Cu deposit formation in the Stikinia terrane (McMillan et al., 1995). Several porphyry deposits constitute the Skeena Arch metallogenic belt in central British Columbia, which are related to Eocene intrusive systems. These include: the Ajax, Bell Moly, and Kitsault Porphyry Mo deposits associated with the 54–48 Ma Alice Arm intrusive suite; the Berg porphyry Cu-Mo, and Ajax porphyry Mo deposits associated with the 54–48 Ma Nanika intrusions; the Equity Silver and

Prosperity-Porter Idaho Ag polymetallic vein deposits associated with the 50–57 Ma Goosly intrusions; the Bell, Gransile, and Morrison porphyry Cu-Au-Mo deposits associated with 54–50 Ma Babine Lake igneous suites; and the Endako porphyry Mo deposit associated with the 50.5 ± 0.5 Ma Francois Lake plutonic suite (Church, 1970, 1972; Carter, 1982; Grainger et al., 2001). These intrusions are calc-alkaline, quartz dioritic to granitic in composition, and form small stocks or dikes (typically less than 1 km in diameter; Carter, 1976), which are mostly emplaced along northwest- and northeast-striking faults (Woodsworth et al., 1991; Cater, 1982; Nokleberg et al., 2005).

Geology of the Babine Lake area

Mesozoic to early Cenozoic volcanic and associated sedimentary rocks form the host rocks for the porphyry deposits in the Babine Lake area. At Morrison, these rocks are composed of three main volcanic and sedimentary units: the Lower to Middle Jurassic Hazelton Group, the Middle Jurassic to Upper Jurassic Bowser Lake Group, and the Lower Cretaceous Skeena Group. These stratified rocks are intruded by Cretaceous to early Cenozoic stocks and dikes (Fig. 3-2).

The Hazelton Group consists mainly of andesitic volcanic rocks and marine to non-marine sedimentary rocks (Carter, 1976; Massey et al., 2005), whereas the Bowser Lake and Skeena Groups are composed mainly of marine to non-marine clastic sedimentary rocks deposited in a fluvial-deltaic to near shore shelf environment (MacIntyre, 2006).

These stratigraphic sequences were uplifted, downfaulted, and tilted by a series of faults in the Babine Lake area, in response to Late Cretaceous to Eocene transpressional to transtensional tectonics. Consequently, several linear horsts and grabens were generated. The Morrison deposit is located in a graben, which is bounded by an unnamed fault to the west and the Morrison Fault to the east (Fig. 3-2; Simpson and Geo, 2007). Within this graben, the Ashman Formation of the Bowser Lake Group forms the immediate host rocks to the Morrison porphyry deposit.

Two groups of faults are recognized in the Morrison area, with dominantly north to northwest, and east to northeast trends (Fig. 3-2; Massey et al., 2005). Carter (1976) suggested

that the faults controlled the emplacement of the Cretaceous to early Cenozoic plutonic rocks, and that the intrusions generally occur along the NNW-trending structures.

The Cretaceous to early Cenozoic plutonic suites mainly range from quartz diorite, quartz monzonite, granodiorite, to granite in composition (Carter, 1976; MacIntyre, 2006). In particular, the plagioclase-hornblende-biotite porphyry stocks and dikes of the Babine Lake intrusive suite are quartz-dioritic to granodioritic in composition (Carson and Jambor, 1974). These intrusions are associated with several porphyry deposits in the northern part of the Babine Lake area, including the Bell, Granisle, Nakinilerak, Dorothy, North Newman, South Newman, Hearne Hill, and Morrison deposits (Carson and Jambor, 1974).

3.3 Morrison Deposit Geology

The central part of the Morrison deposit is relatively well exposed, whereas the surrounding area is mostly covered by Quaternary alluvium and glaciofluvial till, and is heavily forested. In this study, we relied on the previous mapping and geological descriptions of Carson and Jambor (1976), supplemented by our own observations and sampling of a limited number of preserved drill cores. Six drill holes were selected for study (Fig. 3-3), which contain typical examples of the main lithological units, alteration styles, and mineralization types.

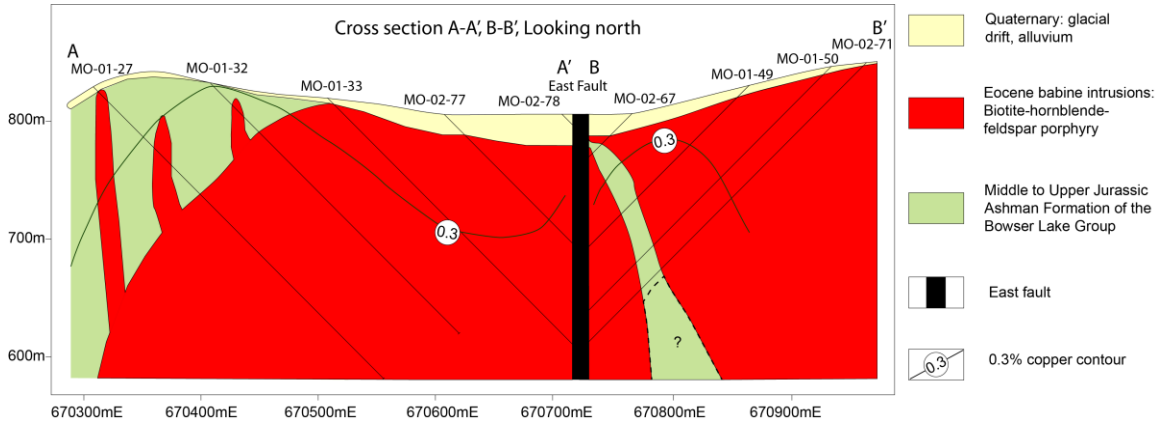

Fig. 3-4. Geological cross-section A-A', B-B' looking north. The cross section is quite schematic due to the limited drillhole coverage.

Eocene plagioclase-hornblende-biotite porphyry

A small stock of plagioclase-hornblende-biotite porphyry and associated dikes intrude the Ashman Formation in the centre of the Morrison property (Figs. 3-3, 3-4). The porphyry stock is interpreted to have been circular with a diameter of about 600 meters, but is now bisected and offset by a north-trending strike-slip fault, named the East Fault, which has a dextral offset of approximately 300 m (Simpson and Geo, 2007).

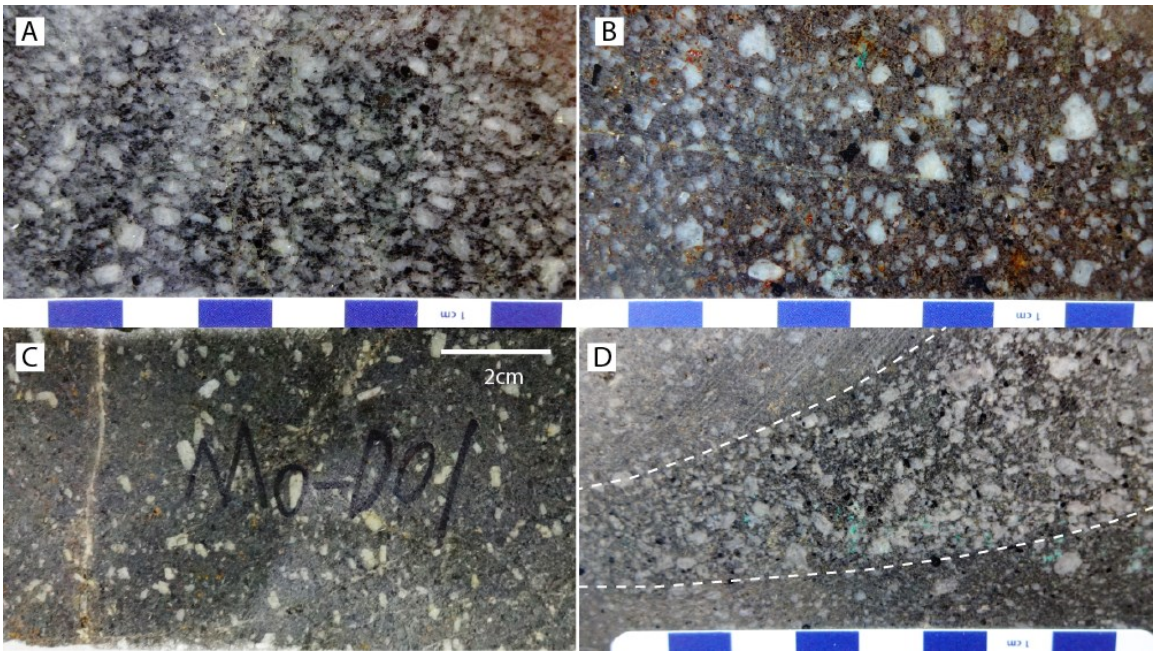

Fig. 3-5. Hand samples of the main intrusive units in the Morrison deposit: (A) Phase A plagioclase-hornblende-biotite porphyry (sample MO128). (B) Phase B plagioclase-hornblende-biotite porphyry (sample MO059). (C) Phase C plagioclase-hornblende-biotite porphyry (sample MO001). (D) Phase A plagioclase-hornblende-biotite porphyry (centre) cutting phase C plagioclase-hornblende-biotite porphyry (sample MO012).

Table 3-1 Characteristics of 3 phases plagioclase-hornblende-biotite porphyry from Morrison

Plagioclase-hornblende-biotite porphyry	Biotite phenocrysts	Hornblende phenocrysts	Plagioclase phenocrysts	Matrix
Phase 1	2-5 mm	3-8 mm	2-6 mm	fine-grained
	8-10%	12-15%	20-25%	50-60%
Phase 2	2-4 mm	3-6 mm	3-5 mm	fine-grained
	2-5%	8-10%	15-20%	65-75%
Phase 3	1-3 mm	3-5 mm	3-5 mm	fine-grained
	1-3%	4-7%	10-15%	75-85%

The plagioclase-hornblende-biotite porphyry is dark grey in color, dioritic to granodioritic in composition, and has a porphyritic texture (Fig. 3-5). The porphyry mainly consists of phenocrysts of biotite, plagioclase, and hornblende, and accessory magnetite and apatite, set in a fine-grained quartzofeldspathic matrix. Carson and Jambor (1976) suggested that the porphyry stock consists of multiple phases, and in this study three distinct phases of porphyry (phases A, B, C) were identified based on contrasting abundances and different grain sizes of phenocrysts (Fig. 3-5A–D; summarized in Table 3-1). Contacts between the three phases were rarely observed in drill cores, and the only boundary spotted in this study indicated that phase A porphyry intruded into phase C porphyry as shown in Figure 3-5D. However, cross-cutting relationships between phase B and phases A and C were not clear.

Sedimentary host rocks

The Ashman Formation sedimentary sequence in the Morrison area strikes N to NW, with a steep dip (Carson and Jambor, 1976). The sequence consists of marine pebble conglomerate at the base overlain by siltstone, sandstone, and greywacke (Simpson and Geo, 2007). The siltstone, which is dominant, is grey to dark-grey, fine- to medium-grained, and mainly composed of detrital quartz and feldspars.

Structure

The most significant structure is the East Fault, which trends north-northwest, dips vertically, and shows dextral strike-slip offset of the main porphyry stock of ~300 m (Figs. 3-3, 3-4; Carson and Jambor, 1976). Based on the description of the faults and sedimentary rocks by Carson and Jambor (1976), the fault is likely to be bedding parallel. Some vertical displacement is also thought to be present because the two segments of the porphyry stock do not fully match (Carson and Jambor, 1976). The East Fault ranges from a few meters to ~50 meters in width, and rocks are strongly fractured along its length. Sericite-carbonate alteration associated with polymetallic vein mineralization is associated with this structure.

Simpson and Geo (2007) also suggested the existence of a second NNW-trending fault cutting sedimentary rocks to the west of the main Morrison deposit (the West Fault), but this fault was not observed in this study.

3.4 Hydrothermal Alteration

Hydrothermal alteration (potassic, propylitic, sericite-carbonate, and argillic) has affected the central porphyry stock and surrounding siltstone at Morrison (Fig. 3-6). Potassic alteration mainly occurs in the central porphyry stock, with minor development in adjacent sedimentary rocks, whereas propylitic alteration mainly occurs in the sedimentary rocks, and only locally affects the porphyry as an overprint on potassic alteration. The potassic alteration is closely related to Cu mineralization, which occurs as vein-hosted and disseminated chalcopyrite and bornite in altered plagioclase-hornblende-biotite porphyry. In contrast, the propylitic-altered rocks only contain minor pyrite. Classic phyllic alteration (sericite-quartz-pyrite), which is common in other porphyry Cu deposits, does not occur at Morrison. Minor sericite-carbonate alteration is restricted to the East Fault, and is associated with late-stage polymetallic sulfide-carbonate veins. Argillic alteration is also restricted to the East Fault, and overprints all other alteration styles; it may be supergene in origin (i.e., related to groundwaters permeating the fault zone).

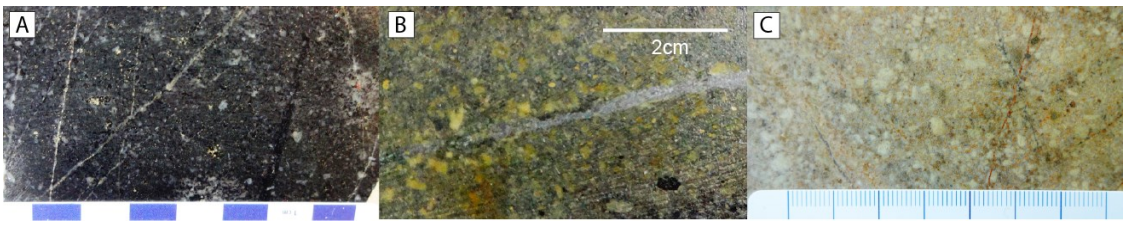

Fig. 3-6. Hand samples showing different alteration types at Morrison: (A) Potassic-altered phase C porphyry (sample MO100). (B) Chlorite alteration overprinting potassic alteration in phase B porphyry (sample MO004). (C) Clay-carbonate-altered phase A porphyry (sample MO037).

Potassic alteration

The potassic alteration is characterized by secondary biotite, which replaces hornblende phenocrysts and occurs as fine-grained crystals in the matrix (Fig. 3-7A). In strongly altered rocks,

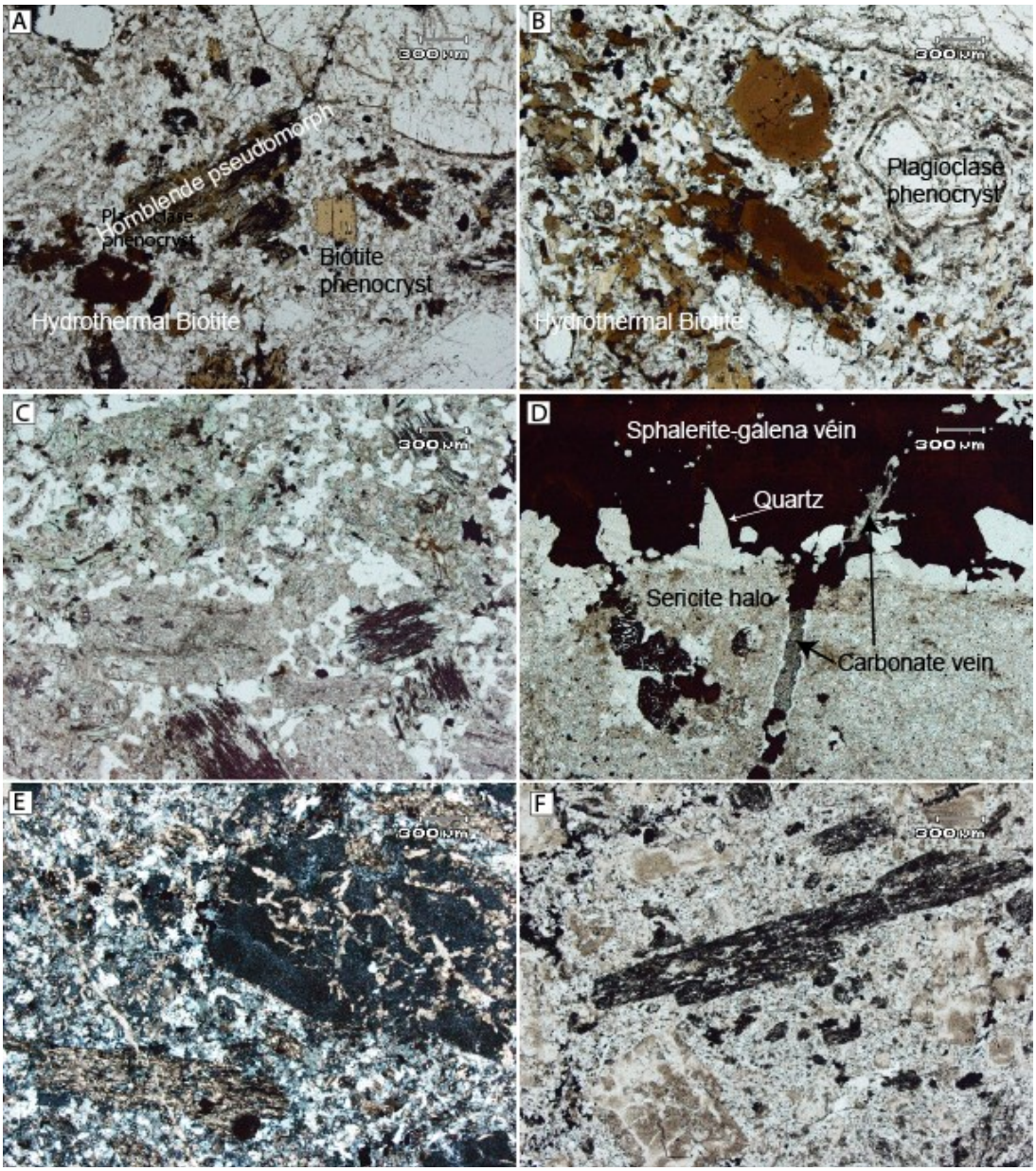

Fig. 3-7. Alteration styles in thin section (A–D and F in plane-polarized light; E in cross-polarized light). (A) Potassic alteration: hydrothermal biotite replaces a hornblende phenocryst, and also occurs in the matrix, whereas a biotite phenocryst was not affected (sample MO014). (B) Strong potassic alteration: the rims of igneous biotite phenocrysts are overgrown by hydrothermal biotite (sample MO010). (C) Chlorite-carbonate alteration: chlorite mainly replaces hornblende phenocrysts, whereas plagioclase and biotite phenocrysts are affected by hydrothermal carbonate minerals (sample MO004). (D) Sericite halo of a quartz-carbonate-polymetallic vein, and a carbonate veinlet cutting the sericite halo (sample MO072). (E) (F) Clay-carbonate alteration: hornblende, biotite, and plagioclase phenocrysts are all replaced by clay and carbonate minerals (sample MO020).

igneous biotite phenocrysts also show overgrowths of hydrothermal biotite (Fig. 3-7B). Early biotite veins are locally present in the potassic zone, with widths between 1–3 mm.

The degree of potassic alteration decreases from the center of the porphyry stock outwards. Hydrothermal biotite in strongly altered rocks is deep brown, coarse-grained, and well developed in the matrix, whereas in more weakly altered rocks it is greenish brown, fine-grained, and only present as alteration of hornblende phenocrysts (Carson and Jambor, 1976).

Propylitic alteration

Propylitic alteration is mainly characterized by secondary chlorite and carbonate minerals. Secondary chlorite replaces hornblende and locally biotite, and carbonate replaces plagioclase phenocrysts (Fig. 3-7C).

Sericite-carbonate and argillic alteration

Sericite-carbonate alteration is mainly characterized by secondary sericite and carbonate. The sericite is present as halos a few millimeters wide around polymetallic sulfide-carbonate veins, whereas dolomite occurs in the center of the veins (Fig. 3-7D).

Argillic alteration is characterized by kaolinite and carbonate minerals (Figs. 3-7E, F), which replace biotite, hornblende, and plagioclase phenocrysts, as well as the matrix of the porphyries. The clay and carbonate minerals in the argillic-altered rocks are primarily kaolinite and dolomite, respectively, based on the X-ray diffraction (XRD) analyses, and XRD results are presented in Appendix A. XRD analyses also identified the presence of other carbonate minerals, including minor ankerite, siderite, and rare calcite.

3.5 Vein relationships

A total of 5 vein types were identified at Morrison based on vein mineralogy and cross cutting relationship, including (1) early biotite (EB) veins; (2) stockwork veinlets of chalcopyrite ± quartz-bornite-pyrite; (3) quartz-chalcopyrite-bornite-pyrite veins with centerline sulfides; (4) quartz-molybdenite ± pyrite veins; (5) polymetallic sulfide-dolomite veins composed of dolomite with quartz-sphalerite-galena-arsenopyrite ± chalcopyrite (Fig. 3-8). These veins can be grouped

into three paragenetic stages based on similarities in timing, mineral assemblages, and related alteration assemblages (Fig. 3-9). Veins types 1 to 4 are associated with potassic alteration, whereas the type 5 veins are related to sericite-carbonate alteration.

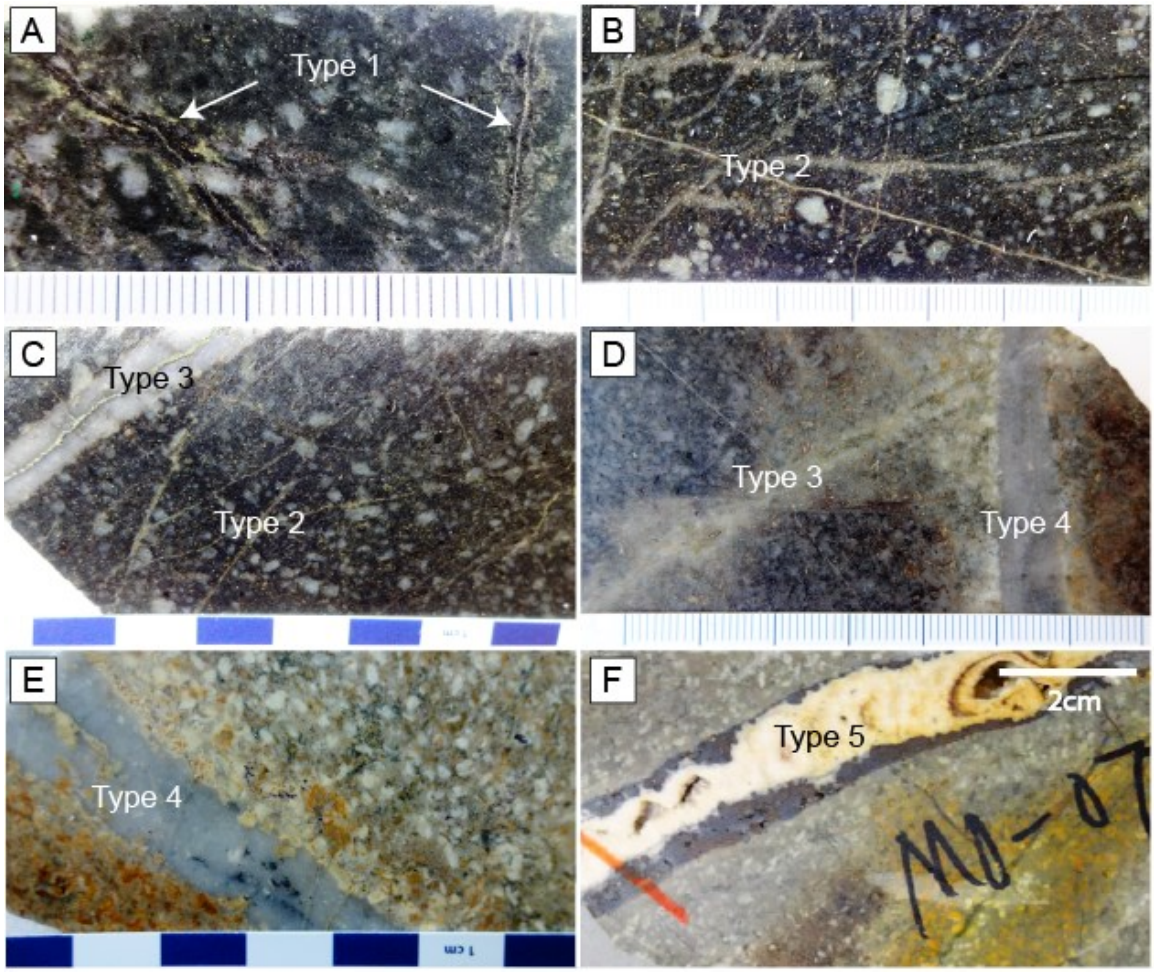

Fig. 3-8. Vein relationships in hand samples: (A) Type 1 biotite veins in strongly potassic-altered porphyry (sample MO010). (B) Type 2 stockwork veinlets of chalcopyrite-bornite-pyrite ± quartz in potassic-altered porphyry (sample MO135). (C) Type 3 quartz-chalcopyrite-bornite-pyrite vein cutting type 2 stockwork veinlets of chalcopyrite-bornite-pyrite ± quartz in potassic-altered porphyry (sample MO135). (D) Type 4 quartz-molybdenite-pyrite vein cutting a type 3 vein in weakly potassic-altered porphyry (sample MO099). (E) Type 4 quartz-molybdenite-pyrite vein in clay-carbonate-altered porphyry, which probably overprints earlier potassic alteration (sample MO098). (F) Type 5 dolomite-sphalerite-galena vein in clay-carbonate-altered porphyry, overprinting previous sericite-carbonate alteration (sample MO072).

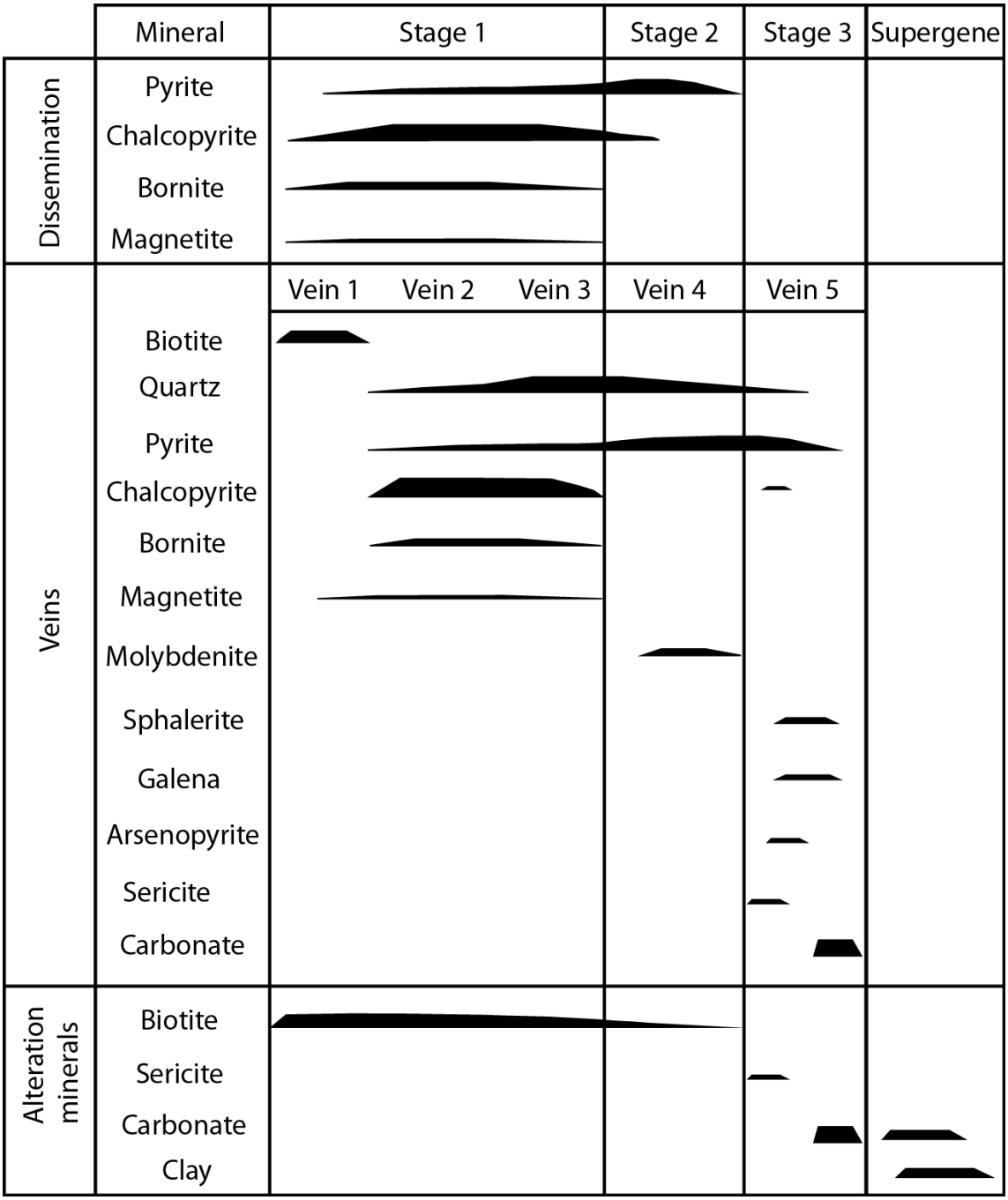

Fig. 3-9. Mineralized vein paragenesis based on hand sample observations and petrographic studies.

The early biotite (EB) veins (type 1) are rare, and only present in the strongly biotite-altered porphyry (Fig. 3-8A, B). These veins are usually 1–3 mm in width, and are mainly composed of dark brown biotite without sulfides. The type 2 and 3 veins are widespread in the biotite-altered porphyry, and are associated with the bulk of the Cu mineralization. Type 2 veins

are usually 1–2 mm in width, and consist of chalcopyrite, minor bornite, magnetite, and pyrite with or without quartz (Fig. 3-8C), whereas type 3 veins are straight, 3–5 mm in width, and mainly composed of coarse-grained quartz with a medial suture line of sulfides (mainly chalcopyrite and minor pyrite; Fig. 3-8D). The type 2 and 3 veins are similar to A and B veins of Gustafson and Hunt (1975). The type 4 quartz-molybdenite ± pyrite veins formed later than the type 2 and 3 veins, and are mainly present in weakly potassic-altered rocks (Fig. 3-8E). They are typically straight and 5–10 mm in width. Type 5 veins are the last hydrothermal stage at Morrison (Fig. 3-8G), and only occur in fractured zones around the East Fault, as infillings of fractures and breccias. These polymetallic sulfide-dolomite veins are 1 cm to a few cm in width, and consist of minor quartz at the vein margin, coarse-grained sulfides (sphalerite, galena, minor arsenopyrite, pyrite, and rare chalcopyrite), and late coarse-grained dolomite filling the vein center and in cross-cutting veinlets (Fig. 3-7D). Narrow (0.5–2 mm) alteration halos consist of sericite-carbonate.

3.6 Mineralization

Most Cu mineralization at Morrison is related to potassic alteration within the plagioclase-hornblende-biotite porphyries. All three phases of porphyry are mineralized, suggesting that they all immediately predated the mineralizing event. Two semicircular copper zones, termed the northwest and southeast zones, have average grades of 0.39% Cu (0.3% Cu cutoff), and are cut and offset by the East Fault (Figs. 3-3, 3-4). The copper zones are surrounded by well-developed annular pyrite halos (Fig. 3-3). Pyrite is usually associated with phyllic alteration in porphyry deposits, but at Morrison it is mainly associated with the chlorite-carbonate alteration. The ratio of chalcopyrite to pyrite decreases from the potassic to the propylitic zone. Some copper mineralization (>0.3% Cu) also occurs in the siltstone country rocks in the northwest zone, but is mainly restricted to the porphyry in the southeast zone (Carson and Jambor, 1976).

The mineralization can be divided into three stages (Figs. 3-9, 3-10). The first stage contains the bulk of the Cu mineralization, and includes vein types 1–3 (Fig. 3-10A–C). Carson and Jambor (1976) noted that seventy to eighty percent of the copper mineralization is hosted by stockworks and small veinlets in this first stage. Sulfides in stage 1 mineralization mainly consist

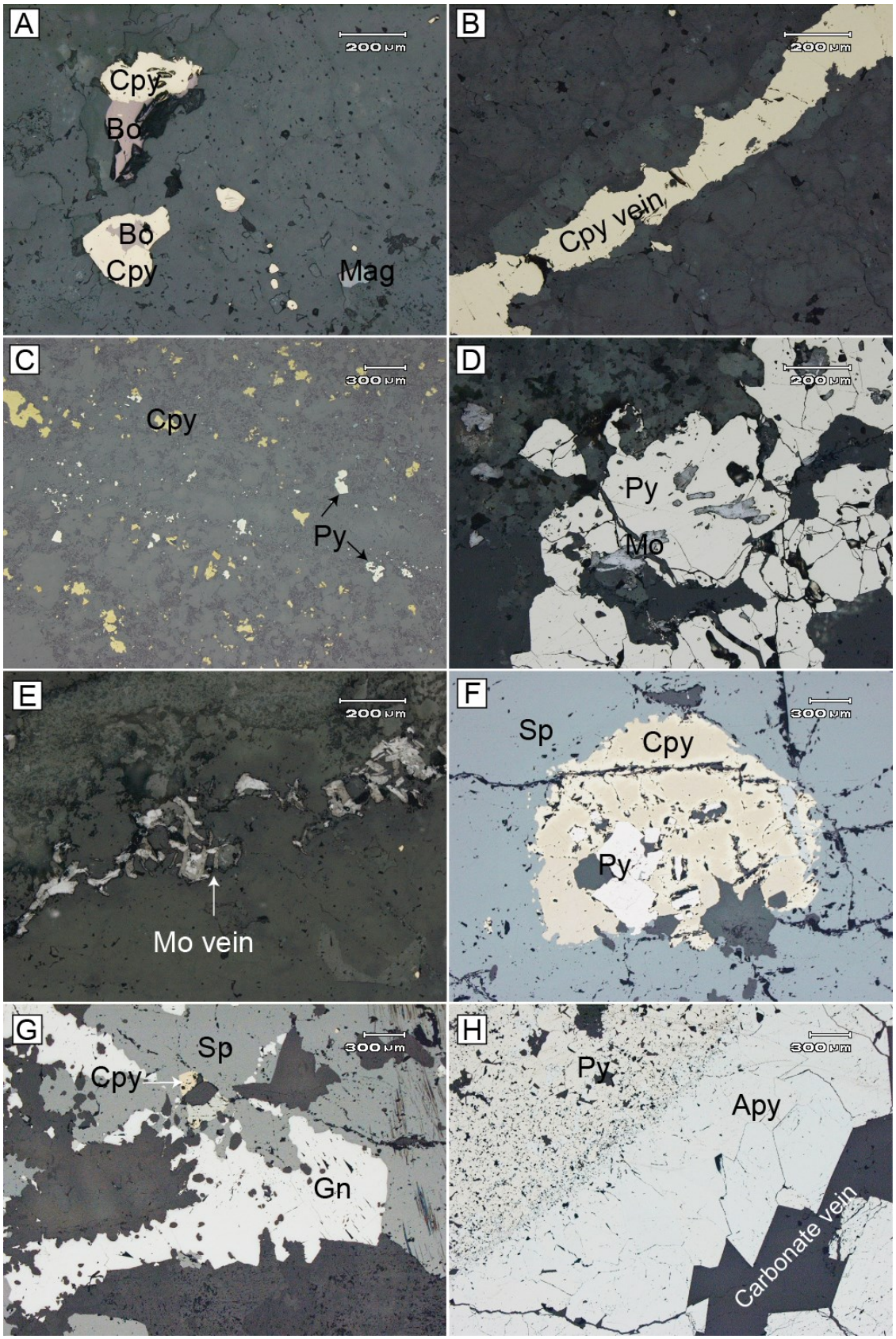
A
200 µm
Cpy
Bo
Bo
Cpy
Mag
B
200 µm
Cpy vein
C
300 µm
Cpy
Py
D
200 µm
Py
Mo
E
200 µm
Mo vein
F
300 µm
Sp
Cpy
Py
G
300 µm
Sp
Cpy
Gn
H
300 µm
Py
Apy
Carbonate vein

Fig. 3-10. Paragenetic relationships between sulfide minerals from the three mineralization stages: (photomicrographs taken in plane-polarized reflected light). Stage 1: (A) Disseminated chalcopyrite intergrown with bornite, accompanied by magnetite (sample MO144). (B) Type 3 chalcopyrite-quartz vein (sample MO135). (C) Disseminated chalcopyrite with minor pyrite (sample MO031). Stage 2: (D) Pyrite overgrowing molybdenite in a type 4 quartz vein (sample MO094). (E) A type 4 quartz-molybdenite vein (sample MO094). Stage 3: (F) Pyrite overgrown by chalcopyrite and then sphalerite in a type 5 polymetallic sulfide-dolomite vein (sample MO072). (G) Sphalerite intergrown with galena in a type 5 polymetallic sulfide-dolomite vein (sample MO072). (H) Pyrite overgrown by arsenopyrite with late dolomite infill in a type 5 polymetallic sulfide-dolomite vein (sample MO071).
Abbreviations: Apy = arsenopyrite, Bo = bornite, Cpy = chalcopyrite, Gn = galena, Mo = molybdenite, Py = pyrite, Sp = sphalerite.

of chalcopyrite, minor bornite, and pyrite, with minor magnetite in veins and disseminations, associated with potassic alteration.

The second stage of mineralization consists of molybdenite-pyrite veins, which mainly occur in weak potassic alteration (Fig. 3-10D, E). Molybdenite mineralization is not correlated with copper, and mainly occurs at the edge of the copper zone (Simpson and Geo, 2007). The molybdenum mineralization is not considered to be economic.

The third stage of mineralization consists of polymetallic sulfide-dolomite veins (sphalerite-galena-arsenopyrite-pyrite ± chalcopyrite; Fig. 3-10F–I), which are present along the East Fault zone. These veins are also considered to be uneconomic.

Gold was detected in the porphyry by assay analyses (207 million tonnes grading 0.2 g/t gold; Simpson and Geo, 2007), but the gold is invisible in hand samples and under the microscope. Gold appears to correlate with copper mineralization based on assay data (Ogryzlo et al., 1995).

3.7 Fieldwork and Analytical methods

Sample selection

A total of 33 drill-core samples from 6 selected diamond drill-holes were collected for this study. The samples are representative of the main lithological units, alteration facies, and mineralization styles in the Morrison deposit. Detailed samples descriptions are provided in Table 3-2, and sampled drill holes are marked on the geological map in Figure 3-3.

Lithogeochemistry

Nine samples of least-altered porphyry intrusions were collected for lithogeochemical analysis. These least-altered samples likely still contain some secondary biotite indicating weak potassic alteration, and many samples have a weak chlorite overprint. Whole-rock geochemical analyses were conducted by Activation Laboratories (Ancaster, Ontario, Canada), using instrumental neutron activation analysis and fusion ICP-MS methods (Actlabs code 4E Research + ICP/MS). As determined by reproducibility of standards and duplicates, accuracy is within 5 and 10 relative percent for major and trace elements, respectively. All major oxide compositions were recalculated to a volatile-free basis for plotting on classification diagrams.

Geochronology

A drill-core sample of phase A plagioclase-hornblende-feldspar porphyry (sample MO128 from drillhole MO-01-26, 215.8 to 217.3 m) was crushed and zircons were separated using standard gravimetric and magnetic methods followed by hand-picking. The zircons were mounted in epoxy, and polished to expose the crystal cores.

Zircons were dated using a multiple collector inductively coupled plasma-mass spectrometer (MC-ICP-MS; Nu-Plasma, Nu Instruments, UK) coupled to a frequency quintupled (λ = 213 nm) Nd:YAG laser ablation system (New Wave Research, USA) at the Canadian Center for Isotopic Microanalysis (CCIM), University of Alberta. Laser pits were approximately 30 μm in width and 20–30 μm in depth. The collector configuration and the analytical protocols are described in detail by Simonetti et al. (2005). International zircon standards (GJ-1-32 and LH94-15) were used for correction of mass bias, and the 2σ reproducibility of the standards was ~3% for U/Pb and 1% for $^{207}Pb/^{206}Pb$. Data are plotted using the Isoplot software (Ludwig, 2003). Concordia intercept ages were calculated by anchoring to a common Pb $^{207}Pb/^{206}Pb$ value of 0.83 ± 0.06 (Stacey and Kramers, 1975).

Two molybdenite samples were analyzed for Re-Os geochronology at the Radiogenic Isotope Facility, University of Alberta. The molybdenite occurs in 1–2 cm-wide type 4 quartz-molybdenite-pyrite veins. Pure molybdenite was separated from the veins by metal-free crushing,

Table 3-2 Sample information from Morrison

Sample ID	Borehole ID	East	North	Elevation (m)	Length (m)	Azimuth	Dip (°)	From (m)	To (m)	Interval (m)	Rock type	Alteration
MO001	MO-02-82	670568.25	6119307.16	800.88	280.42	270	-60	15.24	15.34	0.1	Phase C plagioclase-hornblende-biotite porphyry	Potassic alteration
MO004	MO-02-82	670568.25	6119307.16	800.88	280.42	270	-60	45.4	45.5	0.1	Phase B plagioclase-hornblende-biotite porphyry	Chlorite alteration overprinting potassic alteration
MO010	MO-02-82	670568.25	6119307.16	800.88	280.42	270	-60	116.77	116.87	0.1	Phase C plagioclase-hornblende-biotite porphyry	Potassic alteration
MO012	MO-02-82	670568.25	6119307.16	800.88	280.42	270	-60	136.5	136.65	0.15	Phase A plagioclase-hornblende-biotite porphyry (centre) cutting phase C plagioclase-hornblende-biotite porphyry	Potassic alteration
MO014	MO-02-82	670568.25	6119307.16	800.88	280.42	270	-60	145.6	145.75	0.15	Phase A plagioclase-hornblende-biotite porphyry	Potassic alteration
MO017	MO-02-82	670568.25	6119307.16	800.88	280.42	270	-60	217.8	217.9	0.1	Phase A plagioclase-hornblende-biotite porphyry	Potassic alteration
MO020	MO-02-82	670568.25	6119307.16	800.88	280.42	270	-60	248	248.1	0.1	Phase B plagioclase-hornblende-biotite porphyry	Clay-carbonate alteration
MO031	MO-03-83	670500.00	6119540.00	830.00	309.37	90	-45	139.35	139.5	0.15	Phase C plagioclase-hornblende-biotite porphyry	Potassic alteration
MO037	MO-03-83	670500.00	6119540.00	830.00	309.37	90	-45	203.6	203.7	0.1	Phase A plagioclase-hornblende-biotite porphyry	Clay-carbonate alteration
MO038	MO-03-83	670500.00	6119540.00	830.00	309.37	90	-45	209	209.1	0.1	Phase A plagioclase-hornblende-biotite porphyry	Potassic alteration
MO042	MO-03-83	670500.00	6119540.00	830.00	309.37	90	-45	235.5	235.6	0.1	Sedimentary rock	Chlorite alteration overprinting potassic alteration

MO059	MO-01-37	670568.28	6119122.76	823.15	349.00	90	-61	15.3	15.4	0.1	Phase B plagioclase-hornblende-biotite porphyry	Potassic alteration
MO071	MO-01-37	670568.28	6119122.76	823.15	349.00	90	-61	201.65	201.85	0.2	Phase B plagioclase-hornblende-biotite porphyry	Clay-carbonate alteration
MO072	MO-01-37	670568.28	6119122.76	823.15	349.00	90	-61	203.5	203.7	0.2	Phase B plagioclase-hornblende-biotite porphyry	Clay-carbonate alteration overprinting sericite-carbonate alteration
MO083	MO-01-37	670568.28	6119122.76	823.15	349.00	90	-61	302.1	302.2	0.1	Phase B plagioclase-hornblende-biotite porphyry	Clay-carbonate alteration overprinting sericite-carbonate alteration
MO093	MO-01-31	670268.13	6119541.38	838.72	350.52	90	-45	183.2	183.3	0.1	Phase B plagioclase-hornblende-biotite porphyry	Potassic alteration
MO094	MO-01-31	670268.13	6119541.38	838.72	350.52	90	-45	184.7	184.8	0.1	Phase B plagioclase-hornblende-biotite porphyry	Clay-carbonate alteration overprinting potassic alteration
MO095	MO-01-31	670268.13	6119541.38	838.72	350.52	90	-45	191.2	191.3	0.1	Phase B plagioclase-hornblende-biotite porphyry	Potassic alteration
MO096	MO-01-31	670268.13	6119541.38	838.72	350.52	90	-45	195.2	195.3	0.1	Phase B plagioclase-hornblende-biotite porphyry	Potassic alteration
MO097	MO-01-31	670268.13	6119541.38	838.72	350.52	90	-45	198.4	198.5	0.1	Phase B plagioclase-hornblende-biotite porphyry	Clay-carbonate alteration overprinting potassic alteration
MO098	MO-01-31	670268.13	6119541.38	838.72	350.52	90	-45	229.1	229.3	0.2	Phase B plagioclase-hornblende-biotite porphyry	Clay-carbonate alteration
MO099	MO-01-31	670268.13	6119541.38	838.72	350.52	90	-45	240.33	240.45	0.12	Phase B plagioclase-hornblende-biotite porphyry	Potassic alteration
MO100	MO-01-31	670268.13	6119541.38	838.72	350.52	90	-45	287.45	287.55	0.1	Phase C plagioclase-hornblende-biotite porphyry	Potassic alteration

MO115	MO-01-26	670482.82	6119245.16	820.94	315.47	90	-45	31.4	31.5	0.1	Phase B plagioclase-hornblende-biotite porphyry	Potassic alteration
MO120B	MO-01-26	670482.82	6119245.16	820.94	315.47	90	-45	37.15	37.3	0.15	Phase B plagioclase-hornblende-biotite porphyry	Potassic alteration
MO128	MO-01-26	670482.82	6119245.16	820.94	315.47	90	-45	215.8	217.3	0.4	Phase A plagioclase-hornblende-biotite porphyry	Potassic alteration
MO135	MO-03-89	670350.00	6119540.00	840.00	430.25	90	-45	272.2	272.5	0.3	Phase C plagioclase-hornblende-biotite porphyry	Potassic alteration
MO137	MO-03-89	670350.00	6119540.00	840.00	430.25	90	-45	277.3	277.4	0.1	Phase A plagioclase-hornblende-biotite porphyry	Potassic alteration
MO139	MO-03-89	670350.00	6119540.00	840.00	430.25	90	-45	282.5	282.6	0.1	Phase A plagioclase-hornblende-biotite porphyry	Potassic alteration
MO142	MO-03-89	670350.00	6119540.00	840.00	430.25	90	-45	303.3	303.45	0.15	Phase A plagioclase-hornblende-biotite porphyry	Potassic alteration
MO144	MO-03-89	670350.00	6119540.00	840.00	430.25	90	-45	314	314.1	0.1	Phase A plagioclase-hornblende-biotite porphyry	Potassic alteration
MO149	MO-03-89	670350.00	6119540.00	840.00	430.25	90	-45	402.1	402.2	0.1	Phase A plagioclase-hornblende-biotite porphyry	Potassic alteration
MO151	MO-03-89	670350.00	6119540.00	840.00	430.25	90	-45	416.6	416.7	0.1	Sedimentary rock	Chlorite alteration overprinting potassic alteration

gravity, and magnetic separation. Then the concentrations of ^{187}Re and ^{187}Os in molybdenite were analyzed by isotope dilution mass spectrometry using methods described by Selby and Creaser (2004) and Markey et al. (2007). The model age of molybdenite was calculated based on the equation: $^{187}Os = {}^{187}Re^{*}(e^{\lambda t}-1)$, where the decay constant ($\lambda^{187}Re$) used was $1.666\times 10^{-11}a^{-1}$ (Smoliar et al., 1996). Two sigma uncertainties of the molybdenite Re-Os data are attributed to analytical uncertainty, decay constant uncertainty, and calibration uncertainties.

Stable isotopes

Sulfur isotopes: Sulfide minerals, including chalcopyrite, pyrite, molybdenite, and sphalerite, were separated by crushing, sieving, and hand picking from mineralized rocks. Approximately 5–10 mg of each sample was separated for sulfur analysis, and the purity of each sulfide sample was greater than 90%. Seven sulfide samples were sent for analysis to the Isotope Science Laboratory at the University of Calgary, and data are reported in the usual permil notation relative to the Canyon Diablo Troilite (CDT) standard. The accuracy of sulfur isotope measurements is ±0.3‰.

Oxygen and carbon isotopes: Pure quartz was separated from quartz-sulfide veins by crushing, sieving, and hand picking. Seven quartz samples of approximately 10 mg each were sent to the Geoanalytical Laboratory at the Washington State University for oxygen isotope analyses, using the methods described by Takeuchi and Larson (2005). Isotope ratio measurements were made with a Finnigan MAT Isotope-Ratio Mass Spectrometer, which uses a high-vacuum laser fluorination line for the extraction of oxygen. The UWG-2 garnet standard was used in this analysis (Valley et al., 1995). The accuracy and precision are better than ± 0.1 and 0.05 per mil respectively. All results are reported in per mil notation relative to Vienna Standard Mean Ocean Water (VSMOW). The oxygen stable isotopic compositions of hydrothermal fluids were calculated using the fractionation equation of Clayton et al. (1972), assuming oxygen isotope equilibrium was reached between quartz and hydrothermal fluids at crystallization temperatures estimated from fluid inclusion microthermometry.

Pure dolomite was separated from two stage 3 polymetallic sulfide-dolomite veins by crushing and hand picking. Samples were analyzed for their oxygen and carbon isotope compositions in the Stable Isotope Laboratory at the University of Alberta, using a Finnigan MAT 252 dual inlet mass spectrometer. Results are reported in the usual permil notation relative to the Vienna-Pee Dee Belemnite (VPDB) standard for carbon isotopes, and the Vienna-Standard Mean Ocean Water (VSMOW) standard for oxygen isotopes. Measurement accuracy is ± 0.1 per mil. Oxygen isotopic compositions of hydrothermal fluids, which are assumed to be in equilibrium with the dolomite, were calculated using the fractionation equation of Horita (2014).

Fluid inclusion samples and methodology

Doubly polished thin sections (~100 μm thick) of quartz and dolomite vein samples representing the main mineralization stages were prepared for fluid inclusion analysis. A Linkham THMSG600 heating and freezing stage mounted on an Olympus BX50 microscope was used for microthermometric analyses, and the stage was calibrated using synthetic fluid inclusion standards from Syn Flinc. The analytical precision is about ±0.1°C for low temperature measurements, and ±1°C for high temperature (above ambient) measurements. The measurement accuracy was ±0.2°C for low temperature measurements, and ±2°C above 10°C. Sample chips containing fluid inclusions to be analyzed were cooled to -100°C, and then reheated progressively, recording the temperatures of phase changes, until total homogenization. During the reheating process the melting temperatures of CO_2 (where present; $T_{m(CO2)}$), ice ($T_{m(ice)}$), sylvite ($T_{m(sylvite)}$), and halite ($T_{m(halite)}$), and total homogenization temperature (Th) were recorded. The salinities of fluid inclusions, reported in weight percent NaCl equivalent, were derived from ice melting or halite dissolution temperatures.

3.8 Whole-Rock Geochemistry

Due to the widespread hydrothermal alteration in the area, almost all rocks observed in drill core were at least weakly altered. Nine least-altered (weak biotite alteration) samples of the

various porphyry phases were selected and analyzed for their whole-rock geochemical composition. Major and trace element geochemical data are presented in Table 3-3.

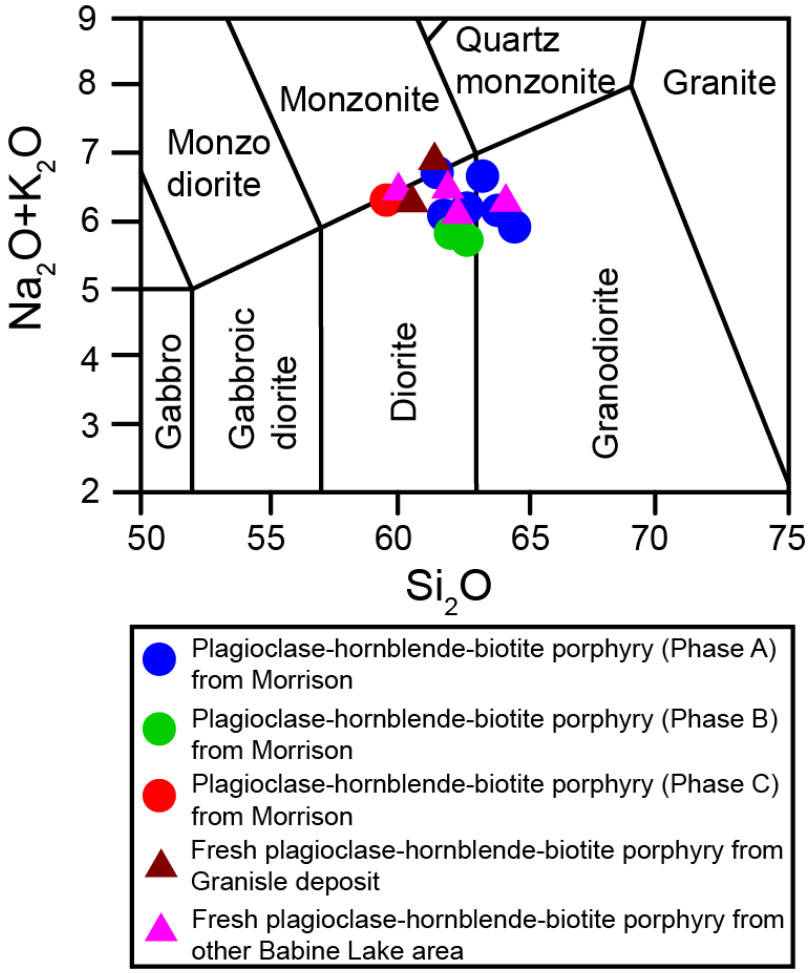

Fig. 3-11. Total alkali versus silica diagram showing the compositions of weakly potassic-altered plagioclase-hornblende-biotite porphyry intrusions from the Morrison area (after Middlemost, 1994). Fresh plagioclase-hornblende-biotite porphyry samples from other Babine Lake intrusions are also shown for comparison (data from Carson and Jambor, 1974, and Ogryzlo et al., 1995).

Major element geochemistry

All major element oxide data were recalculated to 100% volatile free for the purposed of plotting on lithological discrimination diagrams (Figs. 3-11 and 3-12). Most porphyry samples plot within the diorite and granodiorite fields on the total alkali-silica diagram (Fig. 3-11), whereas two samples (MO001 and MO038) straddle the boundary between the monzonite and diorite fields.

Table 3-3 Major and trace element analysis of plagioclase-hornblende-biotite porphyry from the Morrison deposit

Sample ID	MO001	MO017	MO038	MO093	MO120B	MO128	MO139	MO142	MO149
Phase	C	A	A	B	B	A	A	A	A
Weight%									
SiO_2	54.91	59.93	60.04	59.38	60.11	61.34	61.18	58.43	60.73
Al_2O_3	14.59	16.42	15.96	15.91	16.06	15.73	15.69	15.09	15.42
Fe_2O_3	6.37	5.69	5.66	5.74	5.88	4.88	4.90	5.86	5.36
MnO	0.06	0.04	0.07	0.02	0.03	0.04	0.02	0.04	0.05
MgO	4.45	3.26	3.27	3.82	3.34	2.83	2.74	3.05	2.79
CaO	4.99	4.72	5.13	4.24	4.06	4.38	3.86	4.15	4.45
Na_2O	3.18	4.65	4.29	3.37	3.86	4.33	4.00	4.20	4.24
K_2O	2.65	1.27	2.27	2.23	1.65	1.60	1.63	1.59	2.16
TiO_2	0.84	0.84	0.77	0.81	0.78	0.79	0.76	0.71	0.69
P_2O_5	0.26	0.33	0.29	0.34	0.29	0.29	0.23	0.26	0.24
LOI	5.37	1.62	1.90	3.26	3.67	2.44	3.80	3.19	2.81
Total	97.67	98.77	99.65	99.12	99.73	98.65	98.81	96.57	98.94
ppm									
Ba	765	687	1716	546	889	1171	2306	11850	1313
Co	18.9	20.3	16.1	28.3	13.2	13.8	13.6	16.4	12.4
Cr	159	77.2	93.3	123	83.4	74.4	72.2	80.3	78.7
Ni	77	42	45	67	40	47	49	46	44
Pb	7	< 5	< 5	< 5	< 5	< 5	< 5	< 5	< 5
Sc	14.6	8.98	10.2	11.6	9.75	8.87	10.3	9.38	8.53
Sr	502	905	877	775	738	866	928	1639	850
V	164	139	130	134	130	130	131	127	115
Cs	3	2	2.4	3.8	2.4	3	2.4	4	3
Ga	20	21	20	21	21	21	21	21	20
Ge	1.4	1.4	1.3	1.6	1.4	1.7	1.6	1.2	1.3

Hf	2.3	2.8	2.9	3	3	2.9	2.7	2.7	2.9
Nb	6	6.6	6.8	8.1	6.5	6.8	7.1	6.3	7.9
Rb	76	30	39	72	39	39	39	39	38
Sn	1	1	1	2	1	2	1	1	1
Ta	0.39	0.52	0.45	0.51	0.39	0.41	0.43	0.45	0.42
Th	4.21	4.98	5.65	5.91	5.18	5.07	5.07	5.18	5.86
U	1.45	2.39	2.19	2.66	2.37	1.51	1.19	1.15	1.59
Zr	94	113	113	120	118	114	112	112	114
La	21.6	27.4	22.5	27.8	20.8	19	51	25.1	27.9
Ce	40.4	52.4	42.2	50	39	37.5	75.9	44.1	53.1
Pr	4.99	6.41	5.35	5.95	4.85	4.83	7.79	5.24	6.45
Nd	20	25.1	21.5	22.3	19.8	19.5	26.8	20.3	25
Sm	3.89	4.63	3.88	4.09	3.75	3.92	3.99	3.67	4.46
Eu	1.1	1.27	1.12	1.14	1.05	0.938	1.18	1.08	1.13
Gd	3.1	3.37	2.95	3.04	2.85	3.01	2.88	2.87	3.2
Tb	0.43	0.44	0.4	0.4	0.39	0.41	0.39	0.38	0.43
Dy	2.35	2.16	2.06	2.03	2.01	2.12	2.09	2.04	2.13
Ho	0.44	0.38	0.36	0.37	0.37	0.36	0.37	0.36	0.39
Er	1.22	0.97	1.01	1	0.95	0.96	1.04	0.95	1.01
Tl	0.7	0.38	0.35	1.25	0.6	0.4	0.38	0.34	0.42
Tm	0.181	0.147	0.153	0.148	0.139	0.142	0.145	0.135	0.141
Yb	1.11	0.89	0.95	0.91	0.89	0.86	0.94	0.85	0.93
Lu	0.149	0.133	0.142	0.138	0.131	0.125	0.138	0.125	0.145

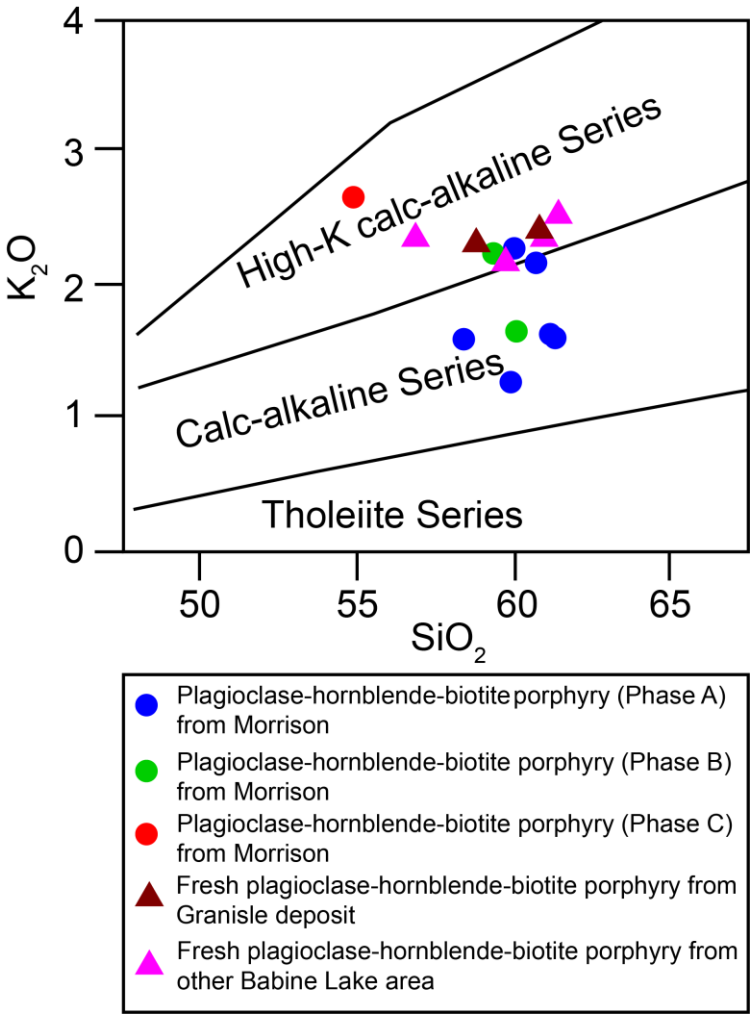

Fig. 3-12. K_2O versus SiO_2 diagram showing the chemical compositions of weakly potassic-altered plagioclase-hornblende-biotite porphyry intrusions from the Morrison area (after Peccerillo and Taylor, 1976). Fresh plagioclase-hornblende-biotite porphyry samples from other Babine Lake intrusions are also shown for comparison (data from Carson and Jambor, 1974, and Ogryzlo et al., 1995).

On a plot of K_2O versus SiO_2, most of the suite plots within the calc-alkaline field, with some extending into the high-K calc-alkaline field (Fig. 3-12). The moderately elevated K_2O contents of some of the samples in this suite might in part be due to weak potassic alteration, but it is noted that the compositional range of the Morrison samples is similar to that of other fresh Babine Lake intrusions (Carson and Jambor, 1974; Ogryzlo, 1995), suggesting that the compositions of the Morrison samples have not been significantly affected by alteration.

The phase A and B porphyries are compositionally similar, whereas a single sample of phase C porphyry (which shows moderate biotite alteration) has slightly higher K_2O and lower SiO_2 content than the others.

Trace element geochemistry

Trace element data for the plagioclase-hornblende-biotite porphyry samples are plotted on primitive mantle-normalized trace element and chondrite-normalized rare earth element (REE) diagrams in Figure 3-13. In the primitive mantle-normalized diagram (Fig. 3-13A), the samples show enrichments in large ion lithophile elements (LILE) but low concentrations of high field strength elements (HFSE) and middle and heavy REE (MREE, HREE). Phase A porphyry samples are somewhat more enriched in LILE (especially Ba, La, Ce, and Sr) than the other samples, whereas the porphyry C sample is slightly more enriched in MREE-HREE. All samples display negative Ta, Nb, and Ti anomalies, which are characteristics of arc-related igneous rocks (Brenan et al., 1994; Foley et al., 2000).

In the chondrite-normalized rare earth element diagram (Fig. 3-13B), all samples show weakly listric-shaped REE patterns, which slope downward from light REE (LREE) to MREE (high $[La/Sm]_n$ ratios from 3.1 to 8.3), and then flatten from MREE to HREE (low $[Dy/Yb]_n$ ratios from 1.4 to 1.7). These listric-shaped REE patterns are likely caused by fractionation of hornblende and/or titanite, because hornblende and titanite preferentially partition MREE (Gromet and Silver, 1987; Klein et al., 1997; Bachmann et al., 2005; Prowatke and Klemme, 2006). An absence of Eu anomalies for most of the samples suggests either that plagioclase did not fractionate extensively from these magmas (Eu^{2+} can substitute for Ca^{2+} in plagioclase; Hanson, 1980) because magmatic water content was high (Naney, 1983; Merzbacher and Eggler, 1984; Rutherford and Devine, 1988; Moore and Carmichael, 1998), and/or that magmatic oxidation state was high (such that most of the Eu was present as Eu^{3+}, and was not incorporated into fractionating plagioclase; Philpotts, 1970; Housh and Luhr, 1991; Sisson and Grove, 1993).

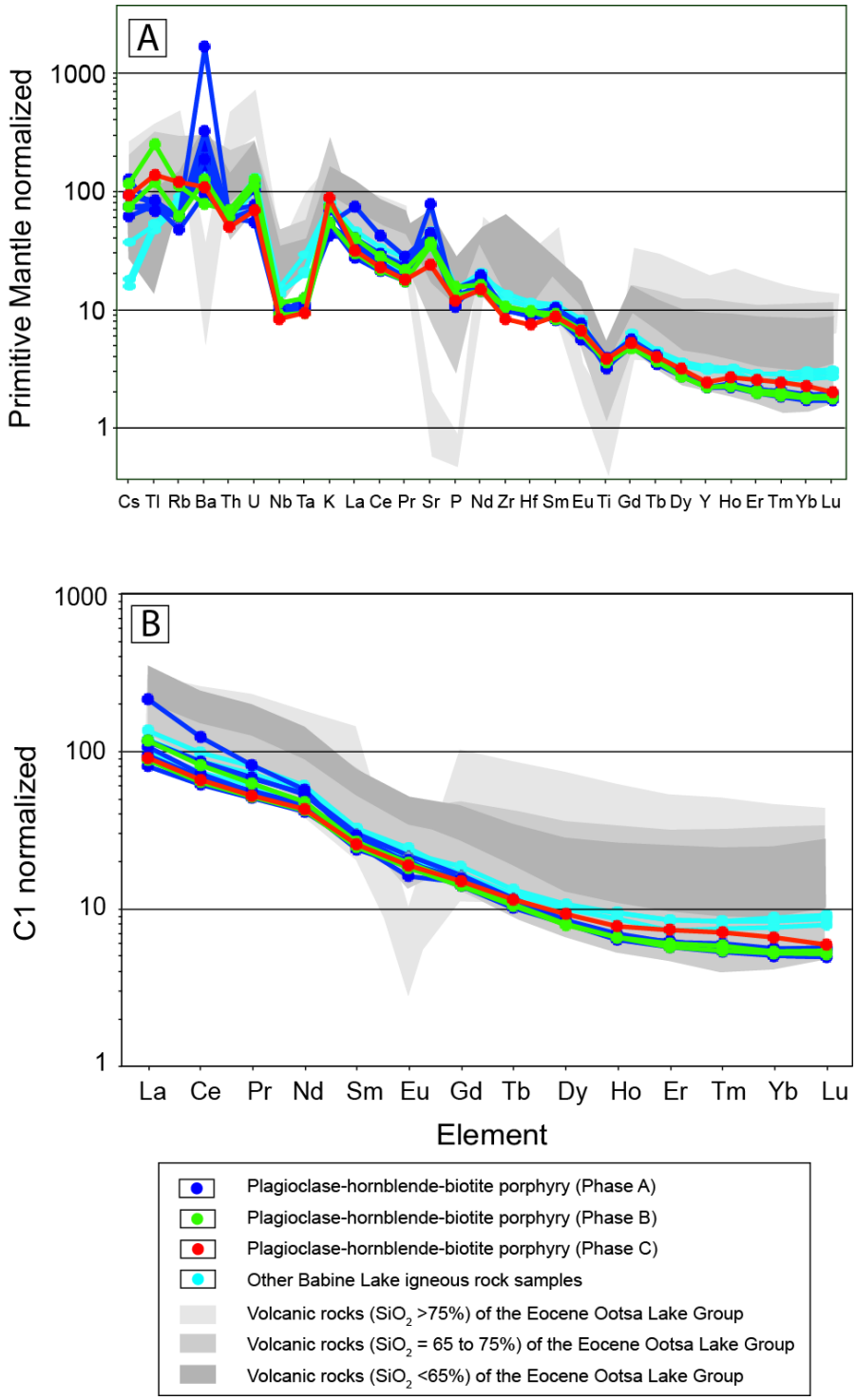

Fig. 3-13. (A) Primitive mantle-normalized trace element diagram, and (B) C1 Chondrite-normalized REE diagram for plagioclase-hornblende-biotite porphyry samples from Morrison (primitive mantle normalization values from Sun and McDonough, 1989). Other Babine Lake igneous rocks from the Babine Lake area, and volcanic rock samples from the Eocene Ootsa Lake Group from nearby areas are shown for comparison (data from Grainger, 2000).

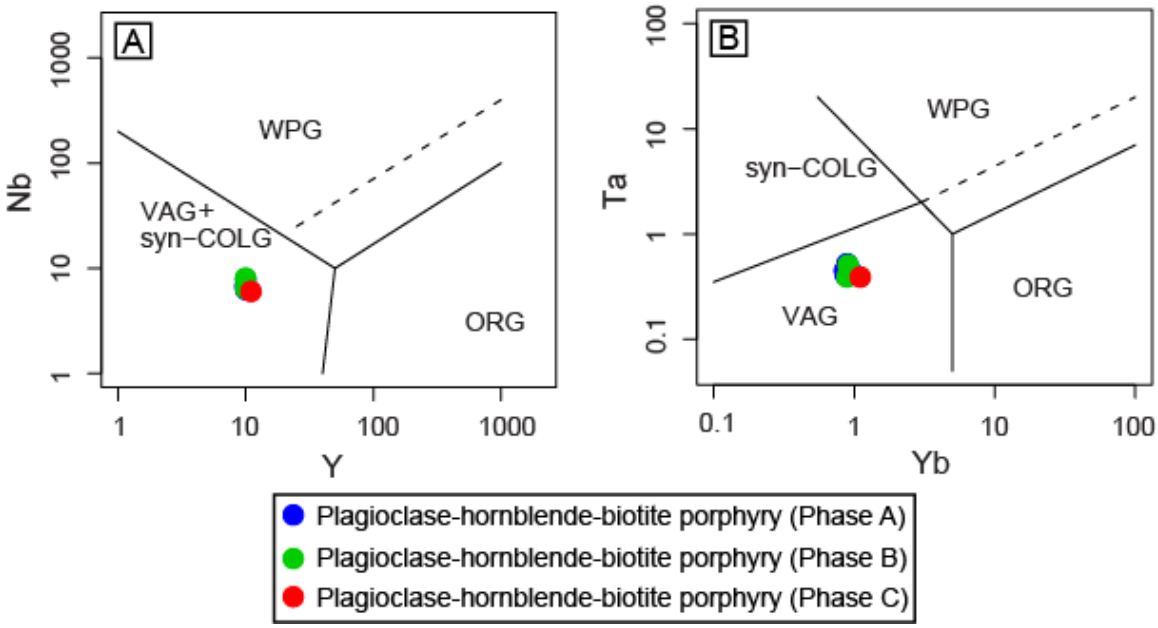

Fig. 3-14. Tectonic discrimination diagrams for plagioclase-hornblende-biotite porphyry from the Morrison deposit (Pearce, 1984). Abbreviations: ACM: active continental margins; MORB: Mid-ocean ridge basalt; WPB: Within plate basalts; WPVZ: within-plate volcanic zones.

All porphyry samples plot in the field of volcanic arc granites on tectonic discrimination diagrams (Fig. 3-14). Thus, the plagioclase-hornblende-biotite porphyry suite is concluded to be of calc-alkaline, dioritic to granodioritic composition, and of arc-related magmatic affinity. The suite also appears to have had a relatively high magmatic water content and/or oxidation state, which is considered to be an indication of fertility for porphyry-type ore formation (Candela, 1992; Richards, 2011).

3.9 Geochronology

U-Pb zircon dating

Zircons from a sample of phase A plagioclase-hornblende-biotite porphyry (MO128) are typical of magmatic crystals: clear, euhedral, and colorless. Weak oscillatory zoning is evident in the backscattered electron images (Fig. 3-15). Twenty-six zircons were analyzed, and all U-Pb isotopic data are summarized in Table 3-4 and plotted on a Concordia diagram in Figure 3-16. The data show a relatively homogeneous population, and yielded a U-Pb Concordia intercept age of 52.21 ± 0.37 Ma (MSWD = 1.6; Fig. 3-16).

Table 3-4 Zircon U-Pb data for phase A plagioclase-hornblende-biotite porphyry sample MO128 from Morrison

Sample ID	$^{207}Pb/^{206}Pb$	2 s	$^{207}Pb/^{235}U$	2 s	$^{206}Pb/^{238}U$	2 s	r	$^{207}Pb^*/^{206}Pb^*$ age (Ma)	2 s error (Ma)	$^{207}Pb^*/^{235}U$ age (Ma)	2 s error (Ma)	$^{206}Pb^*/^{238}U$ age (Ma)	2 s error (Ma)	% discor-dance
MO128-1	0.05741	0.00144	0.06513	0.00222	0.00823	0.00019	0.676	507	54	64	2	53	1	90.0
MO128-3	0.05224	0.00118	0.05869	0.00223	0.00815	0.00025	0.806	296	51	58	2	52	2	82.7
MO128-4	0.05347	0.00098	0.05973	0.00186	0.00810	0.00020	0.811	349	41	59	2	52	1	85.4
MO128-5	0.05575	0.00155	0.06257	0.00250	0.00814	0.00023	0.716	442	61	62	2	52	1	88.5
MO128-6	0.05224	0.00095	0.05808	0.00164	0.00806	0.00017	0.767	296	41	57	2	52	1	82.8
MO128-7	0.06051	0.00150	0.06849	0.00248	0.00821	0.00022	0.728	622	53	67	2	53	1	91.9
MO128-8	0.05603	0.00110	0.06186	0.00213	0.00801	0.00023	0.822	453	43	61	2	51	1	89.0
MO128-9	0.06241	0.00168	0.07051	0.00265	0.00819	0.00021	0.698	688	56	69	3	53	1	92.7
MO128-10	0.05942	0.00175	0.06598	0.00276	0.00805	0.00024	0.710	582	63	65	3	52	2	91.5
MO128-11	0.05537	0.00122	0.06327	0.00202	0.00829	0.00019	0.724	427	48	62	2	53	1	87.9
MO128-12	0.06107	0.00472	0.07185	0.00588	0.00853	0.00023	0.333	642	158	70	6	55	1	91.8
MO128-13	0.05207	0.00108	0.05755	0.00199	0.00801	0.00022	0.801	289	47	57	2	51	1	82.5
MO128-14	0.05656	0.00163	0.06317	0.00264	0.00810	0.00024	0.723	474	63	62	3	52	2	89.4
MO128-15	0.05381	0.00120	0.06175	0.00206	0.00832	0.00021	0.744	363	49	61	2	53	1	85.6
MO128-16	0.05255	0.00081	0.05923	0.00184	0.00818	0.00022	0.869	309	35	58	2	52	1	83.4
MO128-17	0.05528	0.00121	0.06141	0.00230	0.00806	0.00024	0.811	423	48	61	2	52	2	88.1
MO128-19	0.05134	0.00104	0.05777	0.00186	0.00816	0.00020	0.778	256	46	57	2	52	1	79.9
MO128-20	0.05300	0.00115	0.05884	0.00212	0.00805	0.00023	0.799	329	49	58	2	52	1	84.6
MO128-21	0.05024	0.00086	0.05751	0.00182	0.00830	0.00022	0.843	206	39	57	2	53	1	74.5
MO128-24	0.05465	0.00109	0.06176	0.00198	0.00820	0.00021	0.784	398	44	61	2	53	1	87.1
MO128-25	0.05222	0.00103	0.06022	0.00221	0.00836	0.00026	0.842	295	45	59	2	54	2	82.1
MO128-26	0.05412	0.00132	0.06205	0.00239	0.00831	0.00025	0.774	376	54	61	2	53	2	86.2
MO128-27	0.05212	0.00116	0.06116	0.00237	0.00851	0.00027	0.816	291	50	60	2	55	2	81.5
MO128-28	0.05690	0.00157	0.06612	0.00280	0.00843	0.00027	0.760	488	60	65	3	54	2	89.3
MO128-29	0.06088	0.00141	0.07084	0.00248	0.00844	0.00022	0.751	635	49	69	2	54	1	91.8
MO128-30	0.06085	0.00263	0.06977	0.00435	0.00832	0.00037	0.720	634	90	68	4	53	2	92.0

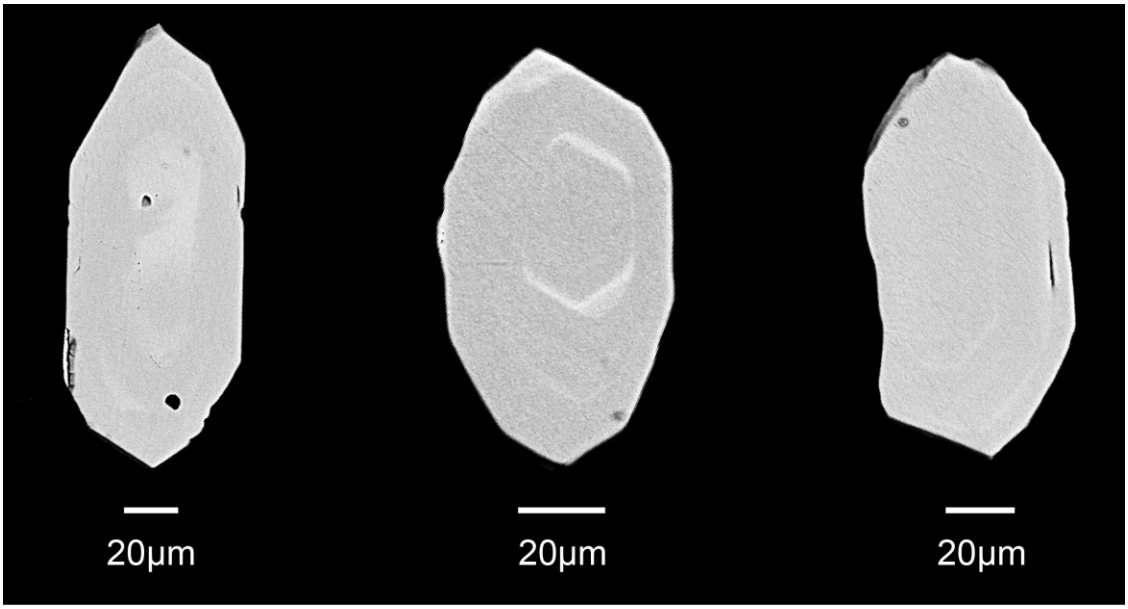

Fig. 3-15. Backscattered electron images of typical zircons from plagioclase-hornblende-biotite porphyry sample MO128. Zircons show weak magmatic oscillatory zoning from center to margin, and dark areas (inclusions) were avoided during analysis.

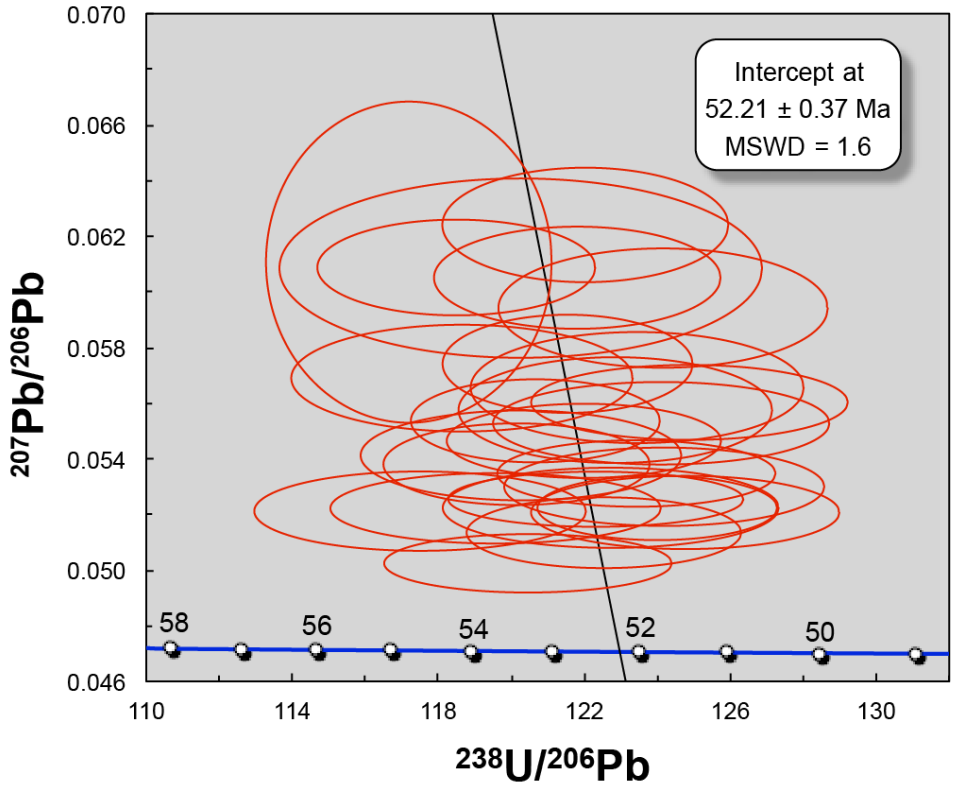

Fig. 3-16. U-Pb Concordia diagram for zircon laser ablation ICPMS data. The error ellipses are 2 sigma.

Molybdenite Re-Os dating

Molybdenite at Morrison occurs as fine-grained crystals in type 4 quartz-molybdenite veins (Fig. 3-8D, E) commonly associated with pyrite. Two samples (MO094 and MO097) of molybdenite-bearing quartz veins were dated by the Re-Os technique. The veins are hosted by clay-carbonate altered plagioclase-hornblende-biotite porphyry, which is probably an overprint on previous potassic alteration. They were collected from drill hole MO-01-031 at depths of 184.5 and 198.5 m respectively. The Re and Os concentrations and model ages of the samples are presented in Table 3-5, and yielded Re-Os ages of 52.54 ± 0.22 and 53.06 ± 0.22 Ma.

Table 3-5 Molybdenite Re-Os data from Morrison

Sample	Re ppm	± 2s	^{187}Re ppm	± 2s	^{187}Os ppb	± 2s	Model Age (Ma)	± 2s (Ma)
MO-094	431.7	1.1	271.3	0.7	237.6	0.2	52.54	0.22
MO-097	559.5	1.5	351.7	0.9	311	0.2	53.06	0.22

3.10 Fluid inclusions

Fluid inclusion types

In this study, primary and pseudosecondary fluid inclusions in quartz and dolomite were analyzed, whereas secondary and necked or leaked inclusions were avoided (using the criteria of Roedder, 1984, and Goldstein and Reynolds, 1994). Primary inclusions were typically found in growth zones of quartz and dolomite crystals, whereas pseudosecondary inclusions generally occur in healed microfractures within crystals. Most measured inclusions have sizes of 5–10 μm.

Two type 3 quartz-chalcopyrite-pyrite veins, two type 4 quartz-molybdenite-pyrite veins, and two type 5 polymetallic sulfide-dolomite veins samples were selected for fluid inclusion analysis after petrographic examination of 7 doubly polished thin sections. Three types of fluid inclusions were recognized based on their features at room temperature: multiphase hypersaline brine inclusions (H) with halite ± sylvite ± opaque minerals and anhydrite daughter crystals (Fig. 3-17A–C, E), two-phase (liquid + vapor) vapor-rich inclusions (V; Fig. 3-17D), and two-phase (liquid + vapor) liquid-rich inclusions (L; Fig. 3-17F). These fluid inclusions occurred in three assemblages (sensu Goldstein and Reynolds, 1994): (1) brine plus vapor-rich inclusions (H + V;

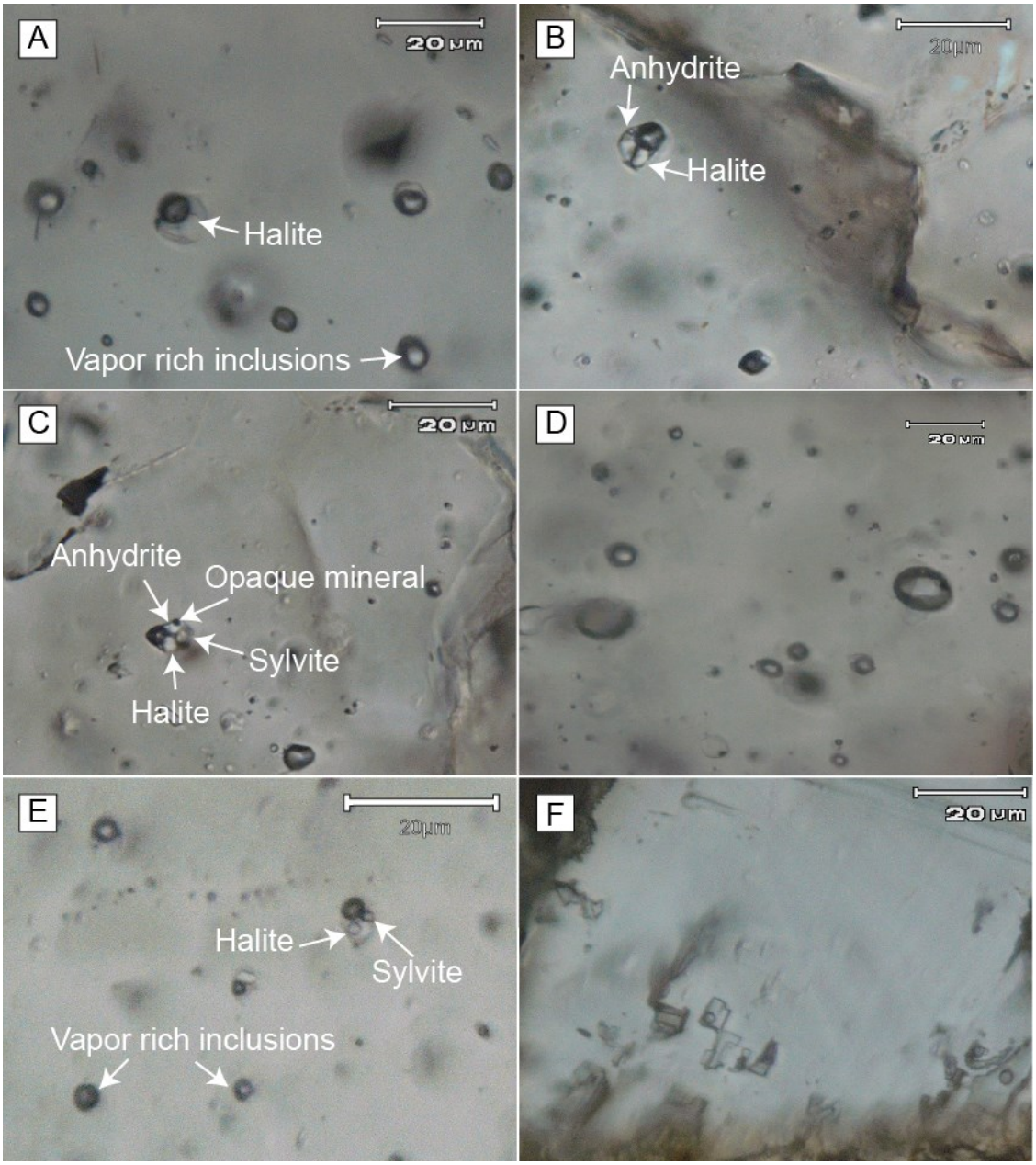

Fig. 3-17. Transmitted light photomicrographs showing primary fluid inclusions from veins at Morrison. (A) A fluid inclusion assemblage with hypersaline inclusions and vapor-rich inclusions from a type 3 quartz-chalcopyrite-pyrite vein (MO135). (B, C) Hypersaline inclusions with halite + liquid + vapor ± additional daughter crystals including sylvite, anhydrite, and opaque crystals from a type 3 quartz-chalcopyrite-pyrite vein (MO135). (D) A vapor-rich inclusion assemblage from a type 3 quartz-chalcopyrite-pyrite vein (MO135). (E) Hypersaline and vapor-rich inclusions from a type 4 quartz-molybdenite-pyrite vein (MO097). (F) Liquid-rich inclusions in a dolomite from a type 5 polymetallic-sulfide-dolomite vein (MO072).

Fig. 3-17A); (2) vapor-rich inclusions (V only; Fig. 3-17D); and (3) liquid-rich inclusions (L only;

Fig. 3-17F). The first and second assemblages occur in both the type 3 quartz-chalcopyrite-pyrite

Table 3-6 Fluid inclusion data from Morrison

Fluid inclusion assemblage ID	$T_{m(CO2)}$ (°C)	$T_{m(ice)}$ (°C)	$T_{m(sylvite)}$ (°C)	$T_{m(halite)}$ (°C)	$T_{h(L)}$ (°C)	T_h (°C)	Salinity wt.% NaCl equiv.	Mode
Quartz-chalcopyrite-pyrite vein (MO135)								
1				338	519	519	41.3	H
				343	509	509	41.8	H
				360	517	517	43.3	H
2				345	493	493	41.9	H
				357	511	511	43.1	H
				360	478	478	43.3	H
				375	524	524	44.8	H
				370	477	477	44.3	H
3			122	385	489	489	45.8	H
				392	507	507	46.6	H
				403	477	477	47.8	H
4				350	430	430	42.4	H
				361	420	420	43.4	H
				385	435	435	45.8	H
5				340	410	410	41.5	H
				353	402	402	42.7	H
				328	422	422	40.4	H
			120	345	400	400	41.9	H
				320	418	418	39.8	H
6				400	432	432	47.4	H
				389	412	412	46.3	H
				370	416	416	44.3	H
7				369	457	457	44.2	H
				342	440	440	41.7	H
				355	420	420	42.9	H
				360	424	424	43.3	H

			102	351	418	418	42.5	H
			113	367	467	467	44.0	H
8	-56.5							V
	-56.6							V
Quartz-chalcopyrite-pyrite vein (MO144)								
9				360	410	410	43.3	H
				365	428	428	43.8	H
				373	423	423	44.6	H
10				353	455	455	42.7	H
				372	475	475	44.5	H
				361	488	488	43.4	H
11				360	507	507	43.3	H
				349	512	512	42.3	H
				352	497	497	42.6	H
12				377	526	526	45.0	H
				363	507	507	43.6	H
				385	517	517	45.8	H
				397	520	520	47.1	H
				347	503	503	42.1	H
Quartz-molybdenite-pyrite vein (MO097)								
1				300	322	322	38.2	H
				311	345	345	39.0	H
				339	349	349	41.4	H
2				290	360	360	37.4	H
				300	358	358	38.2	H
				309	361	361	38.9	H
3				305	396	396	38.6	H
				326	400	400	40.3	H
				323	390	390	40.0	H
4				310	327	327	38.9	H
				319	342	342	39.7	H

				314	320	320	39.3	H
5				310	332	332	38.9	H
				344	358	358	41.9	H
				328	360	360	40.4	H
6				306	401	401	38.6	H
				328	408	408	40.4	H
				285	380	380	37.0	H
7				357	294	357	43.1	H
				348	323	348	42.2	H
				327	301	327	40.4	H
				343	310	343	41.8	H
Quartz-molybdenite-pyrite vein (MO094)								
8				331	288	288	40.7	H
				337	318	318	41.2	H
				344	330	330	41.9	H
				328	292	292	40.4	H
9				337	412	412	41.2	H
				325	397	397	40.2	H
				318	409	409	39.6	H
				332	421	421	40.8	H
				309	393	393	38.9	H
				317	416	416	39.5	H
10				329	360	360	40.5	H
				317	343	343	39.5	H
11				339	358	358	41.4	H
				326	347	347	40.3	H
Polymetallic sulfide-carbonate veins (MO083)								
1					178			L
					182			L
2					168			L
					175			L

3		-1.9			168		3.2	L
		-2.1			170		3.5	L
					185			L
					198			L
					207			L
4					170			L
					163			L
5		-2.1			185		3.5	L
		-1.8			191		3.1	L
		-2.3			195		3.9	L
Polymetallic sulfide-carbonate veins (MO072)								
6					202			L
					205			L
7					189			L
					173			L
					167			L
8					167			L
					184			L
9		-2.1			218		3.5	L
		-1.9			201		3.2	L
		-2.3			210		3.9	L

and type 4 quartz-molybdenite-pyrite veins, whereas the third assemblage only occurs in the polymetallic sulfide-dolomite veins.

The hypersaline inclusions in the veins are irregular to rounded in shape, with cubic halite daughter crystals that account for 20–40% of the inclusion volume. Sylvite daughter crystals are smaller and rounded in shape, and are only observed in a few inclusions. Upon heating, the sylvite crystals dissolve at lower temperatures than halite. Anhydrite crystals are the least common daughter crystals, and are recognized by their rectangular shape and high birefringence. Other minor opaque daughters are too small to be distinguished, and are likely probably sulfides. Neither the anhydrite nor opaque daughter phases dissolved upon heating.

Homogenization temperature/salinity data

A total of 102 fluid inclusions were analyzed from the vein samples, and all microthermometric results are listed in Table 3-6 and illustrated in Figures 3-18 and 3-19. Fluid inclusions were measured in assemblages, and the homogenization temperature and salinities within a single fluid inclusion assemblage were found to be similar (± 50°C, ± 5 wt.% NaCl equiv.), but varied between different assemblages. No data could be recorded from vapor-rich inclusions because of difficulties in observing phase changes in these predominantly dark inclusions (cf. Bodnar et al., 1985). No liquid CO_2 was observed in any inclusions at or below room temperature, but faint melting events close to -56.6°C (interpreted to be the melting of small crystals of solid CO_2) were observed in some vapor-rich inclusions, suggesting the presence of minor amounts of CO_2 in the vapor phase. However, no clathrate melting events were observed in liquid-rich fluid inclusions, so the CO_2 contents of the liquid phase are thought to be low.

Type 3 quartz-chalcopyrite-pyrite vein samples (MO135 and MO144): Forty-four hypersaline inclusions from twelve fluid inclusion assemblages homogenized finally by vapor-bubble disappearance at temperatures between 400–526°C, with a slightly bimodal distribution and an average of 464° ± 42°C. Halite dissolution temperatures ranged from 320 to 403°C, and calculated salinities ranged from 39.8 to 47.8 wt.% NaCl equiv. (mean = 43.6 ± 1.8 wt.% NaCl equiv., n = 42; equation of Sterner et al., 1998). Sylvite was observed in several inclusions, and

the sylvite dissolution temperatures ranged from 102° to 122°C. If the hydrothermal fluid is modeled in the NaCl-KCl-H_2O system, then the composition can be modelled as 32 wt.% NaCl and 21 wt.% KCl based on the phase diagram shown in Figure 3-20 (Roedder, 1984).

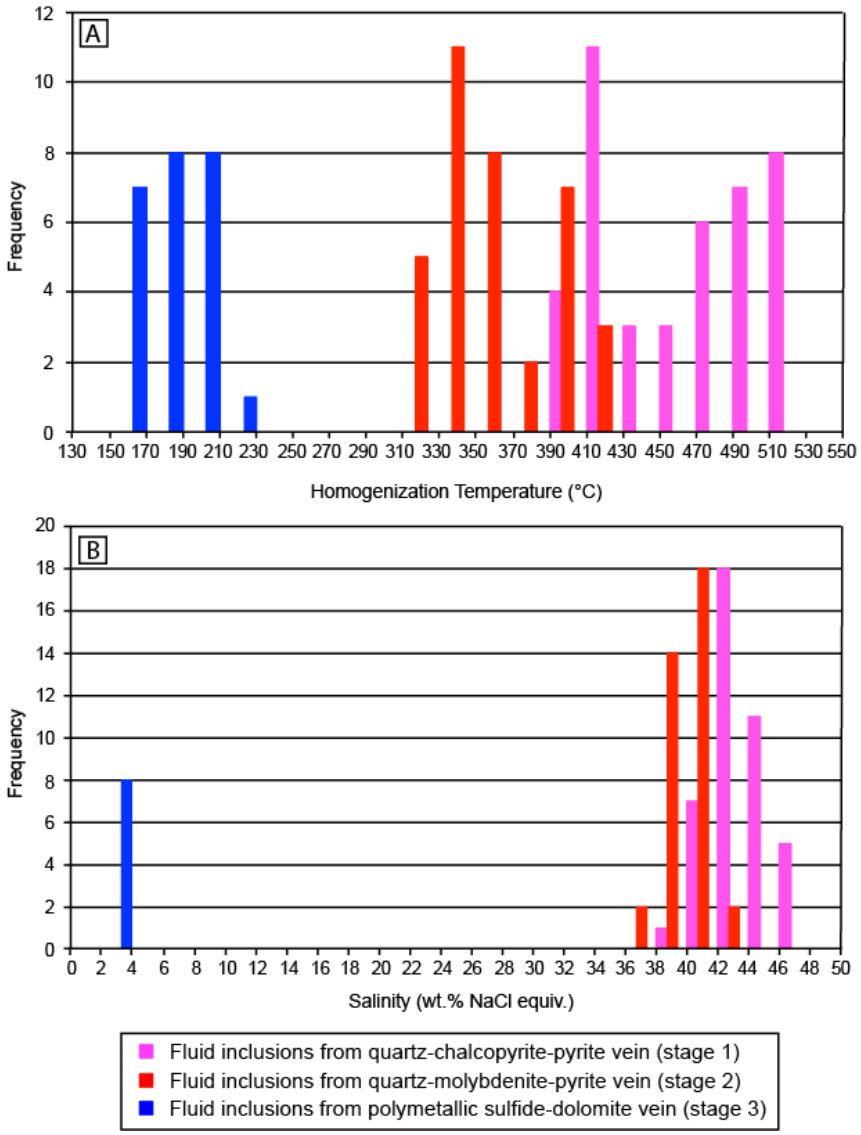

Fig. 3-18. Histograms showing homogenization temperatures and salinities of fluid inclusions from type 3 and 4 quartz-sulfide veins (stage 1 and 2), and type 5 dolomite-sulfide veins (stage 3).

Several fluid inclusion assemblages included vapor-rich fluid inclusions. Although homogenization temperatures and salinities could not be measured on these inclusions due to their dark appearance, the coexistence of vapor-rich and liquid-rich inclusions indicates that

trapping conditions were on the two-phase liquid-vapor curve, and that final homogenization temperatures approximate the trapping temperature.

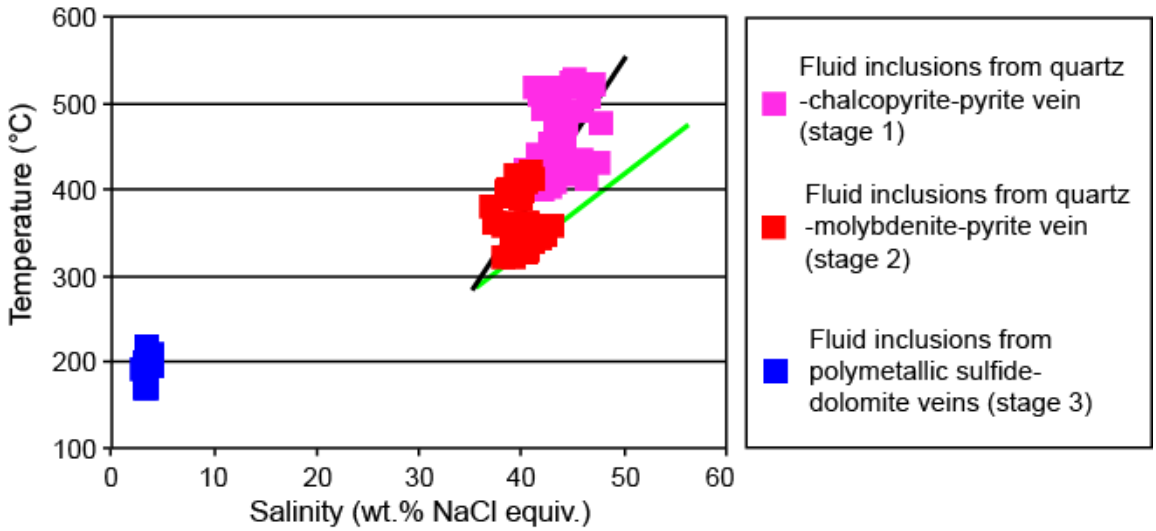

Fig. 3-19. Salinity versus homogenization temperature plot of fluid inclusions from type 3 and 4 quartz-sulfide veins (stage 1 and 2), and type 5 dolomite-sulfide veins (stage 3). The green line is the halite-saturation curve, and the black line shows the evolution trend of the hydrothermal fluids from stage 1 to 2.

Type 4 quartz-molybdenite-pyrite vein samples (MO094 and MO097): Eleven fluid inclusion assemblages containing hypersaline fluid inclusions were measured from this sample. Fluid inclusions in nine of these assemblages homogenized finally by vapor bubble disappearance, with an average $Th_{(L-V)L}$ of 370°± 31°C and Tm_{NaCl} of 40.0 ± 1.2 wt.% NaCl equiv. Fluid inclusions in two assemblages homogenized finally by halite melting temperatures of 327°–357°C, a few degrees above the bubble disappearance temperature of 292°–330°C. Salinities calculated from halite dissolution temperatures range from 37.0 to 43.1 wt.% NaCl equiv. with an average of 40.0 ± 1.4 wt.% NaCl equiv. (n = 36). Sylvite daughter crystals are rare in fluid inclusions from this sample, and no sylvite dissolution temperatures were recorded.

Vapor-rich fluid inclusions also occurred in some of these fluid inclusion assemblages, and final homogenization temperatures are therefore interpreted to approximate the trapping temperature. Halite-bearing inclusions in these fluid inclusion assemblages homogenized by vapor disappearance.

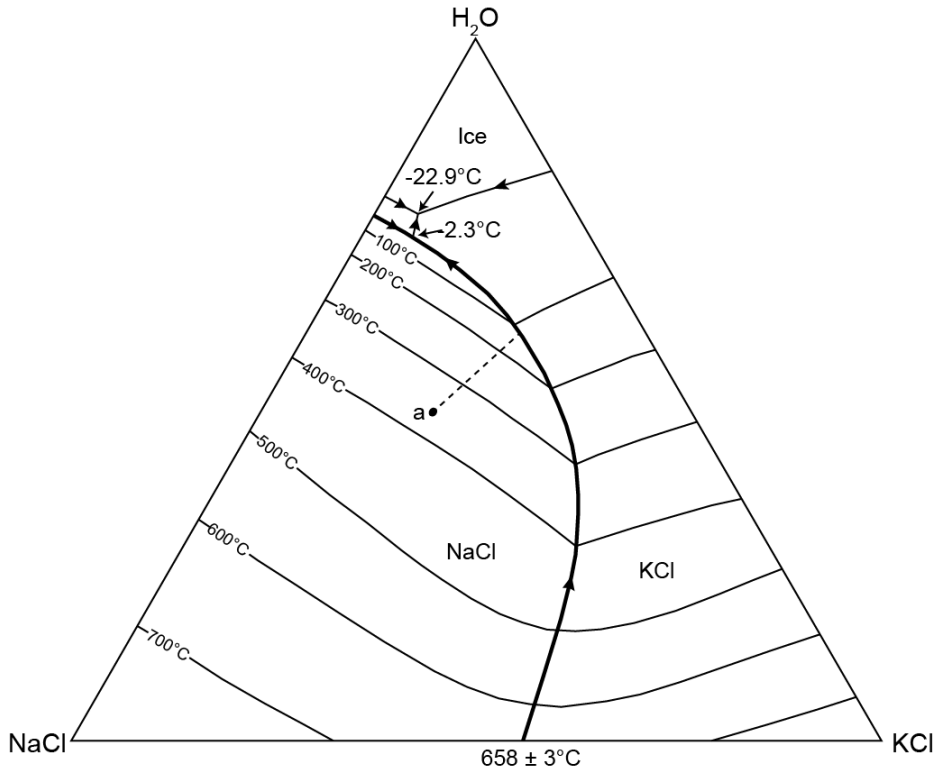

Fig. 3-20. Vapor-saturated NaCl-KCl-H_2O phase diagram (after Roedder, 1984), showing the evolution trend of fluid inclusions containing both halite and sylvite from a type 3 quartz-chalcopyrite-pyrite vein (MO135) (assuming halite is pure NaCl). The average sylvite melting temperature was 114°C, and the average halite melting temperature was 362°C.

Type 5 polymetallic sulfide-dolomite vein samples (MO072 and MO083): Twenty-four liquid-rich fluid inclusions from 9 assemblages in dolomite crystals were measured. Homogenization temperatures range from 163 to 218°C with an average of 185 ± 16°C (n = 24). Fluid salinities calculated from final ice melting temperatures range from 3.1 to 3.9 wt.% NaCl equiv. (mean = 3.5 ± 0.3 wt.% NaCl equiv., n = 8; equation of Bodnar, 1993).

Pressure corrections

No pressure corrections were applied to the homogenization temperatures of liquid-rich fluid inclusions from type 3 and 4 veins, because of the coexistence of liquid- and vapor-rich fluid inclusions, indicating trapping under two-phase (boiling) conditions such that homogenization temperature equals the trapping temperature (and pressure).

However, no vapor-rich fluid inclusions occur in the type 5 polymetallic-sulfide dolomite veins, and so the homogenization temperature is presumed to be a minimum estimate of the trapping temperature, and a pressure correction is required. No independent estimate of pressure is available for this late stage of mineralization, but the trapping pressure of stage 2 fluids can provide a maximum constraint, assuming that pressures fell from stage 2 to stage 3 (perhaps by transition from near lithostatic to hydrostatic pressure conditions, and/or by uplift and erosion). The trapping pressure of stage 2 fluid, was estimated using the program $H_{OKIE}F_{LINCS}$_H_2O-NaCl (Steele-MacInnis, 2012), and yielded a value of ~75 bar. This value is likely to be a minimum estimate, given the observation of small amounts of CO_2 in some vapor-rich fluid inclusions, but nevertheless suggests that fluid pressures during the porphyry stage of mineralization were quite low. Assuming this pressure estimate is approximately correct, a pressure correction of 4°C is indicated for the ~3.5 wt.% NaCl equiv. fluids in stage 3 polymetallic-sulfide dolomite veins. Given that this small correction could be too large (if pressures were significantly less than during phase 2) or too small (if CO_2 added significantly to stage 2 pressures), is seems arbitrary to make any specific correction to stage 3 fluid temperatures, except to note that the trapping temperature might be higher than the homogenization temperature by up to ~5°C, thus indicating an average trapping temperature for stage 3 fluids of ~190° ± ~20°C.

3.11 Oxygen isotope compositions

Quartz was separated from three type 3 (stage 1), two type 4 (stage 2), and two type 5 (stage 3) vein samples for oxygen isotopic analysis. Dolomite was separated from two type 5 (stage 3) vein samples for oxygen and carbon isotopic analysis. $\delta^{18}O$ values of these samples are listed in Table 3-7. Quartz samples range from $\delta^{18}O$ = 7.3 to 8.4‰ for stage 1, 6.1 to 7.7‰ for stage 2, and 9.4 to 10.7‰ for stage 3, and dolomite samples range from $\delta^{18}O$ = 13.6 to 16.6‰. $\delta^{13}C$ values of the two dolomite samples are 0.6 and 0.7‰.

Assuming that O isotopic equilibration occurred between quartz and dolomite and the hydrothermal fluids during crystallization, the $\delta^{18}O$ compositions of the hydrothermal fluids can be derived using the fractionation equations of Clayton et al. (1972) and Horita (2014), and

temperatures derived from fluid inclusion studies. Evidence for phase separation in stages 1 and 2 means that measured fluid inclusion homogenization temperatures approximate the trapping temperatures for these fluids. The average temperature of stage 1 fluids is 464° ± 42°C, and 363° ± 30°C for stage 2, and $\delta^{18}O_{fluid}$ values have been calculated at one standard deviation above and below these average temperatures (Table 3-7 and Figure 3-21). Quartz at the margin of stage 3 polymetallic-sulfide dolomite veins was deposited from early stage 3 hydrothermal fluids, whereas dolomite in the center of the veins was deposited from late stage 3 fluid. No suitable fluid inclusions were found in the quartz, but inclusions in dolomite yielded an average trapping temperature of 185° ± 16°C. A trapping temperature of 190° ± 20°C was used to calculate $\delta^{18}O_{fluid}$ compositions. For early stage 3 fluids, we have calculated fluid isotopic compositions at 300°C and 200°C in order to estimate the likely range of values.

Table 3-7 O isotope data for quartz from quartz veins from stage 1-3 mineralization at Morrison

Sample	Vein stage	Temperature used for calculation of fluid composition	$\delta^{18}O$ (‰)	Maximum $\delta^{18}O_{fluid}$ (‰)[1]	Minimum $\delta^{18}O_{fluid}$ (‰)[2]
MO135-Quartz	Stage 1	464° ± 42°C	8.4	6.3	4.8
MO137-Quartz	Stage 1		8.2	6.1	4.6
MO144-Quartz	Stage 1		7.3	5.2	3.7
MO151-Quartz	Stage 2	363° ± 30°C	6.1	1.9	0.3
MO098-Quartz	Stage 2		7.7	3.4	1.9
MO072-Quartz	Stage 3 (Early)	200° and 300°C	10.7	3.9	-1.0
MO083-Quartz	Stage 3 (Early)		9.4	2.5	-2.3
MO072-Dolomite	Stage 3 (Late)	190° ± 20°C	13.6	3.3	0.8
MO083-Dolomite	Stage 3 (Late)		16.6	6.3	3.7

Note: [1]Maximum oxygen compositions of fluid are calculated with the mean homogenization temperature plus the standard deviation of the mean.
[2]Minimum oxygen compositions of fluid are calculated with the mean homogenization temperature minus the standard deviation of the mean.

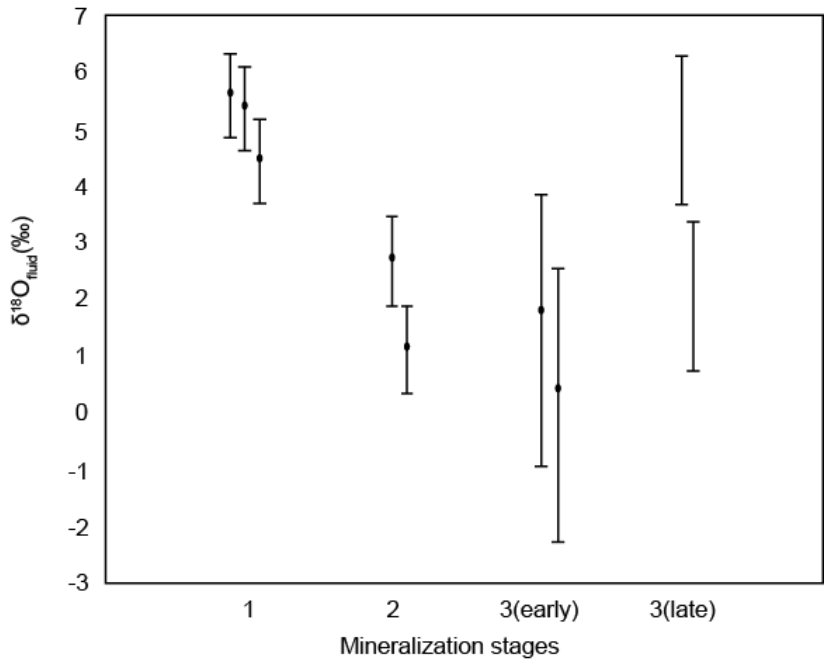

Fig. 3-21. Evolution of the $\delta^{18}O$ composition of the hydrothermal fluids from stages 1 to 3.

Calculated $\delta^{18}O_{fluid}$ values for stage 1 vein fluids range from 3.7 to 6.3‰ (incorporating the error range of the fluid inclusion data), whereas fluid compositions for stage 2 fluids range from 0.3 to 3.4 ‰. The composition of early stage 3 fluids is roughly estimated to be in the range of -2.3 to 3.9‰ (based on the likely fluid temperature range), whereas the composition of late stage 3 fluids is estimated to range between 0.8 and 6.3‰.

3.12 Sulfur isotope compositions

Seven sulfide samples were analyzed for their sulfur isotopic composition: two mixed chalcopyrite and pyrite samples from stage 1 disseminated sulfides in potassic alteration, one molybdenite and one pyrite sample from type 4 quartz-molybdenite-pyrite veins of stage 2 mineralization, and one pyrite and two sphalerite samples from type 5 polymetallic-sulfide-dolomite veins of stage 3 mineralization. The results are reported in Table 3-8.

The two mixed chalcopyrite and pyrite samples (MO095 and MO096) occur as finely intergrown 1–3 mm composite grains that could not be separated, and the analyses therefore

represent a mixture of chalcopyrite and pyrite. However, it is noted that the fractionation of S isotope between these two minerals, and between these minerals and HS^-, is not large (<1‰ at 300-400°C). The $\delta^{34}S$ compositions of these stage 1 sulfides are -0.2 and 0.8‰.

Table 3-8 S isotope data for sulfides from stage 1-3 mineralization at Morrison

Sample	Mineral	$\delta^{34}S$ (‰)	Comments
MO95	Mixture of chalcopyrite and pyrite	-0.8	Stage 1, disseminated sulfides
MO96	Mixture of chalcopyrite and pyrite	0.2	Stage 1, disseminated sulfides
MO042	Molybdenite	-2.1	Stage 2, from type 4 quartz-molybdenite-pyrite vein
MO115	Pyrite	-1.2	Stage 2, from type 4 quartz-molybdenite-pyrite vein
MO072	Pyrite	-5.8	Stage 3, from type 5 polymetallic-sulfide-dolomite vein
MO072	Sphalerite	-7.1	Stage 3, from type 5 polymetallic-sulfide-dolomite vein
MO083	Pyrite	-5.6	Stage 3, from type 5 polymetallic-sulfide-dolomite vein

Molybdenite (sample MO042) and pyrite (sample MO115) from type 4 quartz-molybdenite-pyrite veins (stage 2) yielded $\delta^{34}S$ value of -2.1 and -1.2‰, respectively, and pyrite (samples MO072 and MO083) and sphalerite (sample MO072) from type 5 polymetallic veins (stage 3), and yielded $\delta^{34}S$ values between -7.1 and -5.6‰.

3.13 Discussion

Petrogenesis of the plagioclase-hornblende-biotite porphyry

The U-Pb age of the phase A plagioclase-hornblende-biotite porphyry at Morrison obtained in this study is 52.21 ± 0.37 Ma, which is consistent with the previous K-Ar age (52.1 ± 2.1 Ma) of Carter (1982), but slightly younger than the previous laser $^{40}Ar/^{39}Ar$ age (53. 2 ± 0.5 Ma) of MacIntyre et al. (2001). These ages for Morrison (52–53 Ma) are similar to those of other intrusions in the Babine Lake igneous suite, which range from 48–55 Ma (K-Ar and laser $^{40}Ar/^{39}Ar$ ages from: Carter, 1976, 1982; Villeneuve and MacIntyre, 1997; MacIntyre et al., 2001).

Whole-rock geochemical data indicate that the plagioclase-hornblende-biotite porphyries at Morrison are calc-alkaline to high-K calc-alkaline diorites to granodiorites, and were generated in a continental arc setting. This explanation is consistent with the tectonic setting of central British Columbia in the early Eocene, which involved oblique convergence between the Kula-Farallon and North America plate (Norkleberg et al., 2000).

The Th/La ratio may serve as an indicator for crustal contamination (Taylor and McLennan, 1985). The high Th/La ratio of the Morrison suite (average of ~0.21; n = 9) is higher than the primitive mantle (~0.12; Sun and McDonough, 1989), likely indicating crustal contamination.

The trace element patterns of the porphyry samples from Morrison are similar to those from other Babine Lake intrusions and coeval andesitic–dacitic volcanic rocks (SiO_2 <65%) from the Eocene Ootsa Lake Group (47 to 53 Ma) in central British Columbia (Figure 3-13), although the overall trace element contents of the volcanic rocks are somewhat higher than the intrusive rocks (Grainger, 2000). These patterns show enrichments in LILE and depletions in Nb, Ta, and Ti (Fig. 3-13A), and REE patterns show no europium anomalies (Fig. 3-13B). These geochemical similarities, combined with their similar ages and locations, suggest that these igneous suites are broadly comagmatic. More felsic volcanic rocks (SiO_2 >65%) from the Eocene Ootsa Lake Group show increased depletions in Sr, P, and Ti, and distinct negative Eu anomalies (especially in the rhyolities) with increase in SiO_2 (Fig. 3-13), suggesting extensive fractionation of plagioclase, apatite, and magnetite in these more evolved rocks.

Timing of ore-formation at Morrison

Two molybdenite Re-Os model ages (52.54 ± 0.22 Ma, 53.06 ± 0.22 Ma) were obtained in this study, which are in broad good agreement with the U-Pb age of the host porphyry (52.21 ± 0.37 Ma), suggesting that Mo (and Cu) mineralization was coeval with magmatism (within the error of these geochronological methods).

Ore fluids and genetic model

The coexistence of vapor-rich inclusions and hypersaline inclusions in stage 1 and 2 quartz-sulfide veins indicate the occurrence of fluid immiscibility, and permit the interpretation that homogenization temperatures represent actual trapping temperatures. The microthermometric data from stage 1, type 3 quartz-chalcopyrite-pyrite vein samples show that the early fluids were hot and saline (400° to 526°C; 39.8 to 47.8 wt.% NaCl equiv.), whereas data from stage 2, type 4 quartz-molybdenite-pyrite veins are slightly cooler and less saline (320° to 421°C; 37.0 to 43.1 wt.% NaCl equiv.; Fig. 3-19). Sulfur isotopic compositions of stage 1 disseminated chalcopyrite-pyrite mixtures are +0.8 and -0.2‰, whereas stage 2 vein molybdenite and pyrite are -2.1 and 1.2‰, respectively. Calculated fluid oxygen isotopic compositions range from $\delta^{18}O_{fluid}$ = 3.7 to 6.3‰ in stage 1, and 0.3 to 3.4‰ in stage 2 (Table 3-7). Taken together, these data support a predominantly magmatic origin for the porphyry fluids and contained sulfur, with a possible minor contribution from meteoric water in stage 2. By comparison, Ohmoto and Rye (1979), Ohmoto (1986), Marini et al. (2001), and Simon and Ripley (2011) report a range for magmatic sulfur of $\delta^{34}S = 0 \pm 2$‰, and Sheppard (1977) report ranges for magmatic fluids of $\delta^{18}O_{water}$ = +5.5 to +10.0‰.

The third stage of polymetallic sulfide mineralization is related to localized sericite-carbonate alteration (commonly overprinted by argillic alteration) spatially controlled by the East Fault. Early stage 3 fluids have $\delta^{18}O_{fluid}$ compositions estimated to be roughly between -2.3 and 3.9‰ (imprecisely constrained due to a lack of fluid inclusion temperature information), which is lower than in the stage 1 fluids, but overlaps with stage 2. Sulfur isotopic compositions are also lower than earlier sulfides ($\delta^{34}S$ = -7.1 to -5.6‰; Tables 3-8), indicating a sedimentary source.

Fluids related late stage 3 dolomite precipitation are cooler and much more dilute than in stages 1 and 2 (163° to 218°C; 3.1 to 3.9 wt.% NaCl equiv.), and calculated $\delta^{18}O_{fluid}$ compositions from two dolomite samples have a wide range from 0.8 to 6.3‰, which overlaps the entire range of earlier stages. This wide range can be explained either by mixing of magmatic water and meteoric water, or by wallrock reaction. The latter explanation is supported by carbon isotope compositions ($\delta^{13}C$ = 0.6 to 0.7‰), which are consistent with a marine carbonate origin ($\delta^{13}C \sim 0$; Hoefs, 1987), and may reflect reaction between groundwater and the surrounding sedimentary

wall rocks. In summary, these data suggest that the stage 3 fluids were dominantly of meteoric groundwater origin, and reacted with the surrounding sedimentary rocks.

Comparison with other porphyry deposits in the Babine Lake area

Key characteristics of the Bell, Granisle, and Morrison porphyry deposits are listed in Table 3-9. Based on geological descriptions from Carson and Jambor (1974), Dirom et al. (1995), and Ogryzlo (1995), all three deposits show similarities in host rock ages and compositions, hydrothermal alteration, mineralization style, and ore mineralogy. All deposits are genetically and spatially related to small Eocene plagioclase-hornblende-biotite porphyry stocks, which intruded into Jurassic-Cretaceous volcanic and sedimentary rocks. All porphyries in the Babine Lake area have similar monzonite-diorite-granodiorite compositions (Fig. 3-11) and ages (~52 Ma). Each of the three deposits is centered on a potassic-altered porphyry stock, which is surrounded by a peripheral chlorite-carbonate (propylitic) zone. However, other alteration styles differ in the three deposits: sericite-carbonate alteration and quartz-sericite alteration occur at Bell, sericite-carbonate alteration occurs at Granisle, and minor sericite-carbonate and argillic alteration occur at Morrison. Cu mineralization is mainly associated with potassic alteration generated by magmatic fluids at Granisle and Morrison, whereas it mainly occurs in quartz-sericite stockworks formed by mixtures of magmatic water and groundwater at Bell (Wilson et al., 1980)

The three deposits are similar in many respects to the classic Lowell & Guilbert (1970) model, but differ at Granisle and Morrison in the absence of a large quartz-sericite (phyllic) alteration zone. These differences likely reflect differences in the composition of the country rocks at the three deposits. The Bell porphyry is hosted by Skeena Group siltstone on its western side, which underwent quartz-sericite alteration, and dark green marine tuff (Hazelton Group) on its eastern side, which underwent sericite-carbonate alteration. At Granisle, the porphyry is mainly hosted by intermediate tuff and breccia interlayered with pebble conglomerate of the Lower Jurassic Hazelton Group, which underwent sericite-carbonate alteration. In contrast, at Morrison, the country rocks are mainly siltstones of the Upper Jurassic Ashman Formation, which underwent chlorite-carbonate alteration. The different proportions of sericite, chlorite, and

Table 3-9 Characteristics of three porphyry deposits (Bell, Granisle, and Morrison) in the Babine Lake area

Deposit name	Resource (MT)	Average grades	Country rock	Porphyry age	Porphyry intrusion composition	Alteration types	Mineralization styles	Ore minerals	Hythermal fluid related with mineralization	Source(s)
Morrison	270	0.39% Cu; 0.2 g/t Au; 0.005% Mo	Sedimentary rocks (Siltstones, silty argillites, and minor conglomerates) of Upper Jurassic Ashman Formation of the Bowser Group	52.2 ± 0.37 Ma (U-Pb zircon age)	Diorite to granodiorite	Potassic alteration; chlorite-carbonate alteration; argillic alteration; lack of typical phyllic alteration. Rare phyllic alteration is present as halos of polymetallic veins. Copper mineralization is closely related to the potassic alteration.	Stockwork veins and dissemination	Primarily chalcopyrite, minor bornite, and rare molybdenite, sphalerite, galena, gold, and silver	Magmatic water	Carson and Jambor (1974); Carson and Jambor (1996); Ogryzlo et al. (1995)
Bell	77.2	0.48% Cu; 0.17 g/t Au; <0.01% Mo	Siltstone of the Skeena Group in the west of the main intrusion, and dark green marine tuff of the Hazelton Group in the east of the main intrusion	52.0 ± 0.5 Ma (Biotite Ar-Ar age)	Diorite to granodiorite	Potassic alteration; chlorite-carbonate alteration; sericite-carbonate alteration; quartz-sericite alteration. Copper mineralization is closely associated with the quartz-sericite alteration.	Stockwork veins and dissemination	Primarily chalcopyrite, moderate bornite, minor chalcocite, and rare molybdenite, sphalerite, and galena, gold, and silver.	Mixture of magmatic water and groundwater	Carson and Jambor (1974); Carson et al. (1976); Wilson et al. (1980); Zaluski et al. (1994); Dirom et al. (1995); MacIntyre et al. (2001)
Granisle	52.7	0.43% Cu; 0.13 g/t Au; 0.005% Mo	Intermediate tuff and breccia interlayered with pebble conglomerate of the Lower Jurassic Hazelton Group	51.2 ± 0.6 Ma (Biotite Ar-Ar age)	Diorite to granodiorite	Potassic alteration; chlorite-carbonate alteration; sericite-carbonate alteration. Copper mineralization is closely related to the potassic alteration.	Stockwork veins and dissemination	Primarily chalcopyrite, minor bornite, and rare molybdenite, gold and silver	Magmatic water	Carson and Jambor (1974); Fahrni et al. (1976); Wilson et al. (1980); Zaluski et al. (1994); Dirom et al. (1995); MacIntyre et al. (2001)

carbonate in these alteration zones may reflect different proportions of feldspathic and ferromagnesian minerals, with sericite being more abundant in feldspathic rocks, and chlorite and carbonate in more mafic rocks. Such differences are observed in other porphyry deposits in British Columbia, such as at Schaft Creek, where chloritic alteration predominates due to the mafic nature of the country rocks (Scott et al., 2008).

Hollister (1975) proposed a diorite model for some British Columbia low-silica alkaline porphyries, in which the phyllic alteration zone is poorly developed or absent because iron is not totally consumed by sulfur in the hydrothermal fluid; consequently, chlorite-rich alteration minerals are formed rather than sericite. A similar explanation may apply to Morrison.

3.14 Conclusion

Porphyry Cu mineralization at Morrison is shown to be spatially, temporally, and probably genetically related to Eocene-age calc-alkaline plagioclase-hornblende-biotite porphyry stocks and dikes with continental arc affinity, which were intruded into sedimentary rocks of the Upper Jurassic Ashman Formation of the Bowser Group. Two molybdenite samples yielded Re-Os ages of 52.54 ± 0.22 Ma and 53.06 ± 0.22 Ma, which are broadly in good agreement with the intrusive age. Potassic (biotite) and propylitic (chlorite-carbonate) alteration was developed during the early stages of hydrothermal fluid circulation. The potassic alteration mainly occurs in the plagioclase-hornblende-biotite porphyry, and is closely associated with Cu mineralization. The main Cu ore minerals, chalcopyrite and minor bornite, are primarily located in stockwork veinlets and quartz-sulfide veins, but also occur as disseminations within the altered porphyry. Propylitic alteration is primarily present in peripheral sedimentary rocks, and does not carry Cu mineralization, whereas sericite-carbonate and argillic alteration are associated with a later stage fluid of possible meteoric groundwater origin, and are localized along the East Fault. Sericite-carbonate alteration is restricted to halos around late last stage polymetallic veins, and is locally overprinted by argillic alteration.

The vein paragenesis at Morrison can be classified into five types. Early biotite veins (type 1) consist of fine-grained biotite, lacking sulfides; type 2 veins are stockwork veinlets of

chalcopyrite ± quartz-bornite-pyrite; type 3 veins contain chalcopyrite-quartz-bornite-pyrite with sulfide in the center line. Types 1–3 are closely related to strong potassic alteration, and are grouped as hydrothermal stage 1. Type 4 veins (stage 2) are quartz-rich, with minor molybdenite and pyrite, and are related to weak potassic alteration. Type 5 veins (stage 3) are dolomite rich with polymetallic sulfides (sphalerite-galena-arsenopyrite-pyrite ± chalcopyrite) and minor quartz, and are related to sericite-carbonate alteration.

Oxygen isotope ($\delta^{18}O_{fluid}$ = 3.7 to 6.3‰), sulfur isotope ($\delta^{34}S$ = -0.2 to 0.8‰), and fluid inclusion data indicate that the first stage of mineralization involved a high-temperature (400° to 526°C) and saline (39.8 to 47.8 wt.% NaCl equiv.) fluid of likely magmatic origin, which was responsible for potassic alteration and Cu precipitation. The second stage, with minor molybdenum mineralization, was related to mainly magmatic fluids, but possibly with a minor cooler and dilute groundwater component as indicated by oxygen isotope ($\delta^{18}O_{fluid}$ = 0.3 to 3.4‰), sulfur isotope ($\delta^{34}S$ = -2.1 to -1.2‰), and fluid inclusion data (Th: 320° to 421°C; salinities: 37.0 to 43.1 wt.% NaCl equiv.). In contrast, the third stage of polymetallic-carbonate veining was formed predominantly from meteoric groundwater which had undergone partial isotopic exchange with country rocks: $\delta^{18}O_{fluid}$ = -2.3 to 3.9‰ (derived from early vein quartz); $\delta^{18}O_{fluid}$ = 0.8 to 6.3‰ (derived from late vein dolomite); $\delta^{34}S$ = -7.1 to -5.6‰; $\delta^{13}C$ = 0.6 to 0.7‰; fluid inclusion homogenization temperatures = 163° to 218°C, and salinities = 3.1 to 3.9 wt.% NaCl equiv.).

The Morrison porphyry deposit is similar to other Late Cretaceous-early Cenozoic porphyry deposits in central British Columbia in term of host rocks, age, alteration styles, and ore mineralogy. These deposits are all related to subduction along the western margin of North America in the Paleogene. Plate reconstructions for the Late Cretaceous to Eocene show oblique subduction between the Kula-Farallon and North American plate, which generated intermediate-to-felsic continental-arc magmatism with calc-alkaline affinity, and with high potential for the formation of porphyry Cu ± Mo ± Au deposits such as Morrison.

3.15 References

Bachmann, O., Dungan, M.A., and Bussy, F., 2005, Insights into shallow magmatic processes in

large silicic magma bodies: the trace element record in the Fish Canyon magma body, Colorado: Contributions to Mineralogy and Petrology, v. 149, p. 338–349.

Bodnar, R.J., Burnham, C.W., and Sterner, S.M., 1985, Synthetic fluid inclusions in natural quartz. III. Determination of phase equilibrium properties in the system H_2O–NaCl to 1000°C and 1500 bars: Geochimica et Cosmochimica Acta, v. 49, p. 1861–1873.

Bodnar, R.J., 1993, Revised equation and table for determining the freezing point depression of H_2O-NaCl solutions: Geochimica et Cosmochimica Acta, v. 57, p. 683–684.

Brenan, J.M., Shaw, H.F., Phinney, D.L., and Ryerson, F.J., 1994, Rutile-Aqueous fluid partitioning of Nb, Ta, Hf, Zr, U and Th: Implications for high field strength element depletions in island arc basalts: Earth and Planetary Science Letters, v. 128, p. 327–339.

Candela, P.A., 1992, Controls on ore metal ratios in granite-related ore systems: An experimental and computational approach: Transactions of the Royal Society of Edinburgh, Earth Sciences, v. 83, p. 317–326.

Carson, D.J.T., and Jambor. J.L., 1974, Mineralogy, zonal relationships and economic significance of hydrothermal alteration at porphyry copper deposits, Babine lake area, British Columbia: Canadian Institute of Mining and Metallurgy Bulletin, v. 67, p. 110–133.

Carson, D.J.T., and Jambor. J.L., 1976, Morrison: Geology and evolution of a bisectued annular porphyry copper deposit, in Sutherland, B.A., ed., Porphyry deposits of the Canadian Cordillera: Canadian Institute of Mining and Metallurgy, Special Volume 15, p. 264–273.

Carson, D.J.T., and Jambor. J.L., Ogryzlo, P.L., and Richards, T. A., 1976, Bell copper: Geology, geochemistry, and genesis of a supergene-enriched, biotized porphyry copper deposit with a superimposed phyllic zone, in Sutherland, B.A., ed., Porphyry deposits of the Canadian Cordillera: Canadian Institute of Mining and Metallurgy, Special Volume 15, p. 245–263.

Carter, N.C., 1976, Regional setting of porphyry deposits in west-central British Columbia, in Sutherland, B.A., ed., Porphyry deposits of the Canadian Cordillera: Canadian Institute of Mining and Metallurgy, Special Volume 15, p. 227–238.

Carter, N.C., 1982, Porphyry copper, and molybdenum deposits, west-central British Columbia: British Columbia Ministry of Energy, Mines, and Petroleum Resources, Bulletin 64, 150 p.

Carter, N.C., Dirom, G.E., and Ogryzlo, P.L., 1995, Porphyry copper–gold deposits, Babine Lake area, west-central British Columbia, in Schroeter, T.G., ed., Porphyry Deposits of the Northwestern Cordillera of North America: Canadian Institute of Mining, Metallurgy and Petroleum, Special Volume 46, p. 247–255

Church, B.N., 1970, Geology of the Owen Lake, Parrott Lakes and Goosly Lake area, in Geology, exploration and mining in British Columbia 1969: British Columbia Department of Mines and Petroleum Resources, p. 119–125.

Church, B.N., 1972, Geology of the Buck Creek area, British Columbia, In Geology, exploration and mining in British Columbia 1972: British Columbia Ministry of Energy, Mines and Petroleum Resources, p. 353–363.

Clayton, R.N., O'Neil, J.R., and Mayeda, T.K., 1972, Oxygen isotope exchange between quartz and water: Journal of Geophysical Research, v. 77, p. 3057–3067.

Dirom, G.E., Dittrick, M.P., McArthur, D.R., Ogryzlo, P.L., Pardoe, A.J., and Stothart, 1995, Bell and Granisle porphyry copper-gold mines, Babine region, west-central British Columbia, in Schroeter, T.G., ed., Porphyry Deposits of the Northwestern Cordillera of North America: Canadian Institute of Mining, Metallurgy and Petroleum, Special Volume 46, p. 256–289.

English, J.M., Johnston, S.T., and Mihalynuk, M.G., 2003, The Kutcho Arc and Early Mesozoic intraoceanic amalgamation in the Intermontane Belt, Canadian Cordillera, Program with Abstracts: Geological Association of Canada.

Fahrni, K.C., Kim, H., Klein, G.H., and Carter, N.C., 1976, Granisle, in Sutherland, B.A., ed., Porphyry deposits of the Canadian Cordillera: Canadian Institute of Mining and Metallurgy, Special Volume 15, p. 239–244.

Foley, S.F., Barth, M.G., and Jenner, G.A., 2000, Rutile/melt partition coefficients for trace elements and an assessment of the influence of rutile on the trace element characteristics of subduction zone magmas: Geochimica et Cosmochimica Acta, v. 64, p. 933–938.

Gabrielse, H., Monger, J.W.H., Wheeler, J.O., and Yorath, C.J., 1991, Morphogeological belts, tectonic assemblages, and terranes: Geological Survey Of Canada, Geology of Canada Series, no. 4, p. 15–28.

Goldstein, R.H., and Reynolds, T.J., 1994, Systematics of fluid inclusions in diagenetic materials: Society for Sedimentary Geology Short Course 31, 199 p.

Grainger, N.C., 2000, Petrogenesis of Middle Jurassic to Miocene magmatism within the Nechako plateau, central British Columbia: Insight form petrography, geochemistry, geochronology and tracer isotope studies: Unpublished M.Sc. thesis, University of Alberta, 125 p.

Grainger, N.C., Villeneuve, M.E., Heaman, L.M., and Anderson, R.G., 2001, New U-Pb and Ar/Ar isotope age constraints on the timing of Eocene magmatism, Fort Fraser and Nechako River map areas, central British Columbia: Can. J. Earth Sci., v.38, p. 679–696.

Gromet, L.P., and Silver, L.T., 1987, REE Variations across the Peninsular Ranges batholith: Implications for batholithic petrogenesis and crustal growth in magmatic arcs: Journal of Petrology, v. 28, p. 75–125.

Gustafson, L.B., and Hunt, J.P., 1975, The porphyry copper deposit at El Salvador, Chile: Economic Geology, v. 70, p. 857−912.

Hanson, G., 1980, Rare earth elements in petrogenetic studies of igneous systems: Annual Review of Earth and Planetary Sciences, v. 8, p. 371–406.

Hoefs, J., 1987, Stable isotope geochemistry: Berlin, Springer-Verlag, 241 p.

Hollister, V.F., 1975, An appraisal of the nature and source of porphyry copper deposits: Minerals Science and Engineering, v. 7, p.225–233.

Housh, T.B., and Luhr, J.F., 1991, Plagioclase-melt equilibria in hydrous systems: American Mineralogist, v. 76, p. 477–492.

Klein, M., Stosch, H.G., and Seck, H.A., 1997, Partitioning of high field strength and rare-earth elements between amphibole and quartz-dioritic to tonalitic melts: An experimental study: Chemical Geology, v. 138, p. 257–271.

Logan, J.M., and Mihalynuk, M.G., 2014, Tectonic controls on Early Mesozoic paired alkaline porphyry deposit belts (Cu-Au ± Ag-Pt-Pd-Mo) within the Canadian Cordillera: Economic Geology, v. 109, p. 827–858.

Lowell, J.D., and Guilbert, J.M., 1970, Lateral and vertical alteration-mineralization zoning in

porphyry ore deposits: Economic Geology, v. 65, p. 373−408.

Ludwig, K.R., 2003, Isoplot/Ex, a geochronological toolkit for Microsoft Excel, Version 3.00: Berkeley Geochronology Center, Special Publication No. 4, p. 1–43.

MacIntyre, D.G., 2006, Geology and mineral deposits of the Skeena arch, west-central British Columbia (Parts of NTS 093E, L, M; 094D; 1031, P): Updata on a geoscience BC digital data compilation project: Geological fieldwork 2006, Paper 2007-1, p. 333–340.

MacIntyre, D.G., Villeneuve, M.E., and Schiarizza, P., 2001, Timing and tectonic setting of Stikine Terrane magmatism, Babine-Takla lakes area, central British Columbia: Canadian Journal of Earth Sciences, v. 38, p. 579–601.

Marini, L., Moretti, R., and Accornero, M., 2011, Sulfur Isotopes in Magmatic-Hydrothermal Systems, Melts, and Magmas: Reviews in Mineralogy & Geochemistry, v. 73, p. 423–492

Markey, R., Stein, H.J., Hannah, J.L., Selby, D., and Creaser, R.A., 2007, Standardizing Re-Os geochronology: A new molybdenite reference material (Henderson, UAS) and the stoichiometry of Os salts: Chemical Geology, v. 244, p. 74–87.

Massey, N.W.D., MacIntyre, D.G., Desjardins, P.J., Cooney, R.T., 2005, Digital geology map of British Columbia; whole province: British Columbia Ministry of Energy, Mines and Petroleum Resources, Open-File 2005–01.

McMillan, W.J., Thompson, J.F.H., Hart, C.J.R., and Johnston, S.T., 1995, Regional geological and tectonic setting of porphyry deposits in British Columbia and Yukon Territory, in Schroeter, T.G., eds., Porphyry deposits of the northwestern Cordillera of North America: Canadian Institute of Mining, Metallurgy and Petroleum, Special Volume 46, p. 40–57.

Merzbacher, C., and Eggler, D.H., 1984, A magmatic geohygrometer: application to Mount St. Helens and other dacitic magmas: Geology, v. 12, p. 587–590.

Middlemost, E.A.K., 1994, Naming materials in the magma/igneous rock system: Earth-Science Reviews, v. 37, p. 215–224.

Monger, J.W.H., 1977, Upper Paleozoic rocks of the western Canadian Cordillera and their bearing on Cordilleran evolution: Canadian Journal of Earth Sciences, v. 14, p. 1832–1859

Monger, J.W.H., and Irving, E., 1980, Northward displacement of north-central British Columbia:

Nature (London), v. 285, p. 289–294.

Monger, J.W.H., Price, R.A., and Tempelman-Kluit, D.J., 1982, Tectonic accretion and the origin of two major metamorphic and plutonic welts in the Canadian Cordillera: Geology, v. 10, p. 70–75.

Monger, J., and Price, R., 2002, The Canadian Cordillera: Geology and Tectonic Evolution: CSEG Recorder, v. 2, p.17–36.

Moore, G.M., Carmichael, I.S.E., 1998, The hydrous phase equilibria (to 3 kbar) of an andesite and basaltic andesite from western Mexico: constraints on water content and conditions of phenocryst growth: Contributions to Mineralogy and Petrology, v. 130, p. 304–319.

Naney, M.T., 1983, Phase equilibria of rock-forming ferromagnesian silicates in granitic systems: American Journal of Science, v. 283, p. 993–1033.

Nelson, J., and Colpron, M., 2007, Tectonics and metallogeny of the British Columbia, Yukon and Alaskan Cordillera, 1.8 Ga to the present, in Goodfellow, W.D., eds., Mineral Deposits of Canada: A Synthesis of Major Deposit-Types, District Metallogeny, the Evolution of Geological Provinces, and Exploration Methods: Geological Association of Canada, Mineral Deposits Division, Special Publication v. 5, p. 755–791.

Nokleberg, W.J., Parfenov, L.M., Monger, J. W. H., Norton, I.O., Khanchun, A.I., Stone, D.B., Scotese, C.R., Scholl, D.W., and Fujita, K., 2000, Phanerozoic Tectonic Evolution of the Circum-North Pacific: U.S. Geological survey Professional Paper 1626, 122 p.

Nokleberg, W.J., Bundtzen, T., Eremin, R.A., Ratkin, V.V., Dawson, K.M., Shpikerman, V.V., Goryachev, N.A., Byalobzhesky, S.G., Frolov, Y.F., Khanchuck, A.I., Koch, R.D., Monger, J.W.H., Pozdeev, A.A., Rozenblum, I.S., Rodionov, S.M., Parfenov, L.M., Scotese, C.R. and Sidorov, A.A., 2005, Metallogenesis and tectonics of the Russian Far East, Alaska and the Canadian Cordillera: U.S. Geological Survey Professional Paper 1697, 397 p.

Ogryzlo, P.L., Dirom, G.E., and Stothart, P.G., 1995, Morrison – Hearne Hill copper-gold deposits Babine region, west-central British Columbia, in Schroeter, T.G., ed., Porphyry Deposits of the Northwestern Cordillera of North America: Canadian Institute of Mining, Metallurgy and Petroleum, Special Volume 46, p. 290–303.

Ohmoto, H., and Rye, R.O., 1979, Isotopes of sulfur and carbon, in Barnes, H.L., ed., Geochemistry of hydrothermal ore deposits, second edition: New York, John Wiley and Sons, p. 509–567.

Ohmoto, H., 1986, Stable isotope geochemistry of ore deposits, in Valley, J.W., Taylor, H.P., and O'Neil, J.R., eds, Stable isotopes in high temperature geological processes: Mineral. Soc. Amer., Reviews in Mineralogy, v. 16, p. 491–599.

Pearce, J.A., Harris, N.B.W., and Tindle, A.G., 1984, Trace element discrimination diagrams for the tectonic interpretation of granitic rocks: Journal of Petrology, v. 25, p. 956-983.

Peccerillo, A., and Taylor, S.R., 1976, Geochemistry of Eocene calc-alkaline volcanic rocks from the Kastamonu area, northern Turkey: Contributions to Mineralogy and Petrology, v. 58, p. 63–81.

Philpotts, J.A., 1970, Redox estimation from a calculation of Eu^{2+} and Eu^{3+} concentrations in natural phases: Earth and Planetary Science Letters, v. 9, p. 257–268.

Prowatke, S., and Klemme, S., 2006, Rare earth element partitioning between titanite and silicate melts: Henry's law revisited: Geochimica et Cosmochimica Acta, v. 70, p. 4997–5012.

Richards, J.P., 2011, high Sr/Y magmas and porphyry Cu ± Mo ± Au deposits: Just add water: Economic Geology, v. 106, p. 1075–1081.

Roedder, E., 1984, Fluid inclusions: Reviews in Mineralogy, v. 12, 644 p.

Rutherford, M.J., Devine, J.D., 1988, The May 18, 1980, eruption of Mount St. Helens. 3. Stability and chemistry of amphibole in the magma chamber: Journal of Geophysical Research, v. 93, p. 11949–11959.

Scott, J.E., Richards, J.P., Heaman, L.M., Creaser, R.A., and Salazar, G.S., 2008, The Schaft Creek Porphyry Cu-Mo-(Au) Deposit, Northwestern British Columbia: Canadian Institute of Mining, Metallurgy and Petroleum, v. 17, p. 163–196.

Selby, D., and Creaser, R.A., 2004, Macroscale NTIMS and microscale LA-MC-ICP-MS Re–Os isotopic analysis of molybdenite: Testing spatial restrictions for reliable Re–Os age determinations, and implications for the decoupling of Re and Os within molybdenite: Geochimica et Cosmochimica Acta, v. 68, p. 3897–3908.

Sheppard, S.M.F., 1977, Identification of the origin of oreforming solutions by the use of stable isotopes: Geological Society of London, Special Publications v. 7, p. 25–41.

Sheppard, S.M.F., 1986, Characterization and isotopic variations in natural waters: Reviews in Mineralogy, v. 16, p. 165–183.

Simonetti, A., Heaman, L.M., Hartlaub, R.P., Creaser, R.A., MacHattie, T.G., Bohn, C., 2005, U–Pb zircon dating by laser ablation-MC-ICP-MS using a new multiple ion counting Faraday collector array: Journal of Analytical Atomic Spectrometry, v .20, p. 677–686.

Simpson, R.G., and Geo, P., 2007, Mineral resource update Morrison project: Pacific Booker Minerals Inc. NI43–101 Report, 66 p.

Simon, A.C., and Ripley, E.M., 2011, The role of magmatic sulfur in the formation of ore deposits: Reviews in Mineralogy and Geochemistry, v. 73, p. 513–578.

Sisson, T.W., and Grove, T.L., 1993, Experimental investigations of the role of H_2O in calc-alkaline differentiation and subduction zone magmatism: Contributions to Mineralogy and Petrology, v. 113, p. 143–166.

Smoliar, M.I., Walker, R.J., and Morgan, J.W., 1996, Re-Os ages of Group IIA, IIIA, IVA, and IVB iron meteorites: Sciences, v. 271, p.1099–1102.

Souther, J.G., 1971, Geology and mineral deposits of Tulsequah map-area, British Columbia: Geological Survey of Canada, Memoir 362, 76 p.

——1972, Telegraph Creek map area, British Columbia: Geological Survey of Canada, Paper 71-44, 38 p.

Stacey, J.S., and Kramers, J.D., 1975, Approximation of terrestrial lead isotope evolution by a two-stage model: Earth and Planetary Science Letters, v. 26, p. 207–221.

Sterner, S.M., Hall, D.L., and Bodnar, R.J., 1988, Synthetic fluid inclusions. V. Solubility relations in the system NaCl-KCl-H_2O under vapor-saturated conditions: Geochimica et Cosmochimica Acta, v. 52, p. 989–1005.

Steele–MacInnis, M., Bodnar, R.J., and Naden, J., 2011, Numerical model to determine the composition of H_2O–NaCl–$CaCl_2$ fluid inclusions based on microthermometric and microanalytical data: Geochimica et Cosmochimica Acta, v. 75, p. 21–40.

Sun, S.S., and McDonough, W.F., 1989, Chemical and isotopic systematics of oceanic basalts: Implications for mantle composition and processes. Geological Society of London Special Publication, v. 42: p. 313–345.

Takeuchi, K., and Larson, P.B., 2005, Oxygen isotope evidence for the late Cenozoic development of an orographic rain shadow in eastern Washington, UAS: Geology, v. 33, p. 313–316.

Taylor, S.R., and McLennan, S.M., 1985, The continental crust; its composition and evolution: An Examination of the Geochemical Record Preserved in Sedimentary Rocks, 328 p.

Valley, J.W., Kitchen, N., Kohn, M.J., Niendorf, C.R., and Spicuzza, M.J., 1995, UWG-2, a garnet standard for oxygen isotope ratios: Strategies for high precision and accuracy with laser heating: Geochimica et Cosmochimica Acta, v. 59, p. 5223–5231.

Villeneuve, M.E., and MacIntyre, D.G., 1997, Laser $^{40}Ar/^{39}Ar$ ages of the Babine porphyries and Newman Volcanics, Fulton Lake map area, west-central British Columbia, in Radiogenic age and isotopic studies: Report 10, Geological Survey of Canada, Current Research 1997-F, p. 131–139.

Wilson, J.W.J., Kesler, S.E., Cloke, P.L., and Kelly, W.C., 1980, Fluid inclusion geochemistry of the Granisle and Bell porphyry Copper deposits, British Columbia: Economic Geology, v. 75, p. 45–61.

Woodsworth, G.J., Anderson, R.G., and Armstrong, R.L., 1991, Plutonic regimes, Chapter 15, in Gabrielse, H. and Yorath, C.J., eds., Geology of the Cordilleran Orogen in Canada: Geological Survey of Canada, Geology of Canada, v. 4, p. 491–531.

Zaluski. G., Nesbitt, B., and Muehlenbachs, K., 1994, Hydrothermal alteration and stable isotope systematics of the Babine porphyry Cu deposits, British Columbia: Implications for fluid evolution of porphyry systems: Economic Geology, v. 89, p. 1518–1541.

Chapter 4 Thesis Conclusion

4.1 Conclusion

A large collaborative research project, including geological, ZTEM, magnetotelluric, and magnetic studies, is aimed at improving the effectiveness of ZTEM surveys for deep mineral exploration. As a part of this project, detailed geological studies were conducted on the Newton epithermal and Morrison porphyry deposits in central British Columbia.

The Newton deposit is an intermediate sulfidation epithermal gold deposit, hosted by a Late Cretaceous volcanoplutonic complex. The volcanoplutonic complex is composed of mineralized felsic volcanic rocks (72.1 ± 0.6 Ma; Amarc Resources Ltd., reported in McClenaghan, 2013), quartz-feldspar porphyry (70.9 ± 0.5 Ma; Amarc Resources Ltd., reported in McClenaghan, 2013), feldspar-quartz-hornblende porphyry (72.10 ± 0.48 Ma; this work) stocks and dikes, and a barren diorite intrusive body (69.32 ± 0.43 Ma; this work). The mineralization can be divided into three stages: (1) disseminate pyrite with gold and minor quartz-pyrite ± molybdenite veins, which is associated with quartz-sericite alteration; (2) disseminated marcasite with gold related to quartz-sericite alteration; (3) polymetallic-sulfide veins (pyrite-chalcopyrite-sphalerite-arsenopyrite-dolomite), which cut across quartz-sericite altered rocks, and lack alteration selvedges. Molybdenite yielded a Re-Os age of 72.1 ± 0.3 Ma (McClenaghan, 2013), which suggests a genetic relationship with the Late Cretaceous volcanoplutonic complex. Fluid inclusion data indicate that a relatively hot and saline fluid (313°C, 4.8 wt.% NaCl equiv.) of likely magmatic origin was responsible for the stage 1 mineralization. The precipitation of disseminated gold and associated pyrite/marcasite was likely controlled by cooling and wallrock reaction.

The Morrison deposit is a typical porphyry Cu-Au-Mo deposit in British Columbia. The Eocene plagioclase-hornblende-biotite porphyry stocks and dikes, which intruded into sedimentary rocks of the Upper Jurassic Ashman Formation of the Bowser Group, are the main host rocks for the Cu-Au-Mo mineralization. The porphyry yielded a U-Pb zircon age of 52.21 ± 0.37 Ma. Three stages of mineralization are recognized: stage 1 vein-type and disseminated chalcopyrite and minor bornite related to strong potassic alteration; stage 2 quartz-molybdenite-pyrite veins related to weak potassic alteration; and stage 3 polymetallic-sulfide dolomite veins

related to sericite-carbonate alteration. Molybdenite from stage 2 yielded ages of 52.54 ± 0.22 Ma and 53.06 ± 0.22 Ma, which are broadly in agreement with the porphyry age, indicating a genetic relationship. The first stage of mineralization is related to a high temperature (400° to 526°C) and saline (39.8 to 47.8 wt.% NaCl equiv.) fluid of likely magmatic origin, an origin that is supported by oxygen isotope ($\delta^{18}O_{fluid}$ = 3.7 to 6.3‰) and sulfur isotope data ($\delta^{34}S$ = -0.2 to 0.8‰). The second stage of mineralization is associated with a cooler and slightly less saline fluid (Th = 320° to 421°C; salinities = 37.0 to 43.1 wt.% NaCl equiv.) of magmatic origin, but with a minor meteoric water component as evidenced by oxygen isotope ($\delta^{18}O_{fluid}$ = 0.3 to 3.4‰) and sulfur isotope data ($\delta^{34}S$ = -2.1 to -1.2‰). The third stage of mineralization was formed from predominantly meteoric groundwater with wallrock reaction (Th = 163° to 218°C; salinities = 3.1 to 3.9 wt.% NaCl equiv.; $\delta^{18}O_{fluid}$ = -2.3 to 3.9‰ (derived from early vein quartz); $\delta^{18}O_{fluid}$ = 0.8 to 6.3‰ (derived from late vein dolomite); $\delta^{34}S$ = -7.1 to -5.6‰; $\delta^{13}C$ = 0.6 to 0.7‰).

Based on this research, relevant petrophysical properties will be characterized by our geophysics colleagues, to help reduce the uncertainty of ZTEM survey.

4.2 Reference

McClenaghan, L., 2013, Geology and Genesis of the Newton Bulk-Tonnage Gold-Silver Deposit, Central British Columbia: Unpublished M.Sc. thesis, Vancouver, British Columbia, University of British Columbia, 186 p.

References

Albinson, T., Norman, D.I., Cole, D., and Chomiak, B., 2001, Controls on formation of low-sulfidation epithermal deposits in Mexico: Constraints from fluid inclusion and stable isotope data: Society of Economic Geology Special Publication 8, p. 1–32.

Andrew, K.P.E., 1988, Geology and genesis of the Wolf precious metal epithermal prospect and the Capoose base and precious metal porphyry-style prospect, Capoose Lake area, central British Columbia: MSc. thesis, University of British Columbia, Vancouver, 334 p.

Atwater, T., 1989, Plate tectonic history of the northeast Pacific and western North America, in Winterer, E.L., Hussong, D.M., and Decker, R.W., eds., The eastern Pacific Ocean and Hawaii: Boulder, Colorado, Geological Society of America, Geology of North America, v. N, p. 21–72.

Bachmann, O., Dungan, M.A., and Bussy, F., 2005, Insights into shallow magmatic processes in large silicic magma bodies: the trace element record in the Fish Canyon magma body, Colorado: Contributions to Mineralogy and Petrology, v. 149, p. 338–349.

Bevier, M.L., 1983, Implications of Chemical and Isotopic Composition for Petrogenesis of Chilcotin Group Basalts, British Columbia: Journal of Petrology, v. 24, p. 207–226.

Bevier, M.L., 1983, Regional stratigraphy and age of Chilcotin Group basalts, south-central British Columbia: Canadian Journal of Earth Sciences, v. 20, p. 515–524.

Briqueu, L., Bougault, H., Joron, J.L., 1984, Quantification of Nb, Ta, Ti and V anomalies in magmas associated with subduction zones: petrogenetic implications: Earth and Planetary Science Letters, v. 68, p. 297–308.

Brown, G.G., Thorpe, R.S., and Webb, P.C., 1984, The geochemical characteristics of granitoids in contrasting arcs and comments on magma sources: Journal of the Geological Society, v. 141, p. 413–426.

Bodnar, R.J., Burnham, C.W., and Sterner, S.M., 1985, Synthetic fluid inclusions in natural quartz. III. Determination of phase equilibrium properties in the system H_2O-NaCl to 1000°C and 1500 bars: Geochimica et Cosmochimica Acta, v. 49, p. 1861-1873

Bodnar, R.J., 1993, Revised equation and table for determining the freezing point depression of

H_2O-NaCl solutions: Geochimica et Cosmochimica Acta, v. 57, p. 683–684.

Bodnar, R.J., and Vityk, M.O., 1994, Interpretation of microthermometric data for H_2O-NaCl fluid inclusions, in DeVivo, B., and Frezzotti, M.L., eds., Fluid inclusions in minerals: Methods and applications: Blacksburg, VA, Virginia Polytechnic Institute and State University, p. 117–130.

Bordet, E., Hart, C, and McClenaghan, L., 2011, Epithermal-style Au-Ag mineralization in Cretaceous to Eocene felsic volcanic complexes, central British Columbia, western Canada, in: Barra, F., Reich, M., Campos, E., Tornos, F., eds., Let's Talk Ore Deposits Proceedings of the Eleventh Biennial SGA Meeting Ediciones Universidad Catolica del Norte, Antofagasta, Chile, p. 714–716.

Bozzo, A.T., Chen, H.S., Kass, J.R., and Barduhn, A.J., 1975, The properties of the hydrates of chlorine and carbon dioxide: Desalination, v. 16, p. 303–320.

Brenan, J.M., Shaw, H.F., Phinney, D.L., and Ryerson, F.J., 1994, Rutile-Aqueous fluid partitioning of Nb, Ta, Hf, Zr, U and Th: Implications for high field strength element depletions in island arc basalts: Earth and Planetary Science Letters, v. 128, p. 327–339.

Buchanan, L.J., 2000, The geology of the San Cristobal deposit: Society of Mining Engineers, Abstracts with Programs, Annual Meeting, p. 60.

Bysouth, G.D., Campbell, K.V., Barker, G.E., and Gagnier, G.K., 1995, Tonalite-trondhjemite fractionation of peraluminous magma and the formation of syntectonic porphyry copper mineralization, Gibraltar mine, central British Columbia, in Schroeter, T.G., ed., Porphyry Deposits of the Northwestern Cordillera of North America: Canadian Institute of Mining, Metallurgy and Petroleum, Special Volume 46, p. 201-213.

Candela, P.A., 1992, Controls on ore metal ratios in granite-related ore systems: An experimental and computational approach: Transactions of the Royal Society of Edinburgh, Earth Sciences, v. 83, p. 317–326.

Carson, D.J.T., and Jambor. J.L., 1974, Mineralogy, zonal relationships and economic significance of hydrothermal alteration at porphyry copper deposits, Babine lake area, British Columbia: Canadian Institute of Mining and Metallurgy Bulletin, v. 67, p. 110–133.

Carson, D.J.T., and Jambor. J.L., 1976, Morrison: Geology and evolution of a bisectued annular porphyry copper deposit, in Sutherland, B.A., ed., Porphyry deposits of the Canadian Cordillera: Canadian Institute of Mining and Metallurgy, Special Volume 15, p. 264–273.

Carson, D.J.T., and Jambor. J.L., Ogryzlo, P.L., and Richards, T. A., 1976, Bell copper: Geology, geochemistry, and genesis of a supergene-enriched, biotized porphyry copper deposit with a superimposed phyllic zone, in Sutherland, B.A., ed., Porphyry deposits of the Canadian Cordillera: Canadian Institute of Mining and Metallurgy, Special Volume 15, p. 245–263.

Carter, N.C., 1976, Regional setting of porphyry deposits in west-central British Columbia, in Sutherland, B.A., ed., Porphyry deposits of the Canadian Cordillera: Canadian Institute of Mining and Metallurgy, Special Volume 15, p. 227–238.

Carter, N.C., 1982, Porphyry copper, and molybdenum deposits, west-central British Columbia: British Columbia Ministry of Energy, Mines, and Petroleum Resources, Bulletin 64, 150 p.

Carter, N.C., Dirom, G.E., Ogryzlo, P.L., 1995, Porphyry copper–gold deposits, Babine Lake area, west-central British Columbia, in Schroeter, T.G., ed., Porphyry Deposits of the Northwestern Cordillera of North America: Canadian Institute of Mining, Metallurgy and Petroleum, Special Volume 46, p. 247–255

Casselman, M.J., McMillan, W.J., and Newman, K.M., 1995, Highland valley porphyry copper deposits near Kamloops, British Columbia: A review and update with emphasis on the Valley deposit, in Schroeter, T.G., ed., Porphyry Deposits of the Northwestern Cordillera of North America: Canadian Institute of Mining, Metallurgy and Petroleum, Special Volume 46, p. 161-191.

Chang, Z., Hedenquist, J.W., White, N.C., Cooke, D.R., Roach, M., 2011, Exploration Tools for Linked Porphyry and Epithermal Deposits: Example from the Mankayan Intrusion-Centered Cu-Au District, Luzon, Philippines: Economic Geology, v. 106, p. 1365–1398.

Christie, G., Lipiec, I.T., Simpson, R.G., Horton, J., Borntraeger, B., 2014, Technical report on feasibility study of the Blackwater Gold deposit, British Columbia: New Gold Inc. NI43–101 Report, 336 p.

Church, B.N., 1970, Geology of the Owen Lake, Parrott Lakes and Goosly Lake area, in Geology,

exploration and mining in British Columbia 1969: British Columbia Department of Mines and Petroleum Resources, p. 119–125.

Church, B.N., 1972, Geology of the Buck Creek area, British Columbia, In Geology, exploration and mining in British Columbia 1972: British Columbia Ministry of Energy, Mines and Petroleum Resources, p. 353–363.

Clayton, R.N., O'Neil, J.R., and Mayeda, T.K., 1972, Oxygen isotope exchange between quartz and water: Journal of Geophysical Research, v. 77, p. 3057–3067.

Colpron, M., and Price, R.A., 1995, Tectonic significance of the Kootenay terrane, southeastern Canadian Cordillera: An alternative model: Geology, v. 23, p. 25–28

Colpron, M., Nelson, J.L. and Murphy, D.C., 2006, A tectonostratigraphic framework for the pericratonic terranes of the northern Canadian Cordillera, in Colpron, M. and Nelson, J.L., eds., Paleozoic Evolution and Metallogeny of Pericratonic Terranes at the Ancient Pacific Margin of North America, Canadian and Alaskan Cordillera: Geological Association of Canada Special Paper 45, p. 1–23.

Cooke, D.R., McPhail, D.C., and Bloom, M.S., 1996, Epithermal gold mineralization, Acupan, Baguio district, Philippines: Geology, mineralization, alteration, and the thermochemical environment of ore deposition: Economic Geology, v. 91, p. 243–272.

Cooke, D.R., Deyell, C.L., Waters, P.J., Gonzales, R.I., and Zaw, K., 2011, Evidence for Magmatic-Hydrothermal Fluids and Ore-Forming Processes in Epithermal and Porphyry Deposits of the Baguio District, Philippines: Economic Geology, v. 106, p. 1399–1424.

Diamond, L.W., 1992, Stability of CO_2 clathrate hydrate + CO, liquid + CO_2 vapour + aqueous KCl-NaCl solutions: Experimental determination and application to salinity estimates of fluid inclusions: Geochimica et Cosmochimica Acta, v. 56, p. 273–280.

Dirom, G.E., Dittrick, M.P., McArthur, D.R., Ogryzlo, P.L., Pardoe, A.J., and Stothart, 1995, Bell and Granisle porphyry copper-gold mines, Babine region, west-central British Columbia, in Schroeter, T.G., ed., Porphyry Deposits of the Northwestern Cordillera of North America: Canadian Institute of Mining, Metallurgy and Petroleum, Special Volume 46, p. 256-289.

Edwards, B.R., and Russell, J.K., 1999, Northern Cordilleran volcanic province: A northern Basin

and Range: Geology, v. 27, p. 243–246.

Edwards, B.R., and Russell, J.K., 2000, Distribution, nature, and origin of Neogene-Quaternary magmatism in the northern Cordilleran volcanic province, Canada: GAS bulletin, v. 112, p. 1280–1295.

Einaudi, M.T., Hedenquist, J.W., and Inan, E., 2003, Sulfidation state of hydrothermal fluids: The porphyry-epithermal transition and beyond: Society of Economic Geologists Special Publication 10, p. 285−313.

Engebretson, D.C., Cox, Allan, and Gordon, R.G., 1985, Relative motions between oceanic and continental plates in the Pacific Basin: Geological Society of America, Special Paper 206, 59 p.

English, J.M., Johnston, S.T., and Mihalynuk, M.G., 2003, The Kutcho Arc and Early Mesozoic intraoceanic amalgamation in the Intermontane Belt, Canadian Cordillera, Program with Abstracts: Geological Association of Canada.

English, J.M., and Johnston, S.T., 2004, The Laramide Orogeny: What were the Driving Forces?: International Geology Review, v. 46, p. 833–838.

Fahrni, K.C., Kim, H., Klein, G.H., and Carter, N.C., 1976, Granisle, in Sutherland, B.A., ed., Porphyry deposits of the Canadian Cordillera: Canadian Institute of Mining and Metallurgy, Special Volume 15, p. 239–244.

Foley, S.F., Barth, M.G., and Jenner, G.A., 2000, Rutile/melt partition coefficients for trace elements and an assessment of the influence of rutile on the trace element characteristics of subduction zone magmas: Geochimica et Cosmochimica Acta, v. 64, p. 933–938.

Friedman, R., Diakow, L., Lane, R., and Mortensen, J., 2001, New U Pb age constraints on latest Cretaceous magmatism and associated mineralization in the Fawnie Range, Nechako Plateau, central British Columbia: Canadian Journal of Earth Sciences, v. 38, p. 619–637.

Gabrielse, H., 1991, Late Paleozoic and Mesozoic terrane interactions in north-central British Columbia: Canadian Journal of Earth Sciences, v. 28, p. 947–957.

Gabrielse, H., and Yorath, C.J., 1991, The Cordilleran orogen in Canada. Geoscience Canada, v. 16, p. 67–83.

Gabrielse, H., Murphy, D.C. and Mortensen, J.K., 2006, Cretaceous and Cenozoic dextral orogen-parallel displacements, magmatism and paleogeography, north-central Canadian Cordillera, in Haggart, J.W., Monger, J.W.H., and Enkin, R.J., eds., Paleogeography of the North American Cordillera: Evidence For and Against Large-Scale Displacements: Geological Association of Canada Special Paper 46, p. 255–276.

Gill, J.B., 1981, Orogenic andesites and plate tectonics: New York, Springer-Verlag, 390 p.

Gillespie, J.M., and Heller, P.L., 1995, Beginning of foreland subsidence in the Columbian-Sevier belts, southern Canada and northwest Montana: Geology, v. 23, p. 723–726.

Goldstein, R.H., 2003, Petrographic analisys of fluid inclusions, in Samson, I., Anderson, A., and Marshall, D., eds., Fluid inclusions: Analysis and interpretation: Mineralogical Association of Canada, Short Course Handbook, v. 32, p. 9–53.

Goldstein, R.H., and Reynolds, T.J., 1994, Systematics of fluid inclusions in diagenetic minerals: Society of Economic Paleontologists and Mineralogists, Short Course Handbook, v. 31, 199 p.

Gorton, M.P., and Schandl, E.S., 2000, From continents to Island arcs: A geochemical index of tectonic setting for arc-related and within plate felsic to intermediate volcanic rocks: Canadian Mineralogist, v. 38, p. 1065 – 1073.

Grainger, N.C., 2000, Petrogenesis of Middle Jurassic to Miocene magmatism within the Nechako plateau, central British Columbia: Insight form petrography, geochemistry, geochronology and tracer isotope studies: Unpublished M.Sc. thesis, University of Alberta, 125 p.

Grainger, N.C., Villeneuve, M.E., Heaman, L.M., and Anderson, R.G., 2001, New U-Pb and Ar/Ar isotope age constraints on the timing of Eocene magmatism, Fort Fraser and Nechako River map areas, central British Columbia: Can. J. Earth Sci., v.38, p. 679–696.

Green, T.H., and Pearson, N.J., 1985. Experimental determination of REE partition coefficients between amphibole and basaltic to andesitic liquids at high pressure. Geochimica et Cosmochimica Acta, v. 49, p. 1465–1468.

Gromet, L.P., Silver, L.T., 1983. Rare earth element distributions among minerals in a

granodiorite and their petrogenetic implications. Geochimica et Cosmochimica Acta, v. 47, p. 925–939.

Gromet, L.P., and Silver, L.T., 1987, REE Variations across the Peninsular Ranges batholith: Implications for batholithic petrogenesis and crustal growth in magmatic arcs: Journal of Petrology, v. 28, p. 75–125.

Gustafson, L.B., and Hunt, J.P., 1975, The porphyry copper deposit at El Salvador, Chile: Economic Geology, v. 70, p. 857−912.

Haas, J.L., 1971, The effect of salinity on the maximum thermal gradient of a hydrothermal system at hydrostatic pressure: Economic Geology, v. 66, p. 940–946.

Hanson, G., 1980, Rare earth elements in petrogenetic studies of igneous systems: Annual Review of Earth and Planetary Sciences, v. 8, p. 371–406.

Harms, T. A., 1986, Structural and tectonic analysis of the Sylvester Allochthon, SW McDame map area, northern British Columbia: Implications for paleogeography and accretion, Ph.D. thesis, University of Arizona, Tucson, America, 80 p.

Hedenquist, J.W., Arribas, A., Gonzalez-Urien, E., 2000, Exploration for epithermal gold deposits: Reviews in Economic Geology, v. 13, p. 245–277.

Hollister, V.F., 1975, An appraisal of the nature and source of porphyry copper deposits: Minerals Science and Engineering, v. 7, p.225–233.

Holtham, E., and Oldenburg, D.W., 2010, Three-dimensional inversion of ZTEM data: Geophysical Journal International, v. 182, p. 168–182.

Hoskin, P.W.O., 2000, Patterns of chaos: Fractal statistics and the oscillatory chemistry of zircon: Geochimica et Cosmochimica Acta, v. 64, p. 1905–1923.

Housh, T.B., and Luhr, J.F., 1991, Plagioclase-melt equilibria in hydrous systems: American Mineralogist, v. 76, p. 477–492.

Klein, M., Stosch, H.G., and Seck, H.A., 1997, Partitioning of high field strength and rare-earth elements between amphibole and quartz-dioritic to tonalitic melts: An experimental study: Chemical Geology, v. 138, p. 257–271.

Lamb, S., Hoke, L., Kennan, L., and Dewey, J., 1997, Cenozoic evolution of the Central Andes in

Bolivia and northern Chile: Geological Society [London] Special Publication 121, p. 237–264

Lane, R.A., and Schroeter, T.G., 1997, A review of metallic mineralization in the Interior Plateau, central British Columbia, in: Diakow, L.J., and Newell, J.M., eds., Interior Plateau Geoscience Project, Summary of Geological, Geochemical and Geophysical Studies, BCGS Survey Branch Open File 1996-2, p. 237–256.

Legault, J.M., Kumar, H., Milicevic, B., and Wannamaker, P., 2009, ZTEM tipper AFMAG and 2D inversion results over an unconformity target in northern Saskatchewan: SEG Expanded Abstracts, v. 28, p. 1277-1281.

Lepitre, M.E., Mortensen, J.K. Friedman, R.M., and Jordan, S.J., 1998, Geology and U-Pb geochronology of intrusive rocks associated with mineralization in the northern Tahtsa Lake district, west-central British Columbia, in Geological Fieldwork 1997, British Columbia Ministry of Energy and Mines, Paper 1998-1, p. 1–32.

Logan, J.M., and Mihalynuk, M.G., 2014, Tectonic controls on Early Mesozoic paired alkaline porphyry deposit belts (Cu-Au ± Ag-Pt-Pd-Mo) within the Canadian Cordillera: Economic Geology, v. 109, p. 827–858.

Lowell, J.D., and Guilbert, J.M., 1970, Lateral and vertical alteration-mineralization zoning in porphyry ore deposits: Economic Geology, v. 65, p. 373−408.

Ludwig, K.R., 2003, Isoplot/Ex, a geochronological toolkit for Microsoft Excel, Version 3.00: Berkeley Geochronology Center, Special Publication No. 4, p. 1–43.

Lynch, G., 1995, Geochemical polarity of the Early Cretaceous Gambier Group, southern Coast Belt, British Columbia: Canadian Journal of Earth Sciences, v. 32, p. 675–685.

MacIntyre, D.G., 2006, Geology and mineral deposits of the Skeena arch, west-central British Columbia (Parts of NTS 093E, L, M; 094D; 1031, P): Updata on a geoscience BC digital data compilation project: Geological fieldwork 2006, Paper 2007-1, p. 333–340.

MacIntyre, D.G., Ash, C., and Britton, J., 1994, Geological compilation, Skeena-Nass area, west-central British Columbia, NTS 93E, L, M; 94D; 103G, H, I, J, P; 104A, B: British Columbia Ministry of Energy, Mines and Petroleum Resources, Open File 1994–14.

MacIntyre, D.G., Villeneuve, M.E., and Schiarizza, P., 2001, Timing and tectonic setting of Stikine Terrane magmatism, Babine-Takla lakes area, central British Columbia: Canadian Journal of Earth Sciences, v. 38, p. 579–601.

Marini, L., Moretti, R., and Accornero, M., 2011, Sulfur Isotopes in Magmatic-Hydrothermal Systems, Melts, and Magmas: Reviews in Mineralogy & Geochemistry, v. 73, p. 423–492

Markey, R., Stein, H.J., Hannah, J.L., Selby, D., and Creaser, R.A., 2007, Standardizing Re-Os geochronology: A new molybdenite reference material (Henderson, UAS) and the stoichiometry of Os salts: Chemical Geology, v. 244, p. 74–87.

Massey, N.W.D., MacIntyre, D.G., Desjardins, P.J., Cooney, R.T., 2005, Digital geology map of British Columbia; whole province: British Columbia Ministry of Energy, Mines and Petroleum Resources, Open-File 2005–01.

McClenaghan, L., 2013, Geology and Genesis of the Newton Bulk-Tonnage Gold-Silver Deposit, Central British Columbia: Unpublished M.Sc. thesis, Vancouver, British Columbia, University of British Columbia, 186 p.

McLaren, G., and Rouse, J., 1989, Geology and Geochemistry of the Taseko Lakes Area (NTS 092O/3, 4, 5, 6): British Columbia Ministry of Energy, Mines and Petroleum Resources, Open File 1989–25.

McMillan, W.J., Thompson, J.F.H., Hart, C.J.R., and Johnston, S.T., 1995, Regional geological and tectonic setting of porphyry deposits in British Columbia and Yukon Territory, in Schroeter, T.G., ed., Porphyry deposits of the northwestern Cordillera of North America: Canadian Institute of Mining, Metallurgy and Petroleum, Special Volume 46, p. 40–57.

Merzbacher, C., and Eggler, D.H., 1984, A magmatic geohygrometer: application to Mount St. Helens and other dacitic magmas: Geology, v. 12, p. 587–590.

Middlemost, E.A.K., 1994, Naming materials in the magma/igneous rock system: Earth-Science Reviews, v. 37, p. 215–224.

Mihalasky, M.J., Bookstrom, A.A., Frost, T.P., and Ludington, S., 2011, Porphyry Copper Assessment of British Columbia and Yukon Territory, Canada: U.S. Geological Survey Scientific Investigations Report 2010-5090-C, v.1.1, 128 p.

Mikucki, J.E., 1998, Hydrothermal transport and depositional processes in Archean lode–gold systems: A review: Ore Geology Review, v. 13, p. 307–321.

Monger, J.W.H., 1977, Upper Paleozoic rocks of the western Canadian Cordillera and their bearing on Cordilleran evolution: Canadian Journal of Earth Sciences, v. 14, p. 1832–1859

Monger, J.W.H., and Irving, E., 1980, Northward displacement of north-central British Columbia: Nature (London), v. 285, p. 289–294.

Monger, J.W.H., Price, R.A., and Tempelman-Kluit, D.J., 1982, Tectonic accretion and the origin of two major metamorphic and plutonic welts in the Canadian Cordillera: Geology, v. 10, p. 70–75.

Monger, J., and Price, R., 2002, The Canadian Cordillera: Geology and Tectonic Evolution: CSEG Recorder, v. 2, p.17–36.

Moore, G.M., Carmichael, I.S.E., 1998, The hydrous phase equilibria (to 3 kbar) of an andesite and basaltic andesite from western Mexico: constraints on water content and conditions of phenocryst growth: Contributions to Mineralogy and Petrology, v. 130, p. 304–319.

Naney, M.T., 1983, Phase equilibria of rock-forming ferromagnesian silicates in granitic systems: American Journal of Science, v. 283, p. 993–1033.

Nelson, J., and Colpron, M., 2007, Tectonics and metallogeny of the British Columbia, Yukon and Alaskan Cordillera, 1.8 Ga to the present, in Goodfellow, W.D., eds., Mineral Deposits of Canada: A Synthesis of Major Deposit-Types, District Metallogeny, the Evolution of Geological Provinces, and Exploration Methods: Geological Association of Canada, Mineral Deposits Division, Special Publication No. 5, p. 755–791.

Noble, D.C., Eyzaguirre, V.R., and McKee, E.H., 1990, Precious-metal mineralization of Cenozoic age in the Andes of Peru: Circum-Pacific Council for Energy and Mineral Resources, Earth-Science Series, v. 11, p. 207–212.

Nokleberg, W.J., Parfenov, L.M., Monger, J. W. H., Norton, I.O., Khanchun, A.I., Stone, D.B., Scotese, C.R., Scholl, D.W., and Fujita, K., 2000, Phanerozoic Tectonic Evolution of the Circum-North Pacific: U.S. Geological survey Professional Paper 1626, 122 p.

Nokleberg, W.J., Bundtzen, T., Eremin, R.A., Ratkin, V.V., Dawson, K.M., Shpikerman, V.V.,

Goryachev, N.A., Byalobzhesky, S.G., Frolov, Y.F., Khanchuck, A.I., Koch, R.D., Monger, J.W.H., Pozdeev, A.A., Rozenblum, I.S., Rodionov, S.M., Parfenov, L.M., Scotese, C.R. and Sidorov, A.A., 2005, Metallogenesis and tectonics of the Russian Far East, Alaska and the Canadian Cordillera: U.S. Geological Survey Professional Paper 1697, 397 p.

Ogryzlo, P.L., Dirom, G.E., and Stothart, P.G., 1995, Morrison – Hearne Hill copper-gold deposits Babine region, west-central British Columbia, in Schroeter, T.G., ed., Porphyry Deposits of the Northwestern Cordillera of North America: Canadian Institute of Mining, Metallurgy and Petroleum, Special Volume 46, p. 290–303.

Ohmoto, H., and Rye, R.O., 1979, Isotopes of sulfur and carbon, in Barnes, H.L., ed., Geochemistry of hydrothermal ore deposits, second edition: New York, John Wiley and Sons, p. 509–567.

Ohmoto, H., 1986, Stable isotope geochemistry of ore deposits, in Valley, J.W., Taylor, H.P., and O'Neil, J.R., eds, Stable isotopes in high temperature geological processes: Mineral. Soc. Amer., Reviews in Mineralogy, v. 16, p. 491–599.

Oldenburg, D., Li, Y., and Ellis, R., 1997, Inversion of geophysical data over a copper gold porphyry deposit: A case history for Mt Milligan: Geophysics, v. 62, p. 1419–1431.

Parrish, R.R., Carr, S.D., and Parkinson, D.L., 1988, Eocene extensional tectonics and geochronology of the southern Omineca Belt, British Columbia and Washington: Tectonics, v. 7, p. 181–212.

Pressacco, R., 2012, Technical report on the initial mineral resource estimate for the newton project, central British Columbia, Canada: Amarc Resources Ltd. NI43–101 report, 154 p.

Philpotts, J.A., 1970, Redox estimation from a calculation of Eu^{2+} and Eu^{3+} concentrations in natural phases: Earth and Planetary Science Letters, v. 9, p. 257–268.

Prowatke, S., and Klemme, S., 2006, Rare earth element partitioning between titanite and silicate melts: Henry's law revisited: Geochimica et Cosmochimica Acta, v. 70, p. 4997–5012.

Richards, J.P., 2003, Tectono-magmatic precursors for porphyry Cu-(Mo-Au) deposit formation: Economic Geology, v. 98, p. 1515–1533.

Richards, J.P., 2011, high Sr/Y magmas and porphyry Cu ± Mo ± Au deposits: Just add water:

Economic Geology, v. 106, p. 1075–1081.

Riddell, J. M., 2006, Geology of the Southern Nechako Basin NTS 92N, 92O, 93B, 93C, 93F, 93G: British Columbia Ministry of Energy, Mines and Petroleum Resources, Open-File 2006–01.

Riddell, J., 2011, Lithostratigraphic and tectonic framework of Jurassic and Cretaceous Intermontane sedimentary basins of south-central British Columbia: Canadian Journal of Earth Sciences, v. 48, p. 870–896.

Roback, R. C., Sevigny, J. H., Walker, N. W., 1994, Tectonic setting of the Slide Mountain terrane, southern British Columbis: Tectonics, v. 13, p. 1242–1258.

Roedder, E., and Bodnar, R.J., 1980, Geologic pressure determinations from fluid inclusion studies: Annual Review of Earth and Planetary Sciences, v. 8, p. 263–301.

Roedder, E., 1984, Fluid inclusions: Reviews in Mineralogy, v. 12, 644 p.

Rollinson, H., 1993, Using Geochemical Data: Evaluation, Presentation, Interpretation, 352 p.

Rutherford, M.J., Devine, J.D., 1988, The May 18, 1980, eruption of Mount St. Helens. 3. Stability and chemistry of amphibole in the magma chamber: Journal of Geophysical Research, v. 93, p. 11949–11959.

Scott, J.E., Richards, J.P., Heaman, L.M., Creaser, R.A., and Salazar, G.S., 2008, The Schaft Creek porphyry Cu-Mo-(Au) deposit, Northwestern British Columbia: Exploration and Mining Geology, v. 17, p. 163-196.

Selby, D., Nesbitt, B.E., and Muehlenbachs, K., 2000, Hydrothermal alteration and fluid chemistry of the Endako Porphyry molybdenum deposit, British Columbia: Economic Geology, v. 95, p. 183-202.

Selby, D., and Creaser, R.A., 2004, Macroscale NTIMS and microscale LA-MC-ICP-MS Re–Os isotopic analysis of molybdenite: Testing spatial restrictions for reliable Re–Os age determinations, and implications for the decoupling of Re and Os within molybdenite: Geochimica et Cosmochimica Acta, v. 68, p. 3897–3908.

Seward, T.M., 1989, The hydrothermal chemistry of gold and its implications for ore formation: Boiling and conductive cooling as examples, in: Keays, R.R., Ramsay, W.R.H., Groves,

D.I., eds., The Geology of Gold Deposits: The Perspective in 1988, Economic Geology Monograph Series, v. 6, p. 398–404.

Seward, T.M., 1991, The hydrothermal geochemistry of gold, in: Foster, R.P., ed., Gold Metallogeny and Exploration, p. 37–62.

Sheppard, S.M.F., 1977, Identification of the origin of oreforming solutions by the use of stable isotopes: Geological Society, London, Special Publications, v. 7, p. 25–41.

Sheppard, S.M.F., 1986, Characterization and isotopic variations in natural waters: Reviews in Mineralogy, v. 16, p. 165–183.

Sheppard, S., and Gilg, H., 1996, Stable isotope geochemistry of clay minerals: Clay Minerals, v. 31, p. 1–24.

Sillitoe, R.H., 2010, Porphyry copper systems: Economic Geology, v. 105, p. 3–41.

Sillitoe, R.H., and Hedenquist, J.W., 2003, Linkages between volcanotectonic settings, ore-fluid compositions, and epithermal precious-metal deposits: Society of Economic Geologists Special Publication 10, p. 315−343.

Simpson, R.G., and Geo, P., 2007, Mineral resource update Morrison project: Pacific Booker Minerals Inc. NI43–101 Report, 66 p.

Simonetti, A., Heaman, L.M., Hartlaub, R.P., Creaser, R.A., MacHattie, T.G., Bohn, C., 2005, U–Pb zircon dating by laser ablation-MC-ICP-MS using a new multiple ion counting Faraday collector array: Journal of Analytical Atomic Spectrometry, v .20, p. 677–686.

Sisson, T.W., 1994, Hornblende-melt trace-element partitioning measured by ion microprobe: Chemical Geology, v. 117, p. 331–344.

Sisson, T.W., and Grove, T.L., 1993, Experimental investigations of the role of H_2O in calc-alkaline differentiation and subduction zone magmatism: Contributions to Mineralogy and Petrology, v. 113, p. 143–166.

Smoliar, M.I., Walker, R.J., and Morgan, J.W., 1996, Re-Os ages of Group IIA, IIIA, IVA, and IVB iron meteorites: Sciences, v. 271, p.1099–1102.

Souther, J.G., 1971, Geology and mineral deposits of Tulsequah map-area, British Columbia: Geological Survey of Canada, Memoir 362, 76 p.

——1972, Telegraph Creek map area, British Columbia: Geological Survey of Canada, Paper 71-44, 38 p.

Stacey, J.S., and Kramers, J.D., 1975, Approximation of terrestrial lead isotope evolution by a two-stage model: Earth and Planetary Science Letters, v. 26, p. 207–221.

Sterner, S.M., Hall, D.L., and Bodnar, R.J., 1988, Synthetic fluid inclusions. V. Solubility relations in the system NaCl-KCl-H_2O under vapor-saturated conditions: Geochimica et Cosmochimica Acta, v. 52, p. 989–1005.

Steele–MacInnis, M., Bodnar, R.J., and Naden, J., 2011, Numerical model to determine the composition of H_2O–NaCl–$CaCl_2$ fluid inclusions based on microthermometric and microanalytical data: Geochimica et Cosmochimica Acta, v. 75, p. 21–40.

Stock, J., and Molnar, P., 1988, Uncertainties and implications of the Late Cretaceous and Tertiary position of North America relative to the Farallon, Kula, and Pacific plates: Tectonics, v. 7, p. 1339–1384.

Sun, S.S., and McDonough, W.F., 1989, Chemical and isotopic systematics of oceanic basalts: Implications for mantle composition and processes. Geological Society of London Special Publication, v. 42: p. 313–345.

Takeuchi, K., and Larson, P.B., 2005, Oxygen isotope evidence for the late Cenozoic development of an orographic rain shadow in eastern Washington, UAS: Geology, v. 33, p. 313–316.

Taylor, H.K., 1995, Western Canadian porphyry deposits – economic perspectives, performances and prospects, in Schroeter, T.G., ed., Porphyry Deposits of the Northwestern Cordillera of North America: Canadian Institute of Mining, Metallurgy and Petroleum, Special Volume 46, p. 20-39.

Umhoefer, P.J. and Schiarizza, P., 1996, Latest Cretaceous to early Tertiary dextral strike-slip faulting on the southeastern Yalakom fault system, southeastern Coast belt, British Columbia: Geological Society of America Bulletin, v. 108, p. 768–785.

Valley, J.W., Kitchen, N., Kohn, M.J., Niendorf, C.R., and Spicuzza, M.J., 1995, UWG-2, a garnet standard for oxygen isotope ratios: Strategies for high precision and accuracy with laser

heating: Geochimica et Cosmochimica Acta, v. 59, p. 5223–5231.

Villeneuve, M.E., and MacIntyre, D.G., 1997, Laser $^{40}Ar/^{39}Ar$ ages of the Babine porphyries and Newman Volcanics, Fulton Lake map area, west-central British Columbia, in Radiogenic age and isotopic studies: Report 10, Geological Survey of Canada, Current Research 1997-F, p. 131–139.

Wheeler, J.O., Brookfield, A.J., Gabrielse, H., Monger, J.W.H., Tipper, H.W. and Woodsworth, G.J., 1991, Terrane map of the Canadian Cordillera: Geological Survey of Canada, Map 1713A, scale 1: 2 000000.

Wilson, J.W.J., Kesler, S.E., Cloke, P.L., and Kelly, W.C., 1980, Fluid inclusion geochemistry of the Granisle and Bell porphyry Copper deposits, British Columbia: Economic Geology, v. 75, p. 45–61.

Woodsworth, G.J., Anderson, R.G., and Armstrong, R.L., 1991, Plutonic regimes, Chapter 15, in Gabrielse, H. and Yorath, C.J., eds., Geology of the Cordilleran Orogen in Canada: Geological Survey of Canada, Geology of Canada, v. 4, p. 491–531.

Zaluski. G., Nesbitt, B., and Muehlenbachs, K., 1994, Hydrothermal alteration and stable isotope systematics of the Babine porphyry Cu deposits, British Columbia: Implications for fluid evolution of porphyry systems: Economic Geology, v. 89, p. 1518–1541.

Appendix A X-ray Diffraction

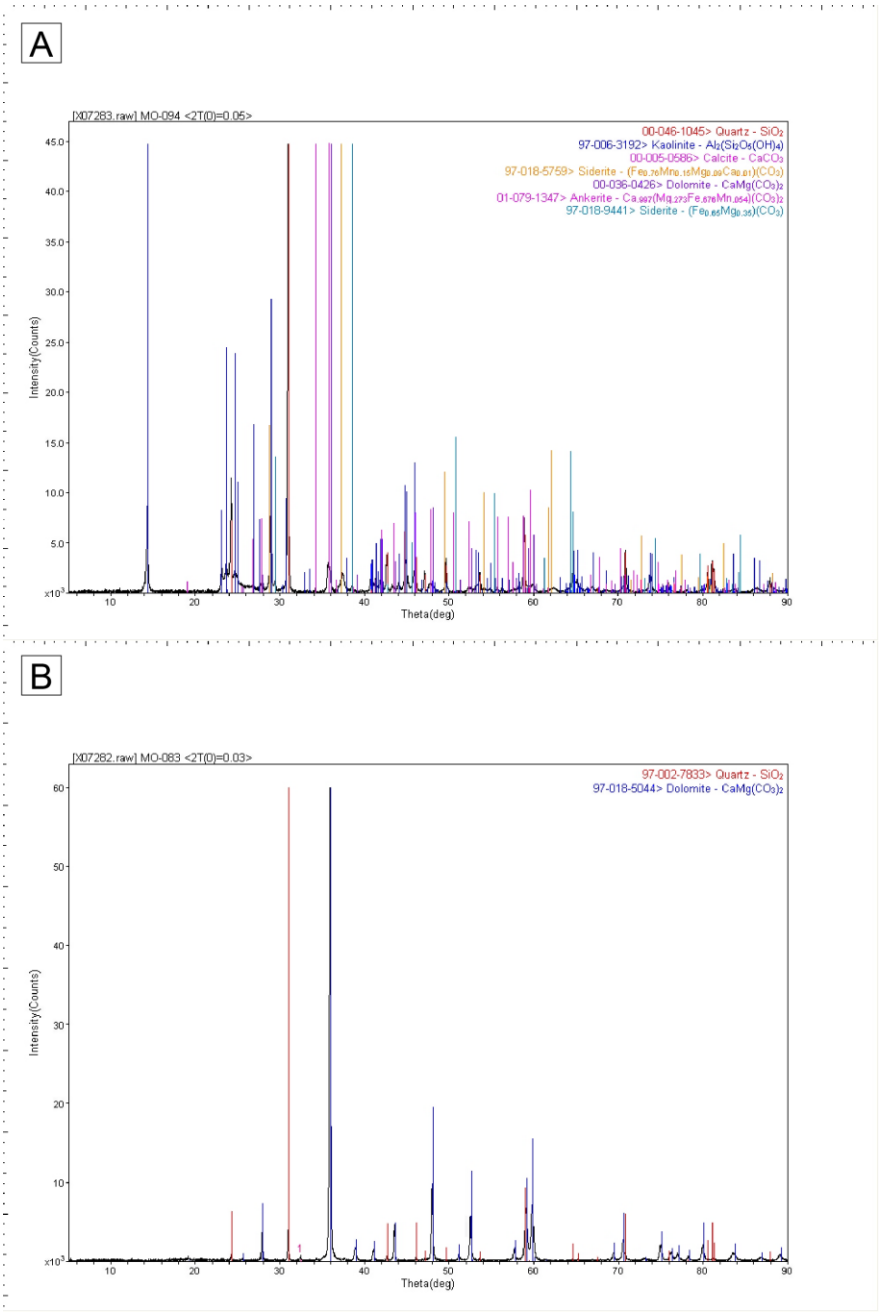

FIG. A1. X-ray Diffraction images of (A) Argillic altered biotite-hornblende-feldspar porphyry from Morrison, and (B) carbonate from polymetallic vein at Morrison.

Clay-carbonate altered porphyry and a carbonate vein samples were ground into fine powder, and analyzed by X-ray diffraction (XRD) at the University of Alberta. The Joint Committee on Powder Diffraction Standards (JCPDS) database and Inorganic Crystal Structure Database (ICSD) were used for identification the diffraction patterns of the samples.

The clay mineral in the argillic altered biotite-hornblende-feldspar porphyry at Morrison is kaolinite (Fig. A1-A). X-ray diffraction analysis in this study also identified various types of carbonate minerals in the argillic altered biotite-hornblende-feldspar porphyry, including dominantly dolomite, ankerite, minor siderite, and rare calcite. Dolomite is the carbonate mineral in the polymetallic vein of stage 3 mineralization of Morrison (Fig. A1-B).